Supplementary material to EMEP Status Report 1/2010
Date: July 2010

METEOROLOGISK INSTITUTT
Norwegian Meteorological Institute

EMEP Unified model performance for acidifying and eutrophying components and photo-oxidants in 2008

EMEP/MSC-W: Haldis Berge and Michael Gauss

EMEP/CCC: Anne-Gunn Hjellbrekke

Supplementary material to EMEP Status Report 1/2010

Contents

CHAPTER 1

Acidifying and eutrophying components: validation and combined maps

Haldis Berge and Anne-Gunn Hjellbrekke

In this chapter the Unified EMEP model is evaluated with respect to acidifying and eutrophying components. Model results for 2008 are validated against measurements from the EMEP network for 2008. The agreement between model results and observations depends on a combination of several elements; the quality and representativeness of the measurement sites, the adequacy of emissions and the model performance. Therefore, the following discussion on model *underestimation* and *overestimation* only implies that the calculated values are lower or higher than the observations and does not necessarily refer to model deficiency.

1.1 Validation

Evaluations of the Unified EMEP model performance for acidifying and eutrophying components have been presented in numerous EMEP reports (e.g. Nyíri and Hjellbrekke 2009, Fagerli and Hjellbrekke 2008, Fagerli and Aas 2008a, Fagerli 2007, Fagerli and Aas 2007, Fagerli 2005, 2004, Fagerli et al. 2003). It has been shown that the EMEP model performance is rather homogeneous over the years (Fagerli et al. 2003), but depends on geographical coverage and quality of the measurement data. The EMEP model has also been validated for nitrogen compounds in Simpson et al. (2006a) and for dry and wet depositions of sulphur, and for wet deposition of nitrogen in Simpson et al. (2006b) with measurements outside the EMEP network. Calculated

trends of total nitrate (HNO_3 and NO_3^-) and ammonia + ammonium in air and precipitation have been evaluated in Fagerli and Aas (2008b) and have shown in general good correspondence to observations.

In last year's EMEP report we presented results from the Unified EMEP model version rv3.1 (EMEP MSC-W & CCC 2009). This year we present results from Unified EMEP model version rv3.6. Changes in the model are described in Simpson et al. (2010). This year the operational Unified EMEP model calculations are based on meteorology from the ECMWF-IFS model. Last year the operational Unified EMEP model calculations were based on meteorology from the HIRLAM model, instead of the PARLAM-PS meteorology used earlier. The meteorological fields from ECMWF-IFS have been interpolated from lon lat coordinates with a resolution of $0.22^\circ \times 0.22^\circ$ to the polar-stereographic 50×50 km^2 grid of EMEP. Test runs with HIRLAM meteorology and the evaluation of results for 2006 were presented in EMEP Report 1/2008 (Fagerli et al. 2008). Results from model runs using different meteorological drivers were evaluated against measurements and the performances of the different model setups were compared. See also discussion of effect of changing the meteorological driver in Tsyro et al. (2010).

The scatter-plots are based on yearly averages for 2008. The lines on the scatter-plots display deviations in the scatter of 30% ('30% line') and 50% ('50% line') relative bias, respectively. Relative bias is defined here as $\frac{Mod-Obs}{0.5\,(Mod+Obs)} \times 100\%$, where 'Mod' refers to yearly averaged modelled concentrations, while 'Obs' refers to yearly averaged measured concentrations.

Table 1.1 shows for each component the number of stations where measurements were available and data coverage criteria was satisfied (N_{stat}), measured yearly average over all stations (Obs), modelled yearly average over all stations (Mod), bias ($\frac{Mod-Obs}{Obs} \times 100\%$), correlation between observation and model for station yearly averages (Corr), root mean square error, Rmse ($\sqrt{\frac{1}{n}\sum_{i=1}^{n}(m_i - o_i)^2}$ where m_i and o_i are modelled and measured concentration in monitoring station *i*), and index of agreement, IOA ($1 - \frac{\sum_{i=1}^{N_{stat}}(m_i - o_i)^2}{\sum_{i=1}^{N_{stat}}(|m_i - Obs| + |o_i - Obs|)^2}$). IOA is introduced for the first time this year to give a more robust evaluation of the model result. IOA varies from 0 (theoretical minimum) to 1 (perfect agreement between observed and predicted values) and gives the degree to which model predictions are error free. IOA varies between 0.71 and 0.88 for all components except ammonia and nitric acid (which are 0.52 and 0.54 respectively).

1.1.1 Sulphur dioxide in air

In 2008 the modelled yearly averages for most acidifying and eutrophying components are lower than the observations. An exception is SO_2, for which modelled air concentrations are in average 48% higher than measured ones. This is a higher overestimation than last year (27%) which is probably due to changes in the SO_2 deposition in the Unified EMEP model (Simpson et al. 2010).

It can be noted (Figure 1.1) that the largest over-prediction for SO_2 is at the stations

Component	N_{stat}	Obs.	Mod.	Bias (%)	Corr.	RMSE	IOA
NO_2 (μg(N) m^{-3})	40	1.70	1.49	-12	0.77	0.90	0.85
SO_2 (μg(S) m^{-3})	51	0.42	0.62	48	0.60	0.45	0.71
SO_4^{2-} (μg(S) m^{-3})	58	0.56	0.32	-42	0.64	0.32	0.65
NH_3 (μg(N) m^{-3})	22	1.02	0.90	-11	0.32	0.90	0.52
NH_4^+ (μg(N) m^{-3})	37	0.67	0.50	-26	0.78	0.29	0.82
NH_3+NH_4^+ (μg(N) m^{-3})	45	1.42	1.19	-16	0.68	0.77	0.79
HNO_3 (μg(N) m^{-3})	21	0.18	0.11	-38	0.47	0.16	0.54
NO_3^-+HNO_3 (μg(N) m^{-3})	47	0.49	0.44	-11	0.81	0.16	0.88
NO_3^- (μg(N) m^{-3})	30	0.34	0.37	8	0.68	0.17	0.81
SO_4^{2-} wd (μg(S)m^{-2})	63	17673.34	14130.44	-20	0.69	142.77	0.80
SO_4^{2-} cp (μg(S)l^{-1})	63	0.33	0.26	-19	0.72	0.16	0.83
NH_4^+ wd (μg(N)m^{-2})	63	20448.06	16912.60	-17	0.67	171.50	0.80
NH_4^+ cp (μg(N)l^{-1})	63	0.38	0.30	-21	0.64	0.19	0.76
NO_3^- wd (μg(N)l^{-1})	64	15928.30	12968.05	-19	0.69	129.93	0.80
NO_3^- cp (μg(N)l^{-1})	64	0.28	0.23	-17	0.79	0.10	0.86
precip. mm	64	63988.72	65489.11	2	0.72	316.54	0.84

Table 1.1: Comparison of model results and observations for 2008. Annual averages over all EMEP sites with measurements. N_{stat}= number of stations, wd=wet deposition, cp= concentration in precipitation, Corr.= spatial correlation coefficient, RMSE = root mean square error, IOA= index of agreement.

SK02, SE14, DK08, IS02 and RU18. Two of these sites (SE14 and DK08) are situated on the coast of southern Sweden and on an island outside the eastern coast of Denmark. The overestimation of SO_2 at these two sites might indicate that the ship emissions included in the EMEP inventory are somewhat too high.

The Slovak site SK02 and the Swiss site CH01 are both mountain sites (2008 and 3578 m.a.s, respectively). Because of their high elevation, for a long-term run, these sites will often be above the boundary layer, especially in the winter. With the coarse topography in the regional scale model, this cannot be well captured by the model. Consequently, sulphur dioxide concentrations are overestimated. This applies also for sulphate.

For the Russian site, Danki (RU18), high discrepancies between the modelled and observed values have been identified also for other components and in previous years. Danki lies relatively close to Moscow, and this local influence might be the reason of the poor performance for this site.

For the Norwegian site, Zeppelin (NO42), underestimations of all components have been identified. Zeppelin is located on Svalbard and underestimation at this site reflects the model's difficulties in modelling transport to the Arctic.

Time series for SO_2 are shown in Figures 1.4–1.9. As it can be seen from the time series, overestimation is generally highest during winter time and autumn. In the

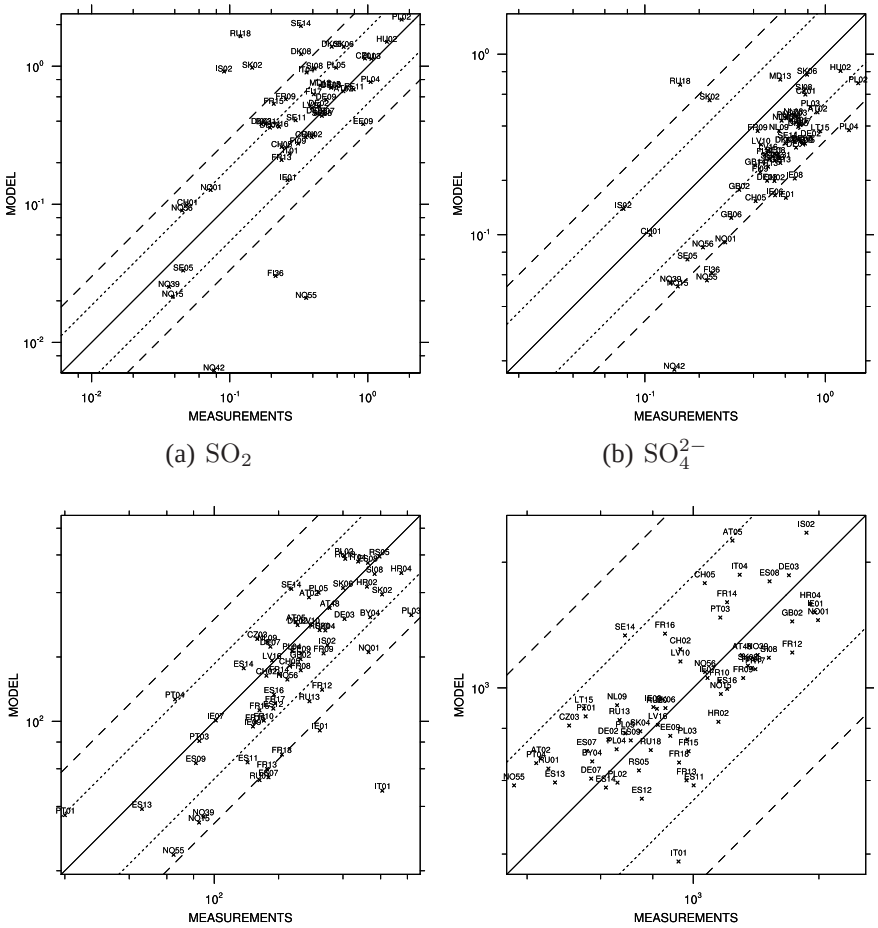

(a) SO_2 (b) SO_4^{2-}

(c) SO_4^{2-} wet dep. (d) Precipitation

Figure 1.1: Scatter-plots of modelled versus observed concentrations of sulphur dioxide and sulphate in air (μg(S) m^{-3}), wet deposition of sulphur (μg(S)m^{-2}) and precipitation (mm).

model seasonal variation of the emissions is considered based on data provided by the University of Stuttgart, IER, for 1990. However, it is likely that the seasonal variation of emissions has changed over time. Nowadays a larger part of emissions is released during the summer time with increasing use of air condition, and more importantly, the growth of telecommunications and computer hardware use.

1.1.2 Sulphate in air

For 2008 the modelled concentrations of sulphate in air are 42% underestimated. This is in the same range as in last year (underestimated by 41%). This is a significantly higher underestimation than in previous years (before 2007), and is probably caused by the change of the meteorological driver (Nyíri and Hjellbrekke (2009)). A similar underestimation of sulphate in air was found in a test run with HIRLAM meteorology

for 2006 (Fagerli et al. 2008).

A scatter-plot for modelled versus measured sulphate concentrations in air for 2008 is presented in Figure 1.1. While 84% of the annual mean concentrations for the different sites are within a relative bias of 50%, only 40% of the sites are within the 30% lines.

For several sites SO_4^{2-} is underestimated while there is an overestimation of SO_2 (e.g. NO01, SE14, DK08, HU02, PL02), while for other sites the model under-predicts both SO_4^{2-} and SO_2, with a higher underestimation for sulphate (e.g. NO15, NO39, SE05, IE01, PL04). This might indicate that there is too little oxidation of SO_2 to sulphate in the model. The bulk production of SO_4^{2-} results from the oxidation of SO_2 to sulphuric acid in liquid clouds, primarily by H_2O_2 and O_3. Of these two, H_2O_2 is by far the most important oxidant. The production of sulphate is limited by both the available SO_2 and the oxidizing capacity of the atmosphere.

The large decrease in sulphur emissions during the last decades has also lead to changes in the pH in the cloud liquid water. The oxidation rate for the SO_2 + O_3 aqueous reaction grows with increasing pH, and this pathway therefore becomes increasingly important.

There might be other reasons for the too low modelled air concentrations of sulphate, e.g. dry deposition velocity or fast wash out. The latter, hovewer, is not very likely, since the wet deposition of sulphur is also underestimated (Section 1.1.5).

Two mountain sites, CH01 and SK02 overestimate both SO_2 and particulate sulphate in air. As it was explained in Section 1.1.1, measurement sites with high elevation in general can not be well modelled with a coarse grid resolution, and air concentrations are expected to be overestimated.

Time series for sulphate in air are shown in Figures 1.10–1.15.

1.1.3 Ammonia and ammonium aerosol in air

For 2008, as for the previous years, there is a rather limited number of sites (45 in 2008) that report measurements for NH_3+NH_4^+ (NH_x). In order to evaluate the model performance for NH_x properly, ammonia and ammonium should be studied separately. However, the number of measurements for 2008 where the gaseous and particle phase are analyzed both separately and at the same time is rather limited.

The individual concentrations of ammonia and ammonium are biased when using the common filter-pack method due to the volatile nature of ammonium nitrate. Separation of these gases and particles by a simple aerosol filter is unreliable, and to obtain better quality data it is necessary to use denuders. However, this is a much more demanding method and several sites in the EMEP network are still using the filter-pack method and report the individual concentrations of ammonia and ammonium based on this.

Scatter-plots for modelled versus measured concentrations for ammonia, aerosol ammonium and total ammonium+ammonia in air in 2008 are presented in Figure 1.2, while time series for NH_3+NH_4^+ are shown in Figures 1.21–1.25. In table 1.1 the

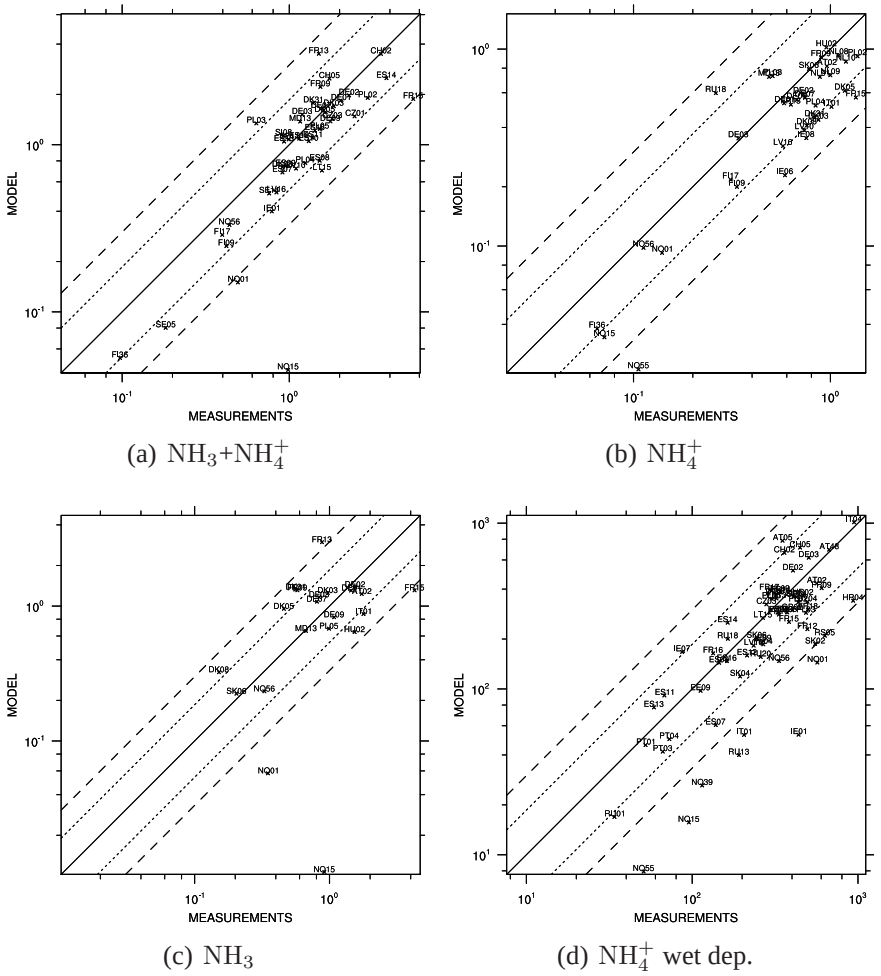

(a) NH_3+NH_4^+ (b) NH_4^+

(c) NH_3 (d) NH_4^+ wet dep.

Figure 1.2: Scatter-plots of modelled versus observed concentrations of total ammonium+ammonia, aerosol ammonium and ammonia in air (μg(N) m^{-3}) and wet deposition of reduced nitrogen (μg(N)m^{-2}).

Norwegian station Zeppelin (NO42) is included, this station is outside the range of Figure 1.2 because of low modelled values (less than 10^{-7} μg(N) m^{-3}). Figure 1.25 shows timeseries of the sum of ammonia and ammonium in air.

The modelled yearly average of the concentration of the sum of ammonia and ammonium in air is underestimated by 16% compared with the monitoring data. The spatial correlations for NH_3+NH_4^+ and NH_4^+ are among the highest for the modelled acidifying compounds, while NH_3 have a low spatial correlation. The much worse correlation this year (r=0.33 versus r=0.93 last year) reflects the dependency on the selection of stations.

1.1.4 Nitrate and nitric acid in air

Measurements of airborne nitrate are expected to have a rather large uncertainty due to the very different physical characteristics of the compounds making up total nitrate. Whilst nitric acid is a spatially variable volatile gas with fast dry deposition, particulate nitrate dry deposits only slowly and hence concentrations are more determined by long range transport.

In Figure 1.3 we show scatter-plots for total nitrate, particulate nitrate and nitric acid in air. Time series for total nitrate in air are shown in Figures 1.16–1.20.

Normally, the results for nitrate aerosol and nitric acid are somewhat worse than for total nitrate, because the monitoring data quality for these components are in general not as good as for total nitrate. The reason for this is that, similarly to the total ammonia+ammonium (as described in Section 1.1.3), the individual concentrations of nitrate and nitric acid are biased when using the common filter-pack method. This has also been shown in the evaluation of the EMEP model performance for nitrogen compounds using intensive measurement data from two sampling periods, June 2006 and January 2007 (Fagerli and Aas 2008a). One should keep in mind, that the meteorological driver for the model runs used in the evaluation of the model performance against the intensive measurement data was still PARLAM-PS, while this year we applied ECMWF-IFS meteorology (see Section 1.1).

In this year's model results, NO_3^- was overestimated by 8%, HNO_3 was underestimated by 27% and the sum of NO_3^-+HNO_3 was 11% underestimated. We have changed the model since last year's report (r3_6 versus rv3_1). Different performance might be caused by changes in dry deposition velocities of aerosols and changes in gaseous deposition (Simpson et al. 2010).

1.1.5 Concentrations in precipitation and wet depositions

The ability of the model to predict concentrations in precipitations and wet depositions is limited by the accuracy of the precipitation fields used in the model. The precipitation field pattern is very patchy (e.g. influenced by local topographic effects), and the regional scale model is unable to resolve this sub grid scale distribution. A typical problem arises with small scale showers. In reality precipitation is high in a small area of a given grid, but a large fraction of the grid should remain dry. Within the model, however, this precipitation is averaged out to cover the whole grid at a lower intensity. Thus, even though average precipitation amounts may be simulated well, the model experiences precipitation more often, but in lower amounts, than occur in reality. On a shorter time scale, e.g on daily basis, this may lead to too high concentrations in precipitation for episodes when it rains only in a small part of the grid square. For a regional scale model it is more sensible to compare the bulk concentrations, i.e the sum of the wet deposited compounds divided by the sum of precipitation.

The correlation between model and measurements for concentrations in precipitation and wet depositions will to a large extent depend on the model precipitation

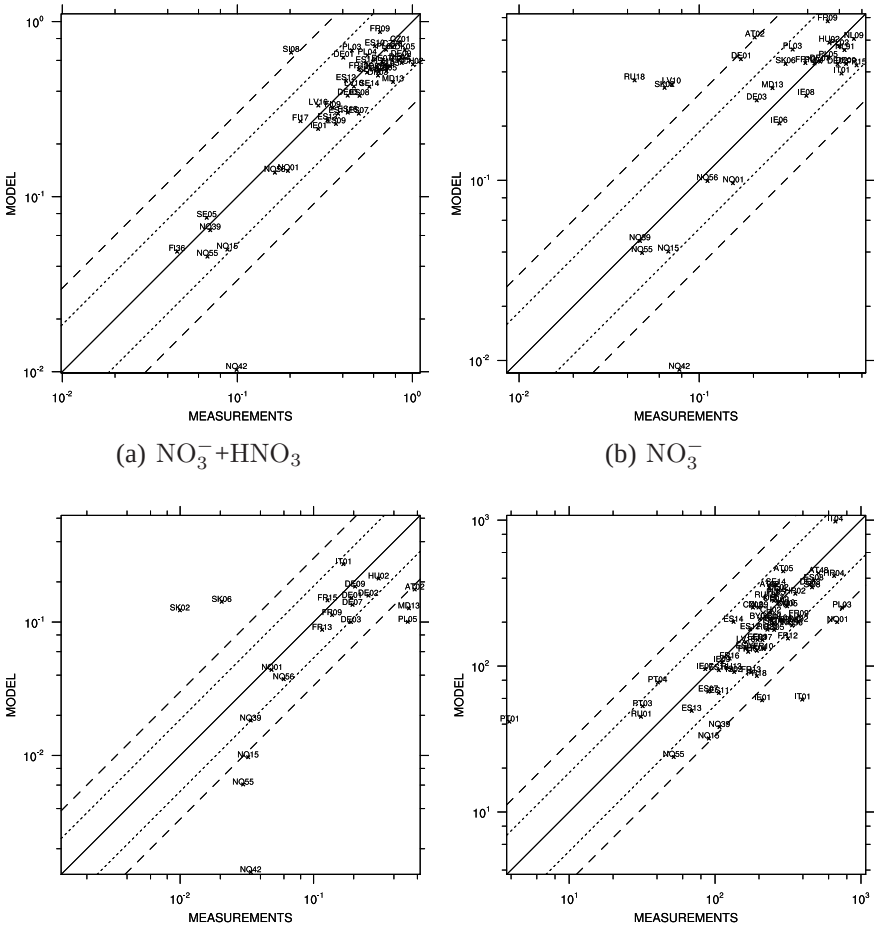

(a) NO_3^-+HNO_3 (b) NO_3^-

(c) HNO_3 (d) NO_3^- wet dep.

Figure 1.3: Scatter-plots of modelled versus observed concentrations of total nitrate, nitrate aerosol, nitric acid (μg(N) m^{-3}) and wet deposition of oxidized nitrogen (μg(N)m^{-2}).

field.

Scatter-plot for modelled versus observed precipitation is shown in Figure 1.1(d). In average, the observed and modelled precipitation is very similar (bias=2 %). The spatial correlation coefficient is 0.72.

Model calculations of wet depositions and concentrations in precipitation are lower than the observations ranging from 15% (reduced nitrogen in wet deposition) to 20% (wet deposition of sulphur). However, concentrations in precipitation and wet depositions of oxidized nitrogen are somewhat less underestimated in 2008 than in 2007.

The highest underestimation is found for sulphur both for wet deposition and concentration in precipitation (20% and 19%, respectively).

Scatter-plots for modelled versus observed wet depositions of sulphur, reduced nitrogen and oxidized nitrogen are shown in in Figures 1.1(c), 1.2(d) and 1.3(d), respectively.

Time series for sulphur, oxidized nitrogen and reduced nitrogen concentrations in precipitation are shown in Figures 1.26–1.32, Figures 1.33–1.39 and Figures 1.40–1.46, respectively.

1.2 Time series

In this section we present time series plots for all stations supplying data on a selection of acidifying and eutrophying components to EMEP CCC in 2008. The plots show daily model results and measurements, where available. Time series are shown also for those measurement sites which were excluded from the scatter-plots. In those cases where there is more than one day between measurements we only plot the measurement points. Time series for sulphur dioxide in air are shown in Figures 1.4–1.9, for sulphate in air in Figures 1.10–1.15, for total nitrate in air in Figures 1.16–1.20 and for ammonia+ammonium in air in Figures 1.21–1.25. In addition, time series are shown for sulphur, oxidized nitrogen and reduced nitrogen concentrations in precipitation in Figures 1.26–1.32, Figures 1.33–1.39 and Figures 1.40–1.46, respectively.

Sulphur dioxide in air

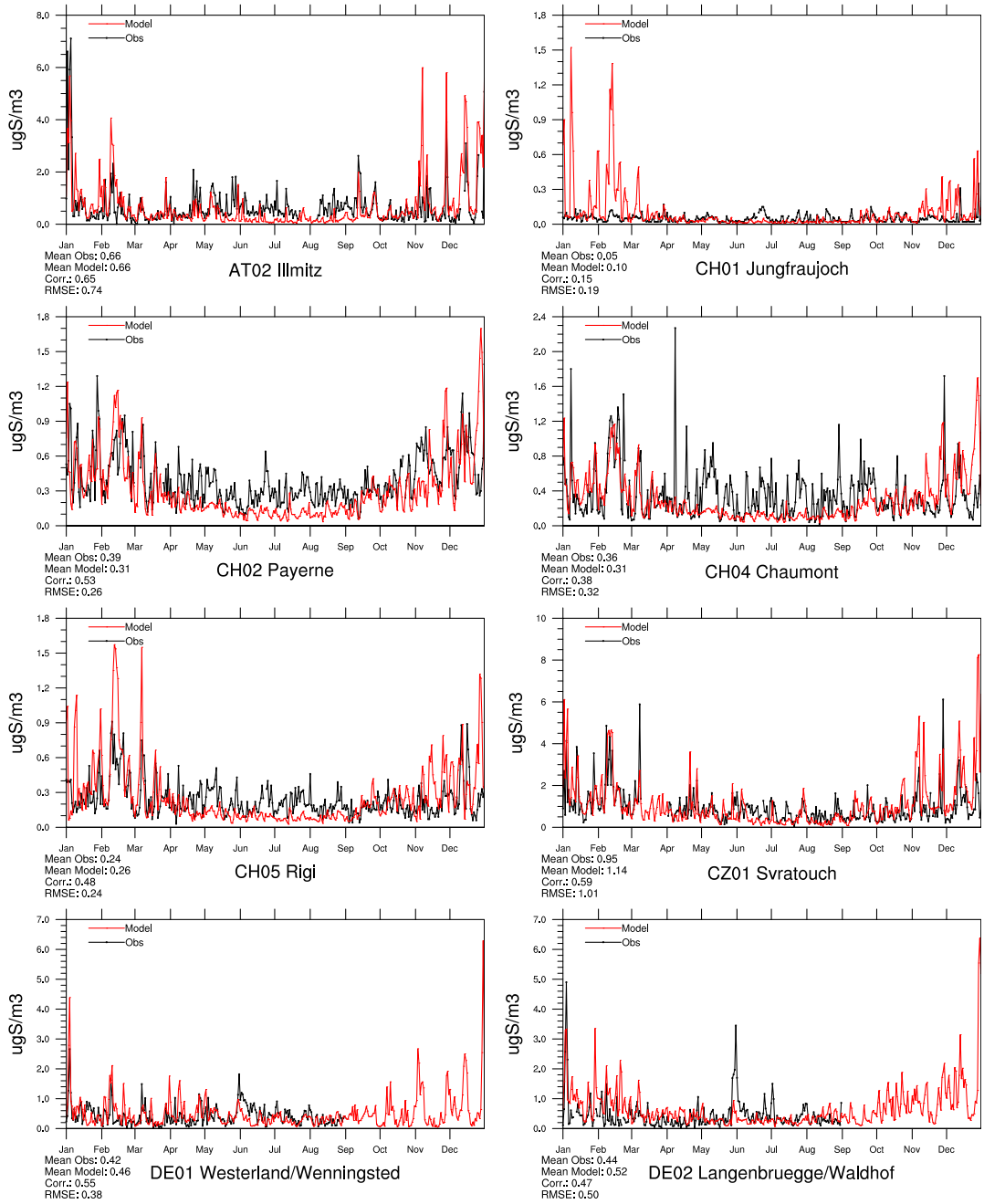

Figure 1.4: Comparison of model results and measurements (daily) for SO_2 in air (ugS) for stations that have measured SO_2 in 2008.

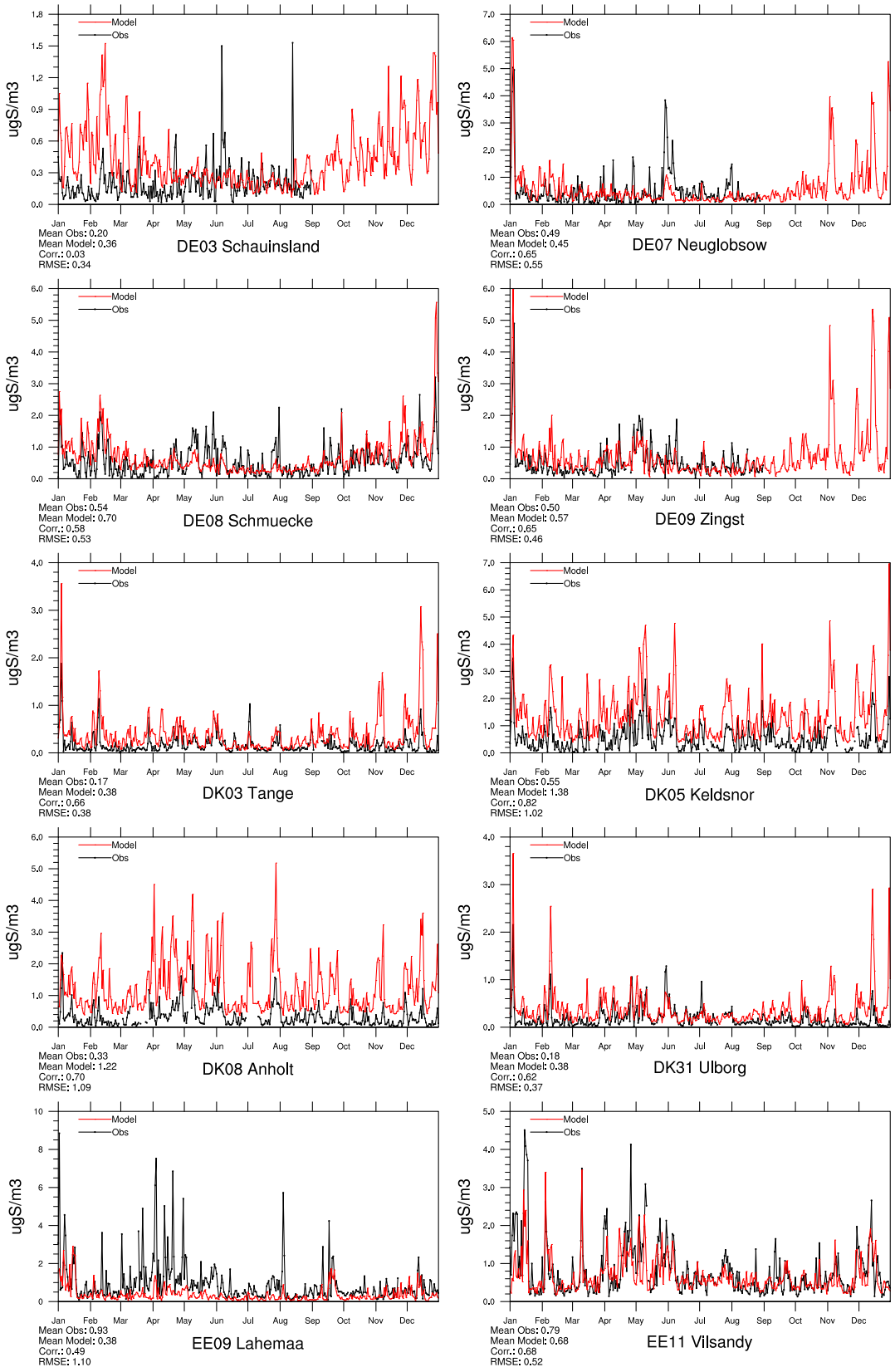

Figure 1.5: Comparison of model results and measurements (daily) for SO_2 in air (ugS) for stations that have measured SO_2 in 2008.

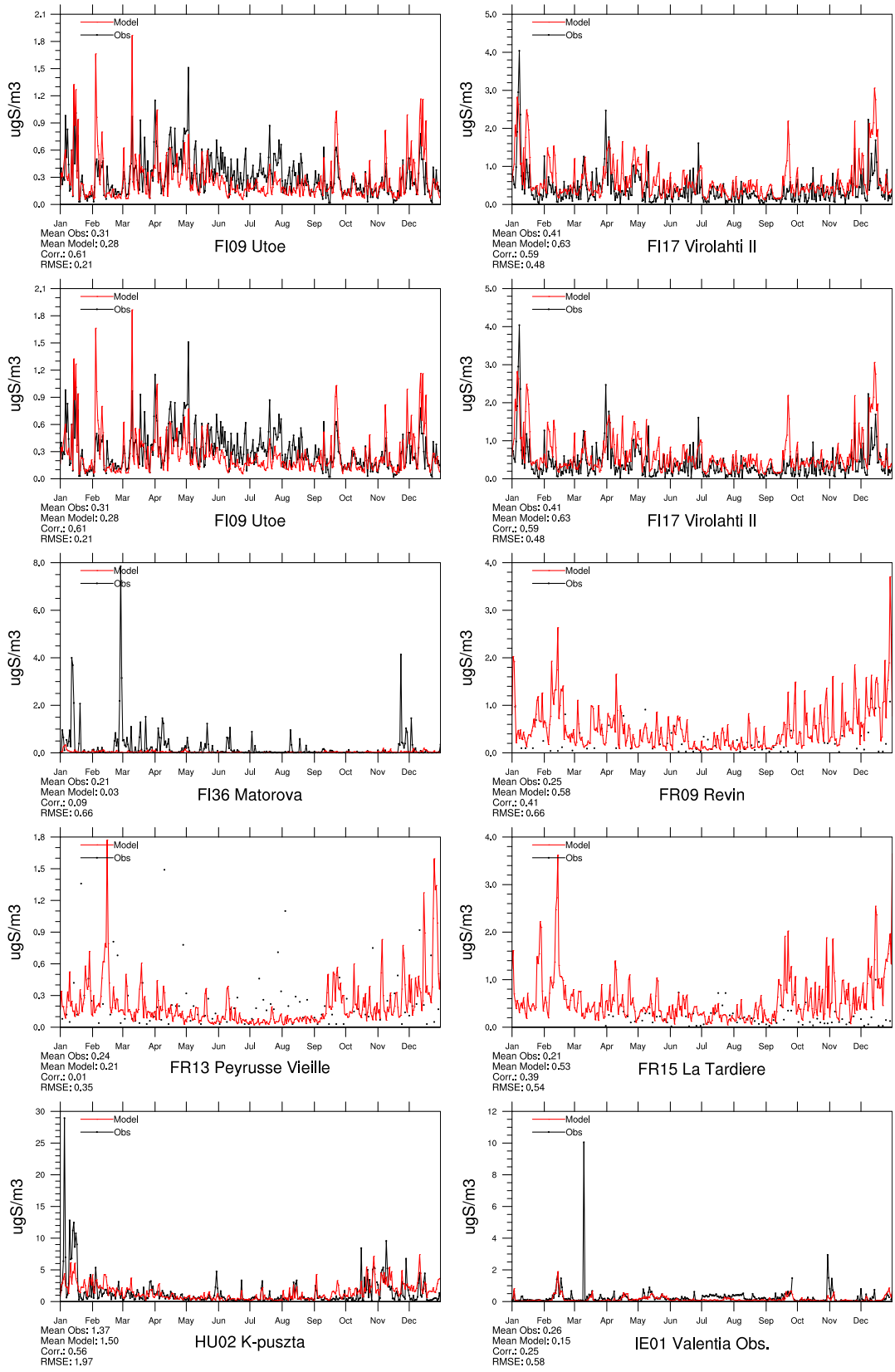

Figure 1.6: Comparison of model results and measurements (daily) for SO_2 in air (ugS) for stations that have measured SO_2 in 2008.

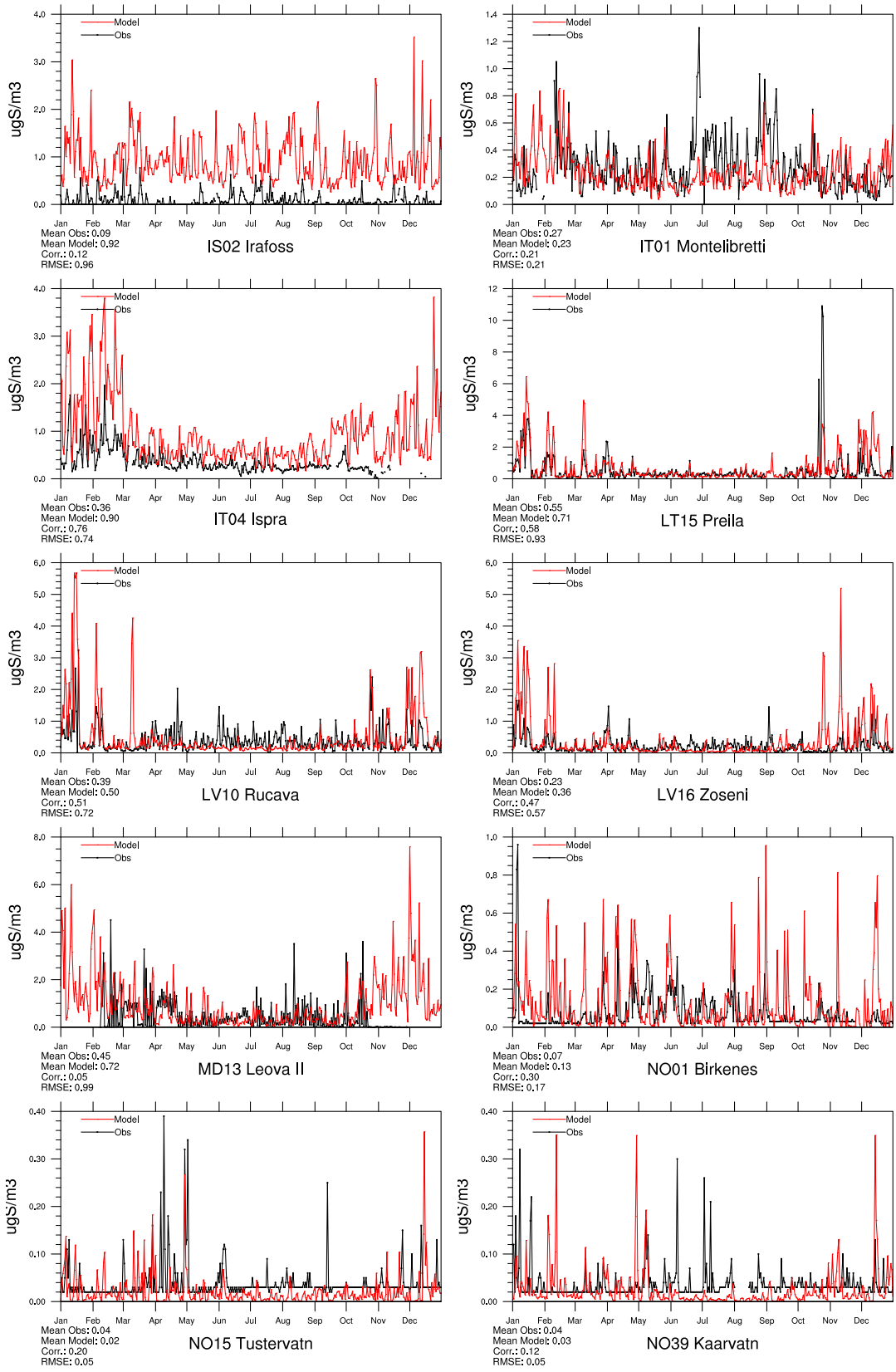

Figure 1.7: Comparison of model results and measurements (daily) for SO_2 in air (ugS) for stations that have measured SO_2 in 2008.

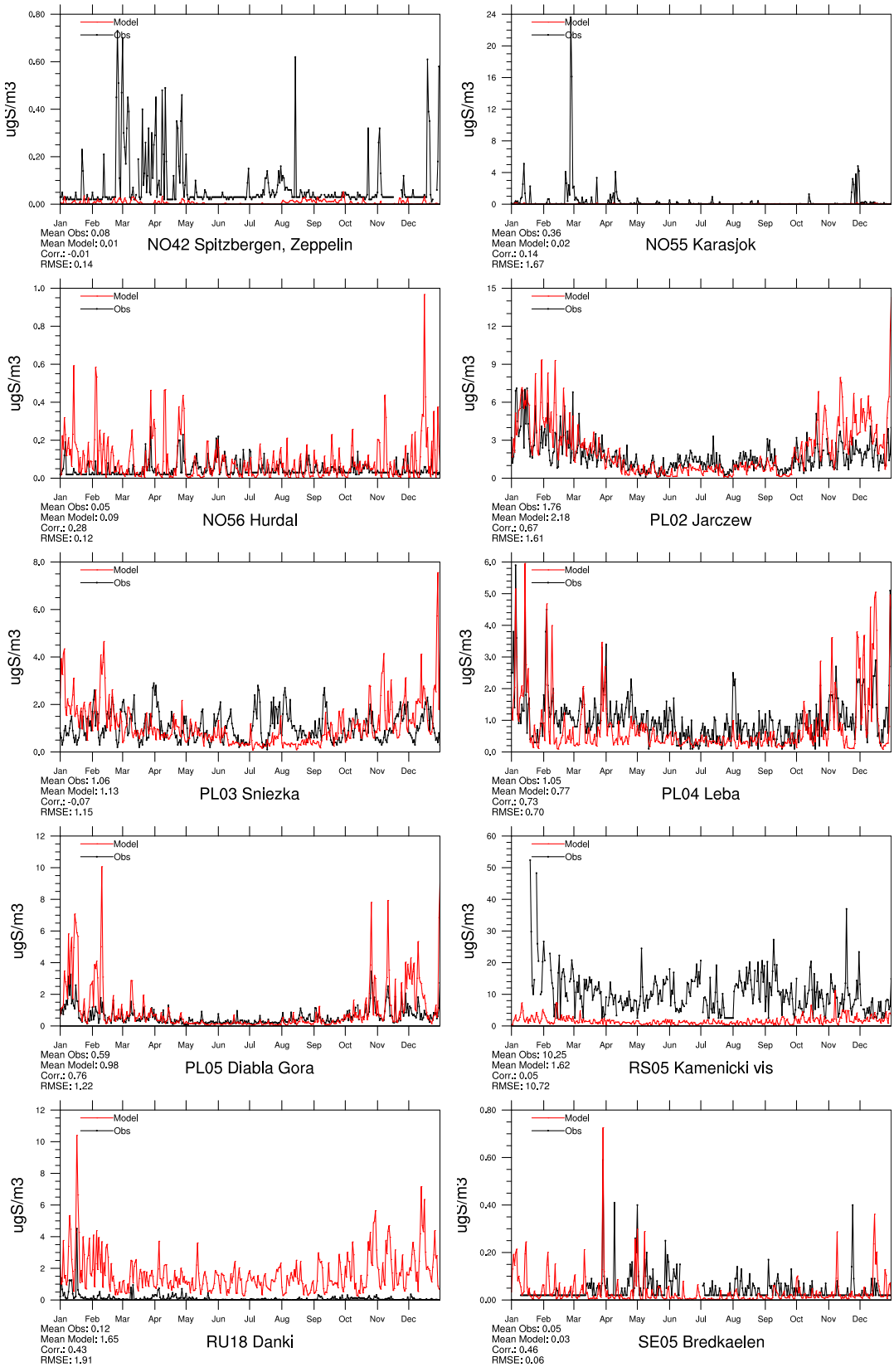

Figure 1.8: Comparison of model results and measurements (daily) for SO_2 in air (ugS) for stations that have measured SO_2 in 2008.

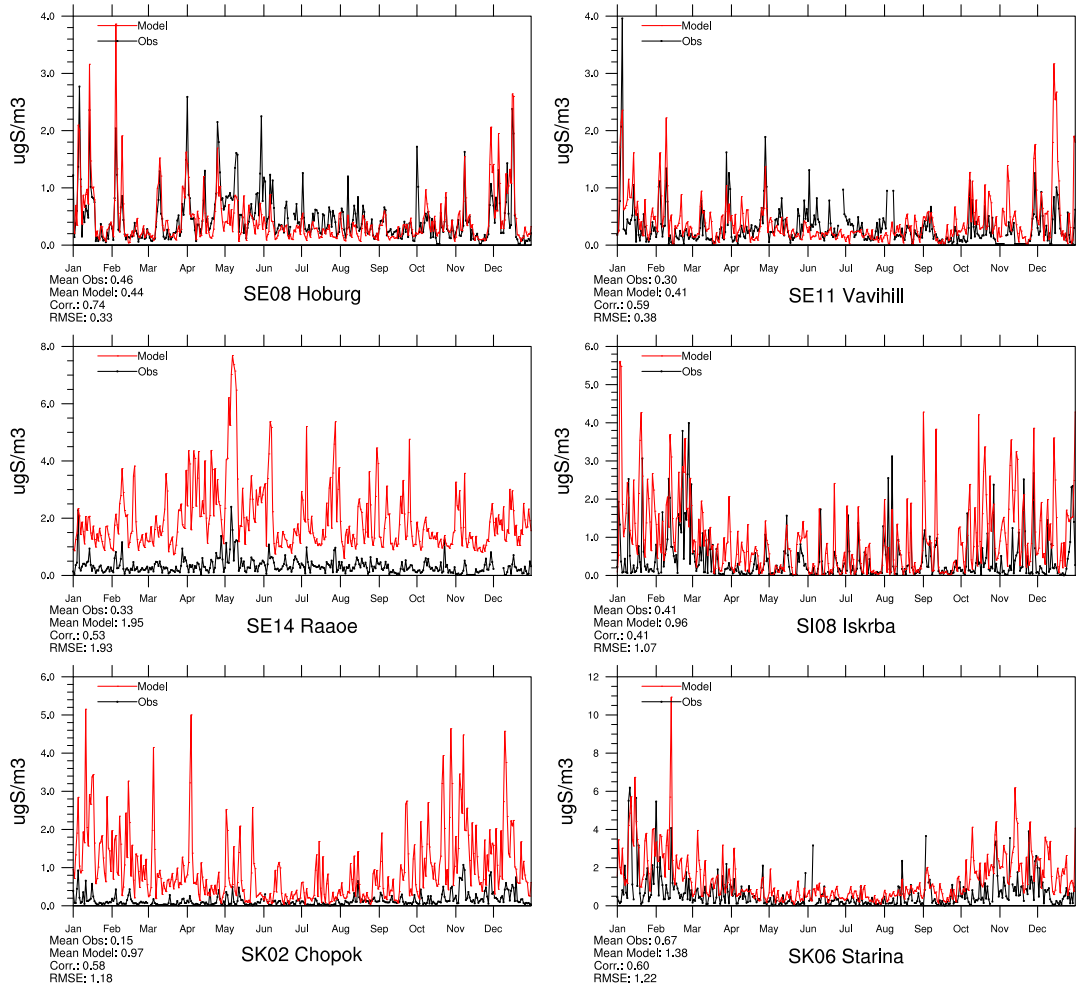

Figure 1.9: Comparison of model results and measurements (daily) for SO_2 in air (ugS) for stations that have measured SO_2 in 2008.

Sulphate in air

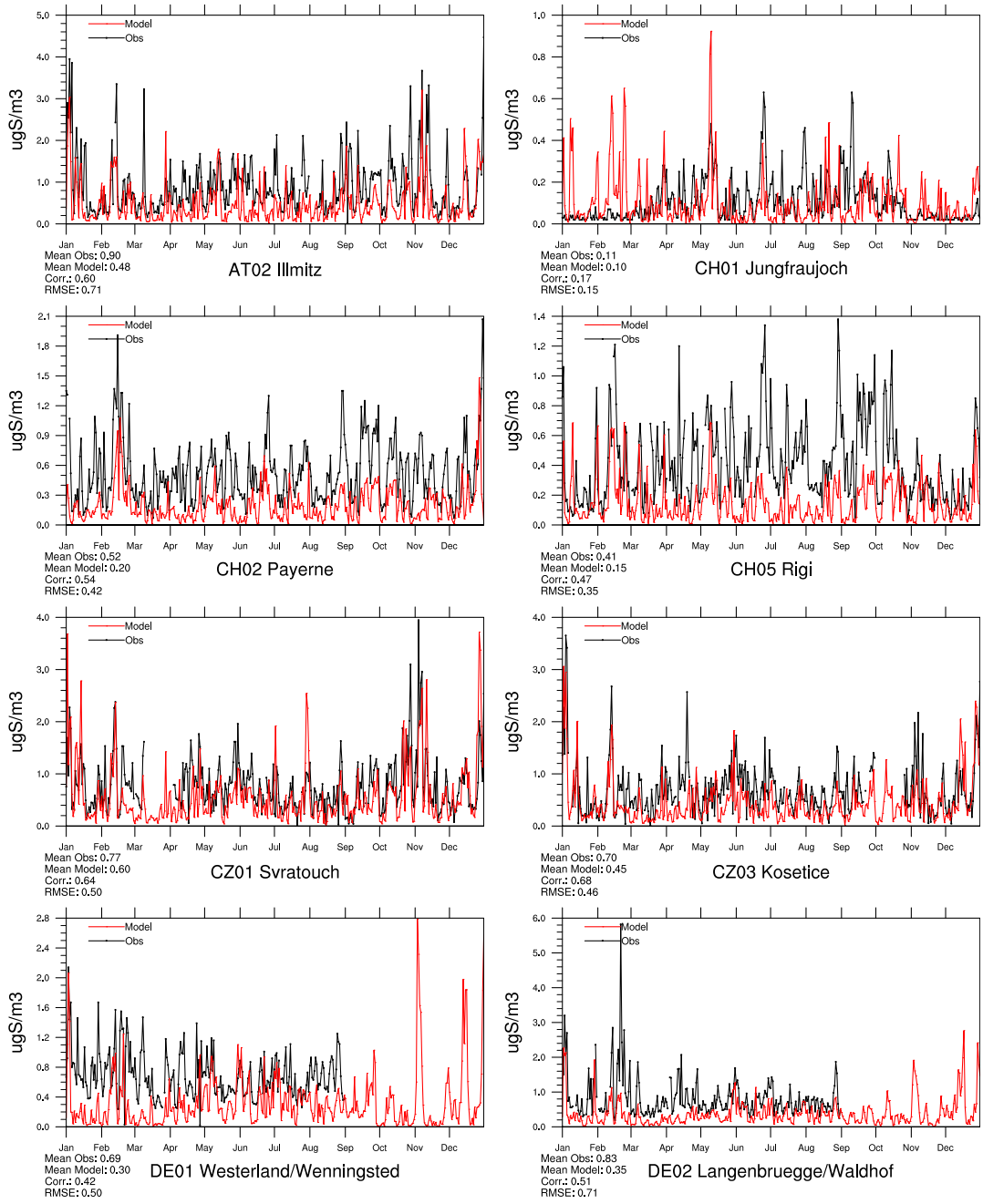

Figure 1.10: Comparison of model results and measurements (daily) for sulphate in air (ugS) for stations that have measured sulphate in 2008.

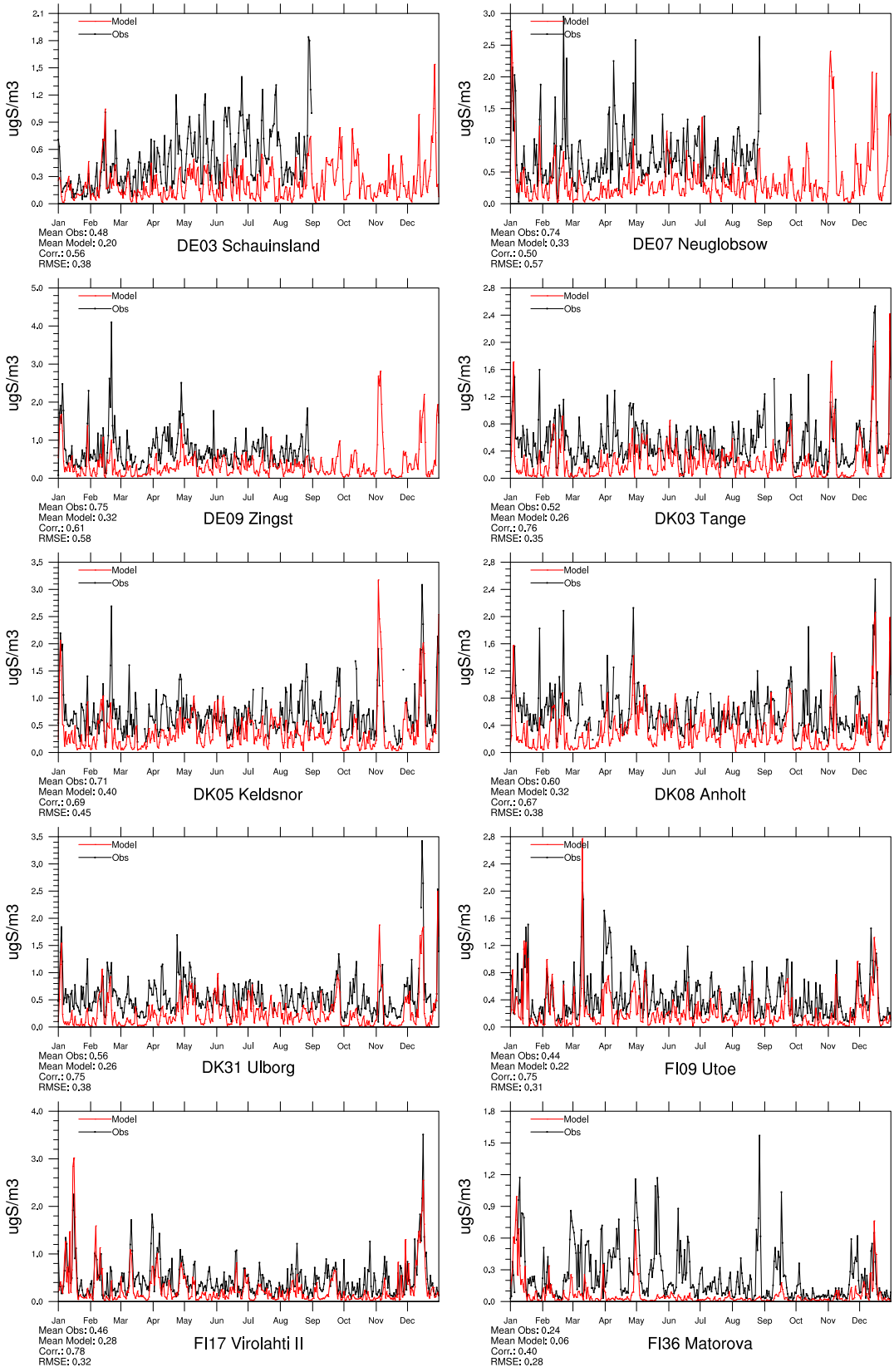

Figure 1.11: Comparison of model results and measurements (daily) for sulphate in air (ugS) for stations that have measured sulphate in 2008.

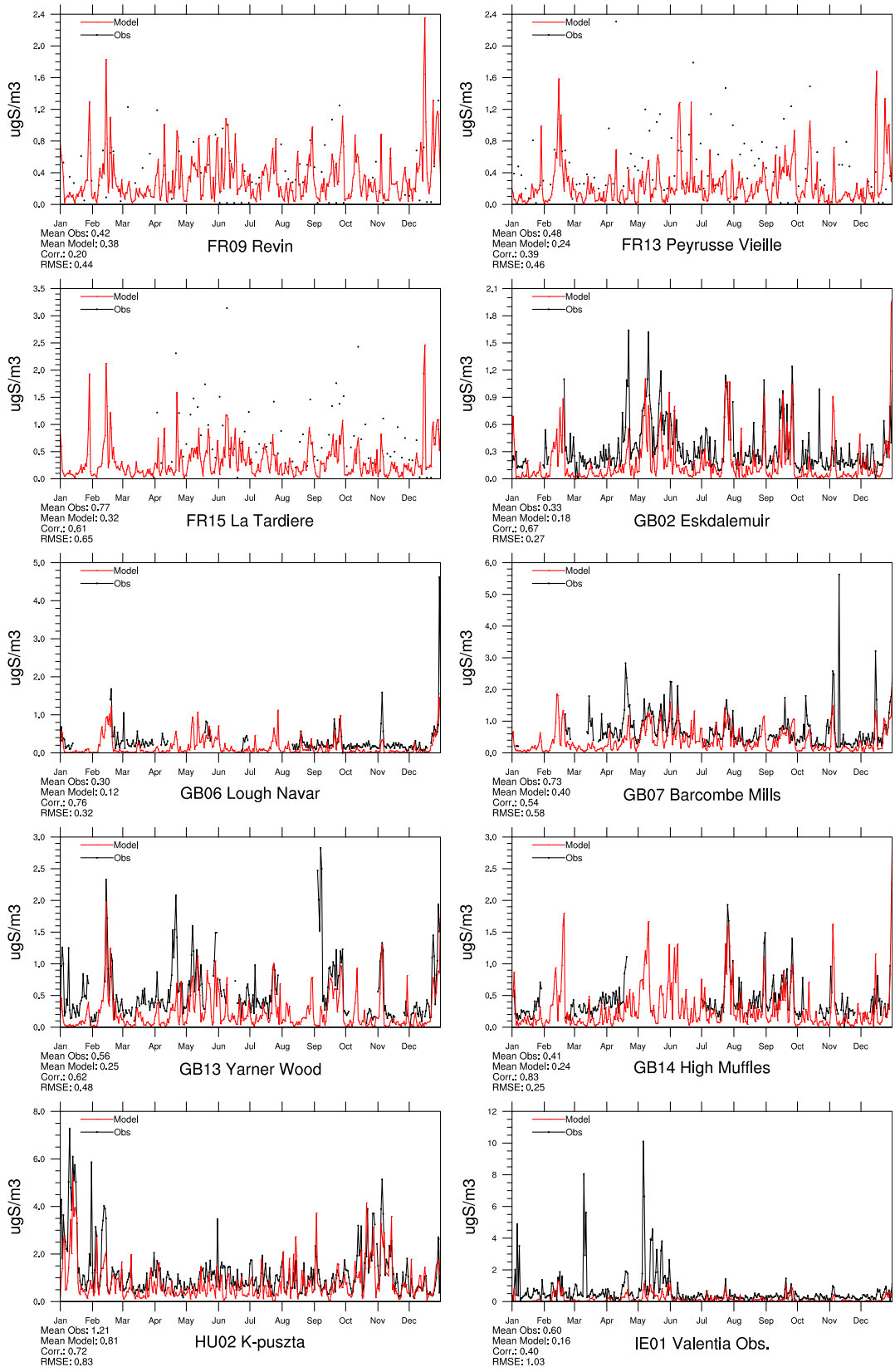

Figure 1.12: Comparison of model results and measurements (daily) for sulphate in air (ugS) for stations that have measured sulphate in 2008.

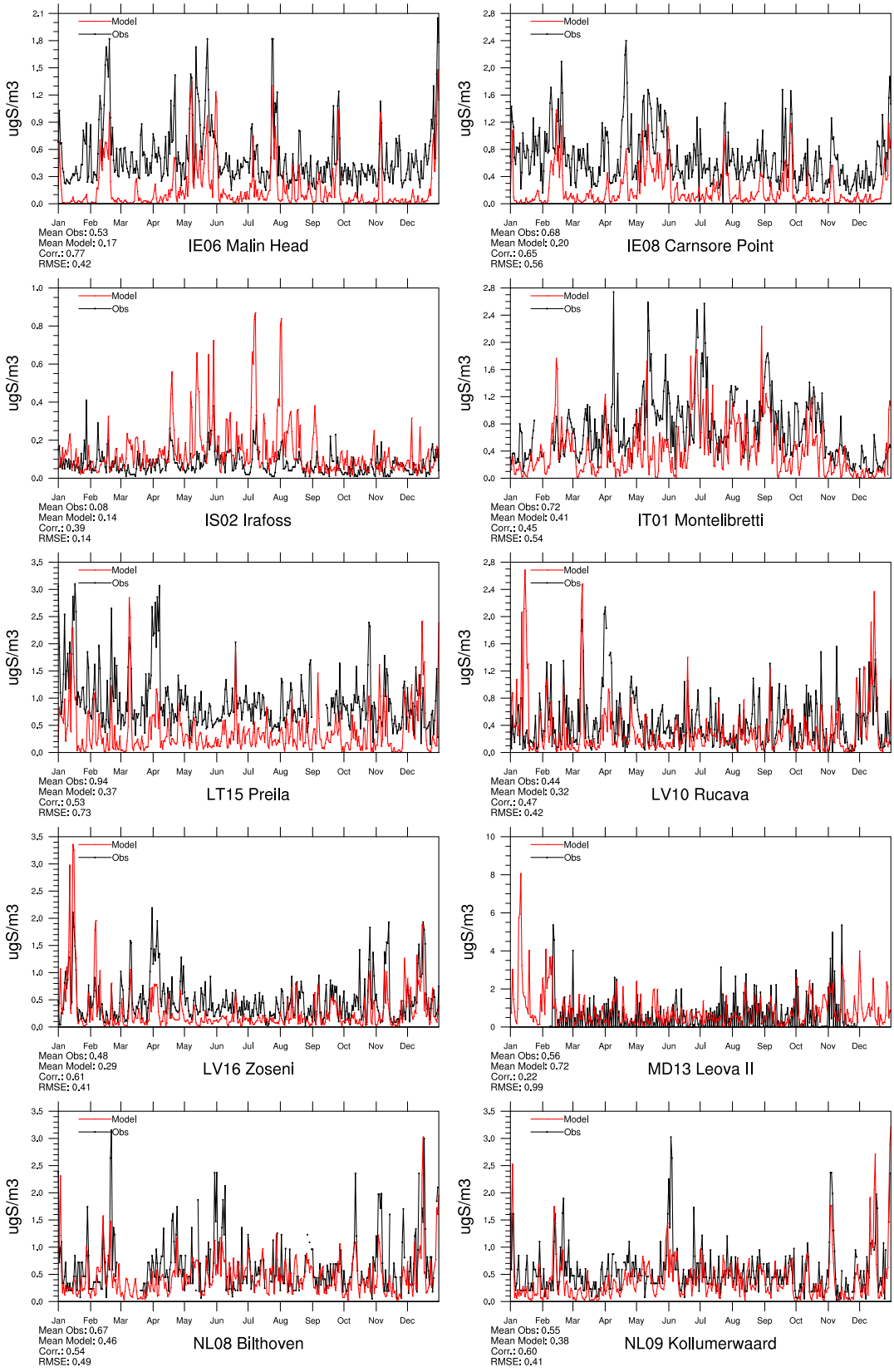

Figure 1.13: Comparison of model results and measurements (daily) for sulphate in air (ugS) for stations that have measured sulphate in 2008.

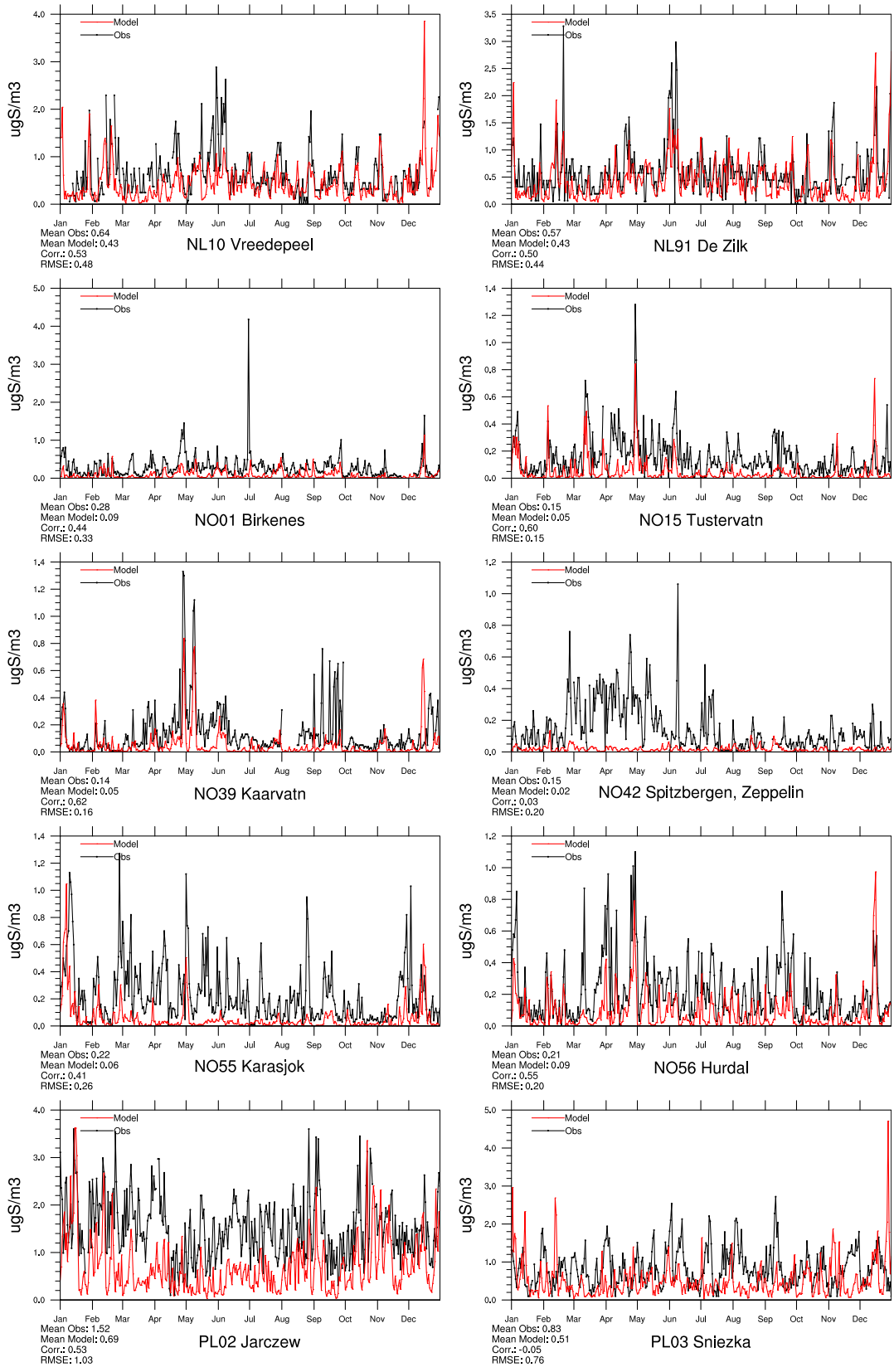

Figure 1.14: Comparison of model results and measurements (daily) for sulphate in air (ugS) for stations that have measured sulphate in 2008.

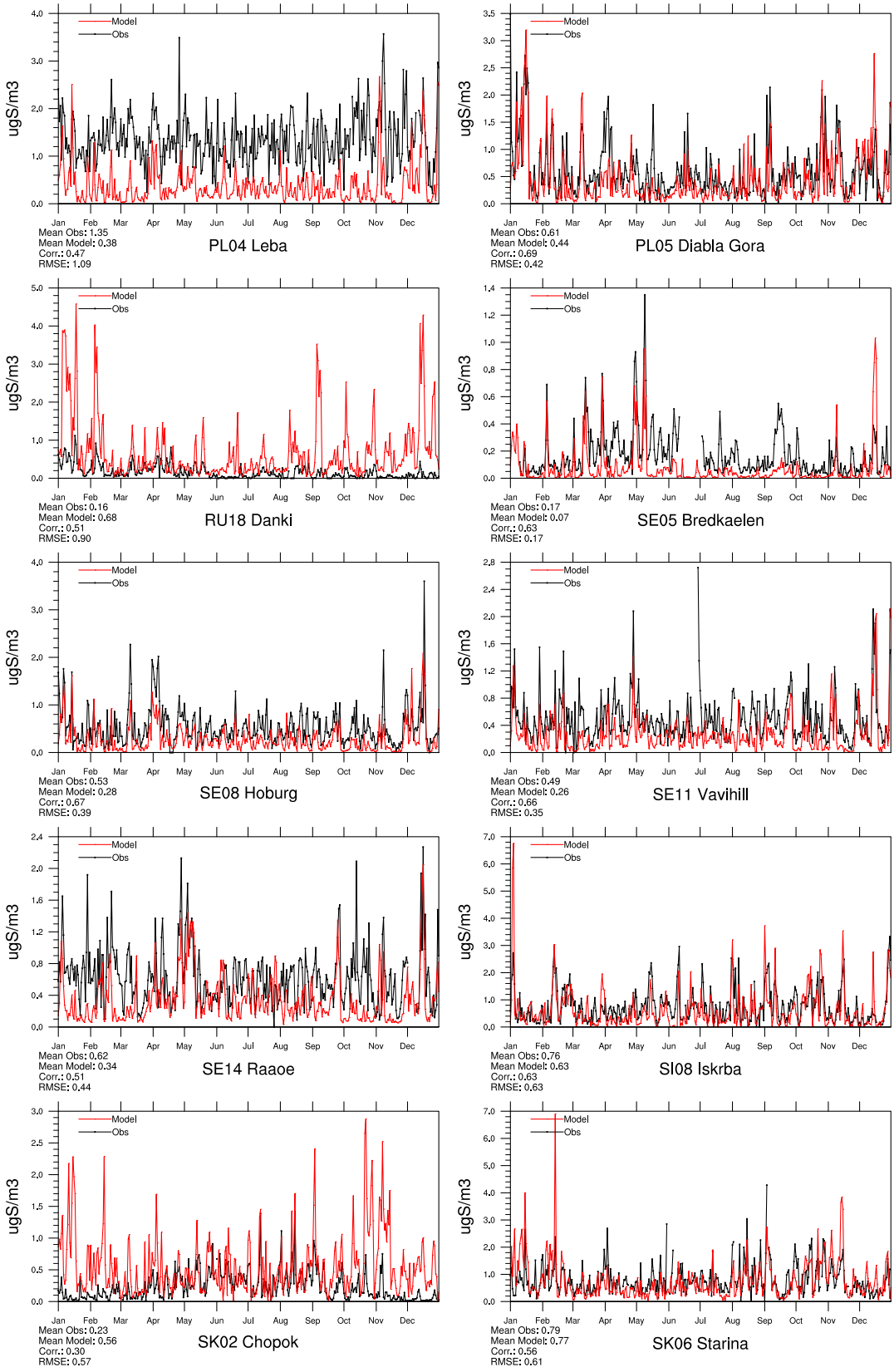

Figure 1.15: Comparison of model results and measurements (daily) for sulphate in air (ugS) for stations that have measured sulphate in 2008.

Total nitrate in air

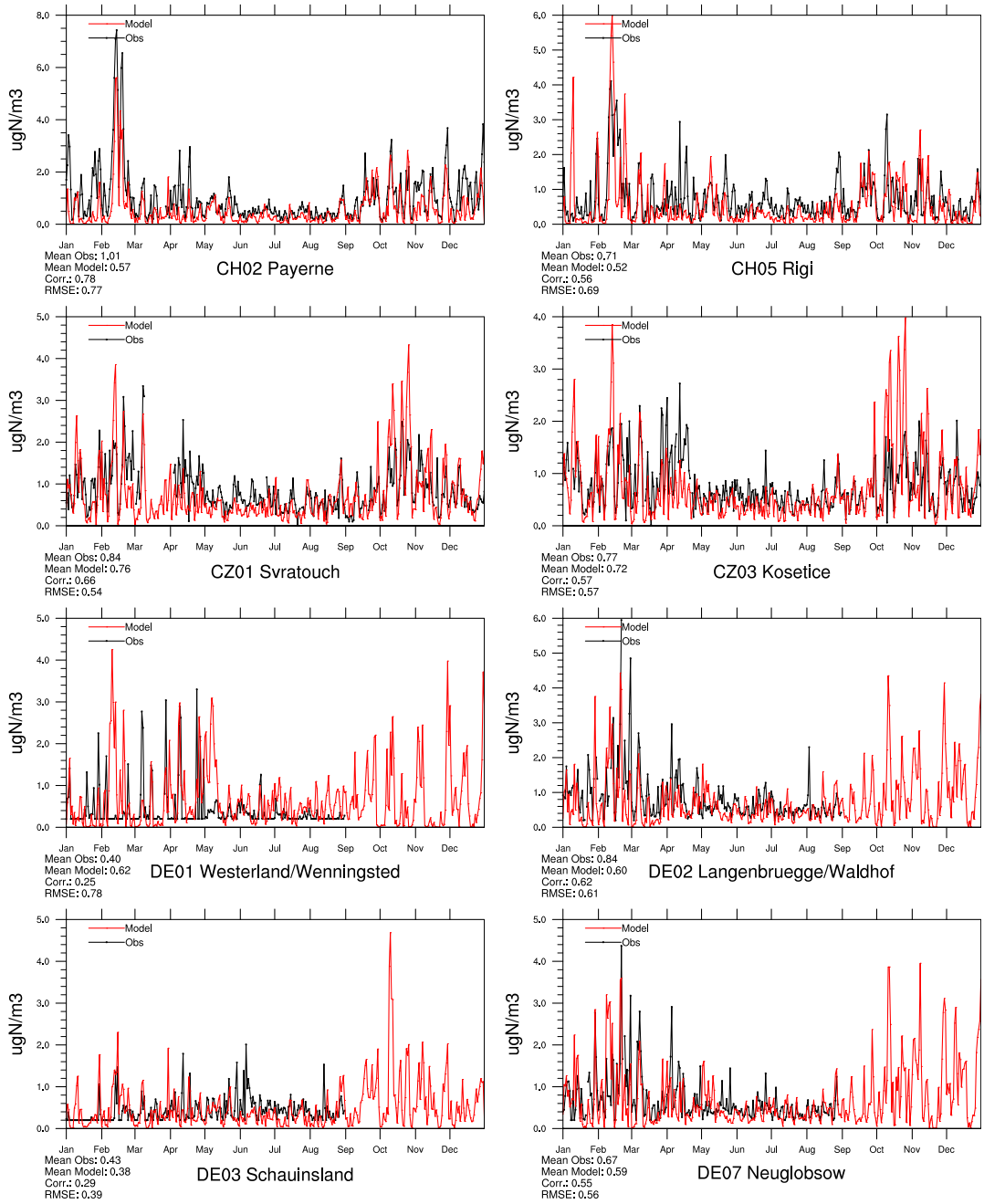

Figure 1.16: Comparison of model results and measurements (daily) total nitrate concentrations (μg(N) m^{-3}) for stations that have measured total nitrate in 2008.

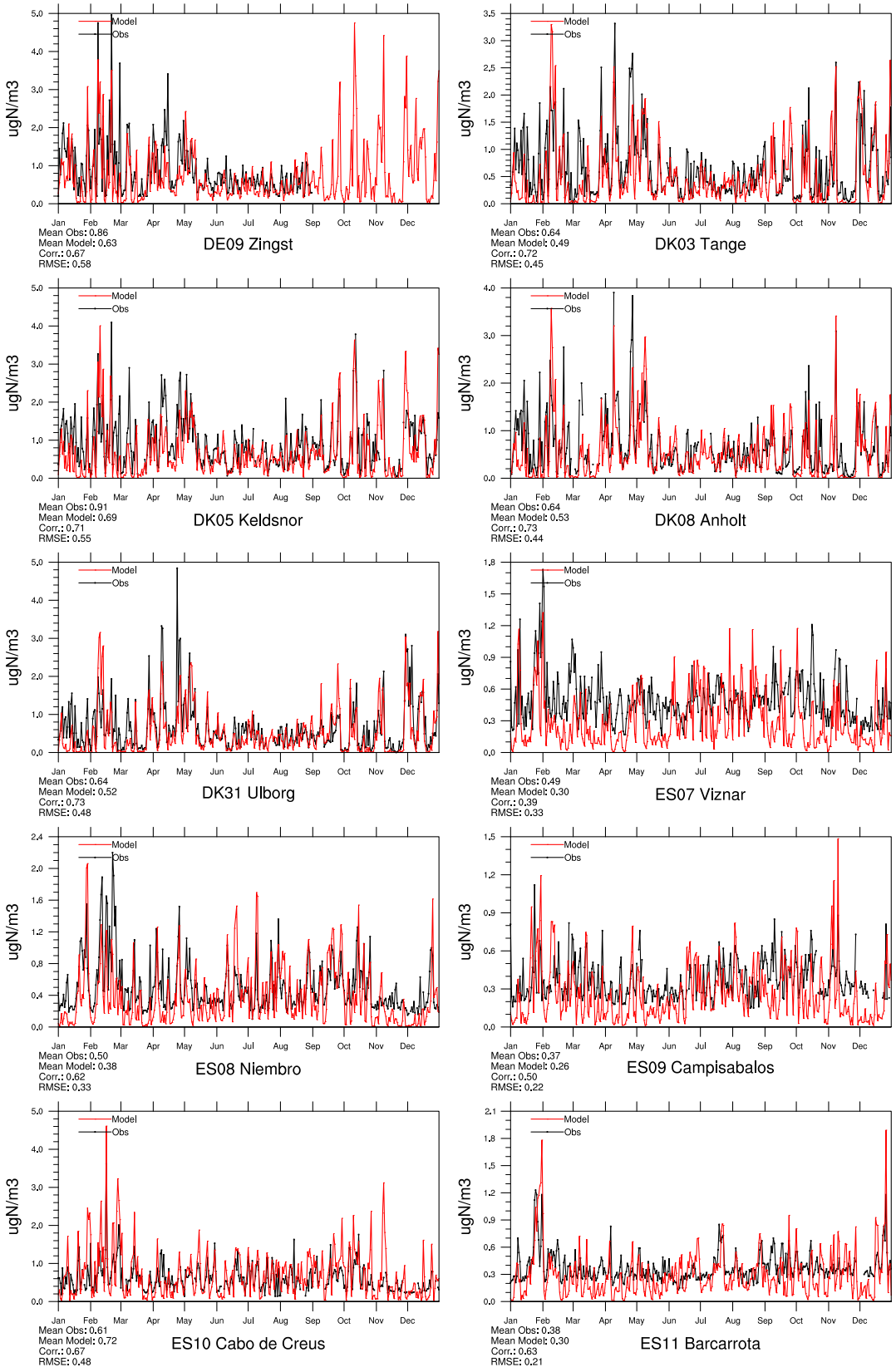

Figure 1.17: Comparison of model results and measurements (daily) total nitrate concentrations (μg(N) m^{-3}) for stations that have measured total nitrate in 2008.

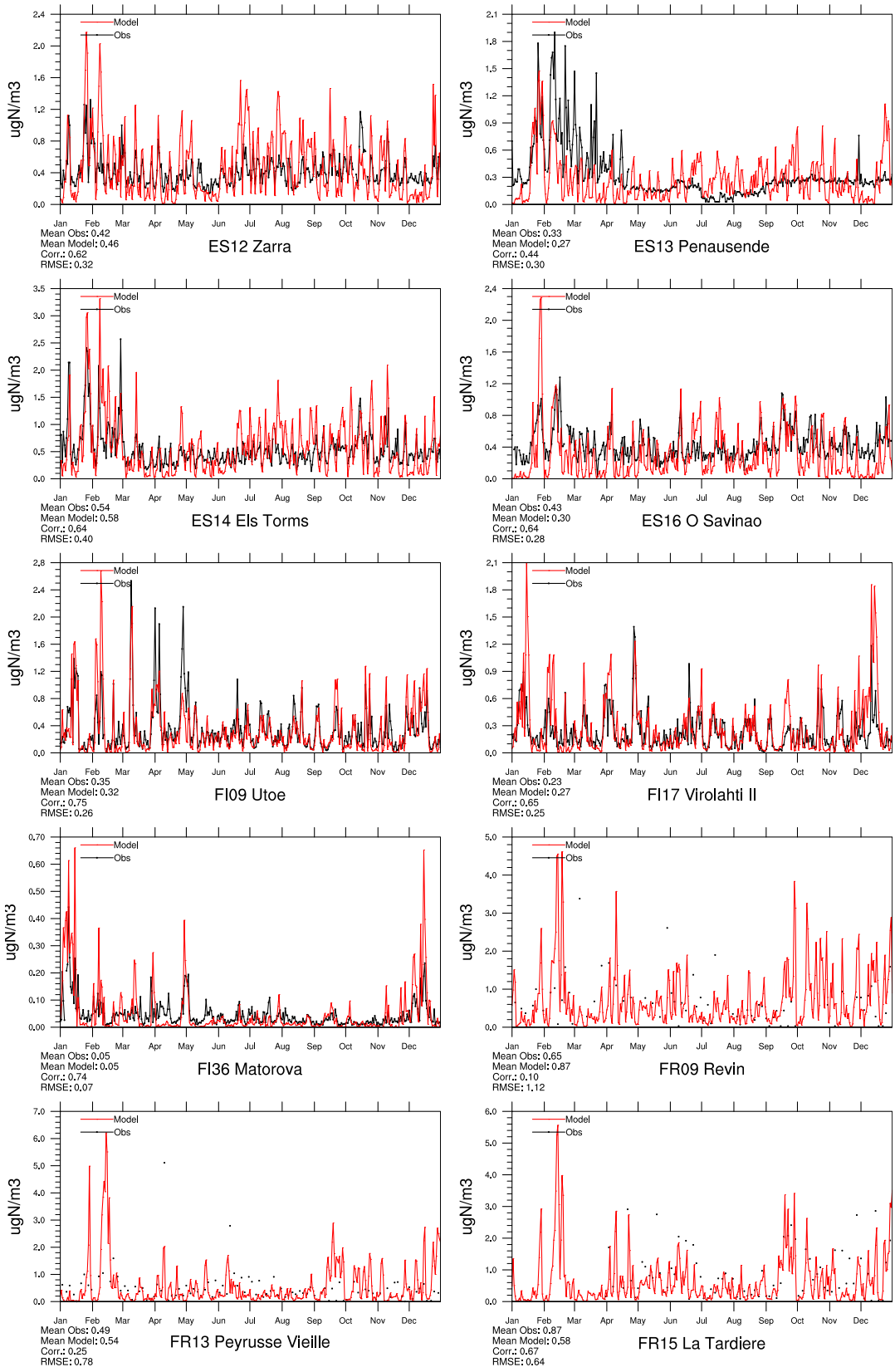

Figure 1.18: Comparison of model results and measurements (daily) total nitrate concentrations (μg(N) m^{-3}) for stations that have measured total nitrate in 2008.

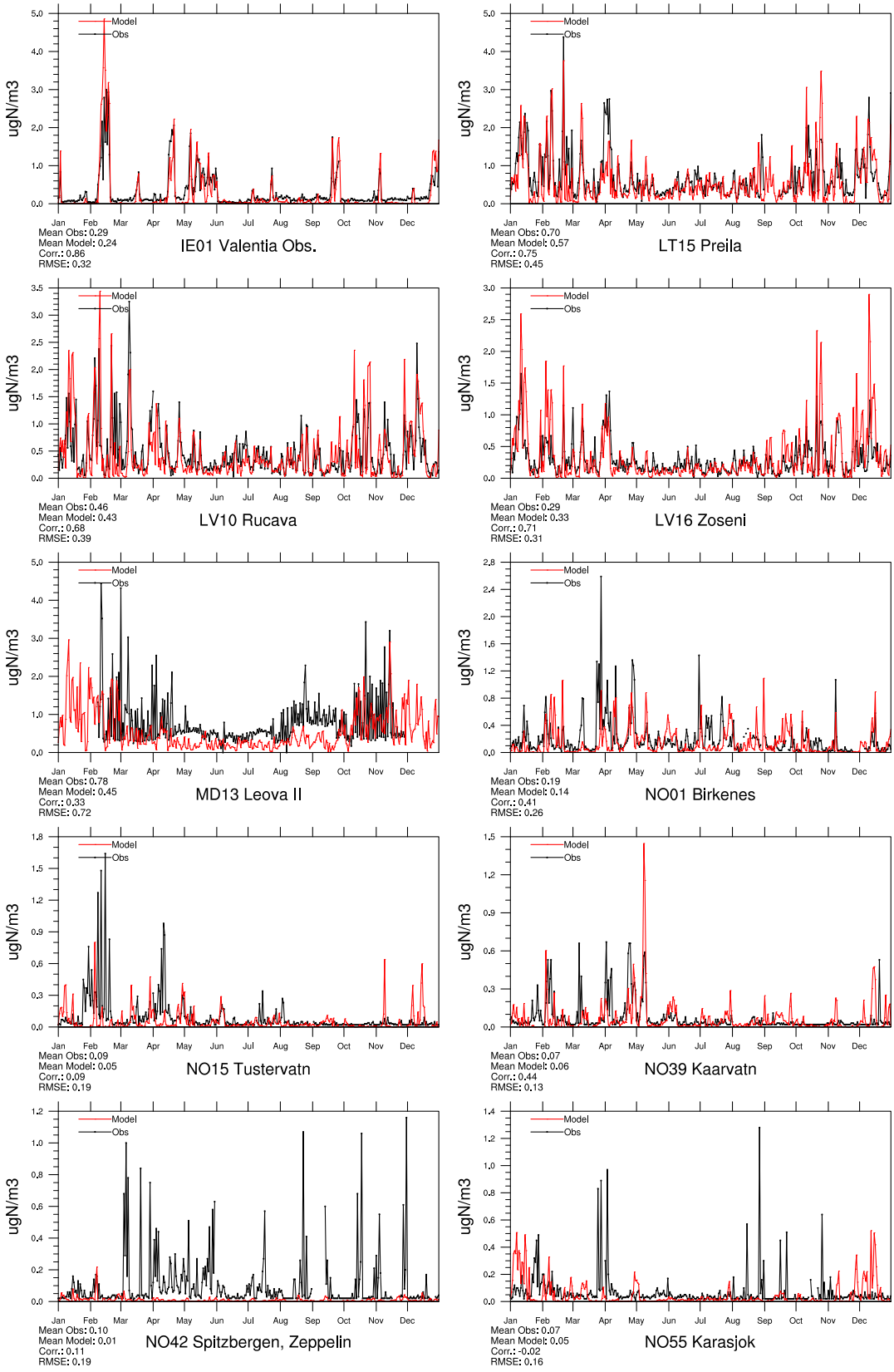

Figure 1.19: Comparison of model results and measurements (daily) total nitrate concentrations (μg(N) m^{-3}) for stations that have measured total nitrate in 2008.

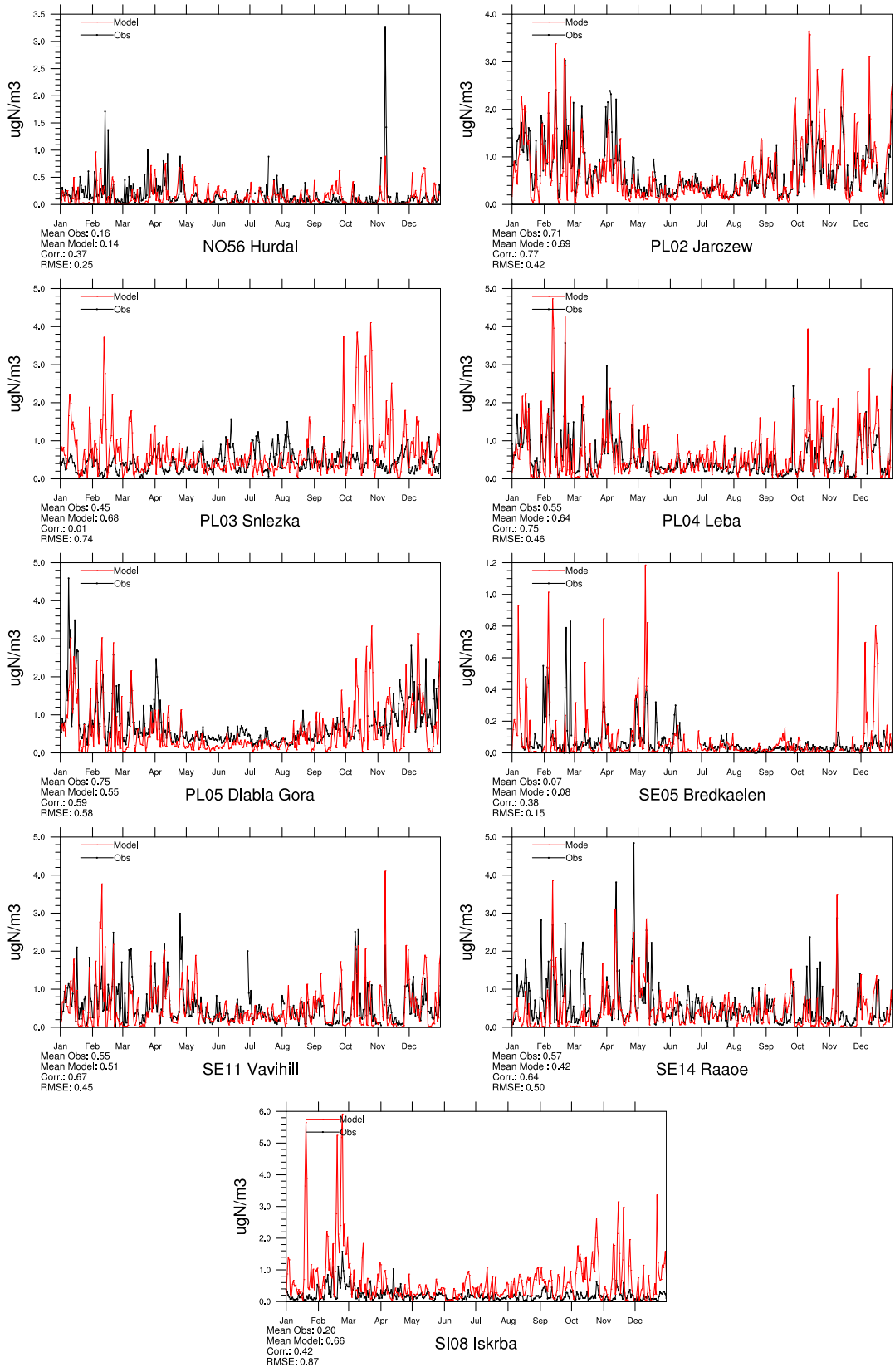

Figure 1.20: Comparison of model results and measurements (daily) total nitrate concentrations (μg(N) m^{-3}) for stations that have measured total nitrate in 2008.

Ammonia+ammonium in air

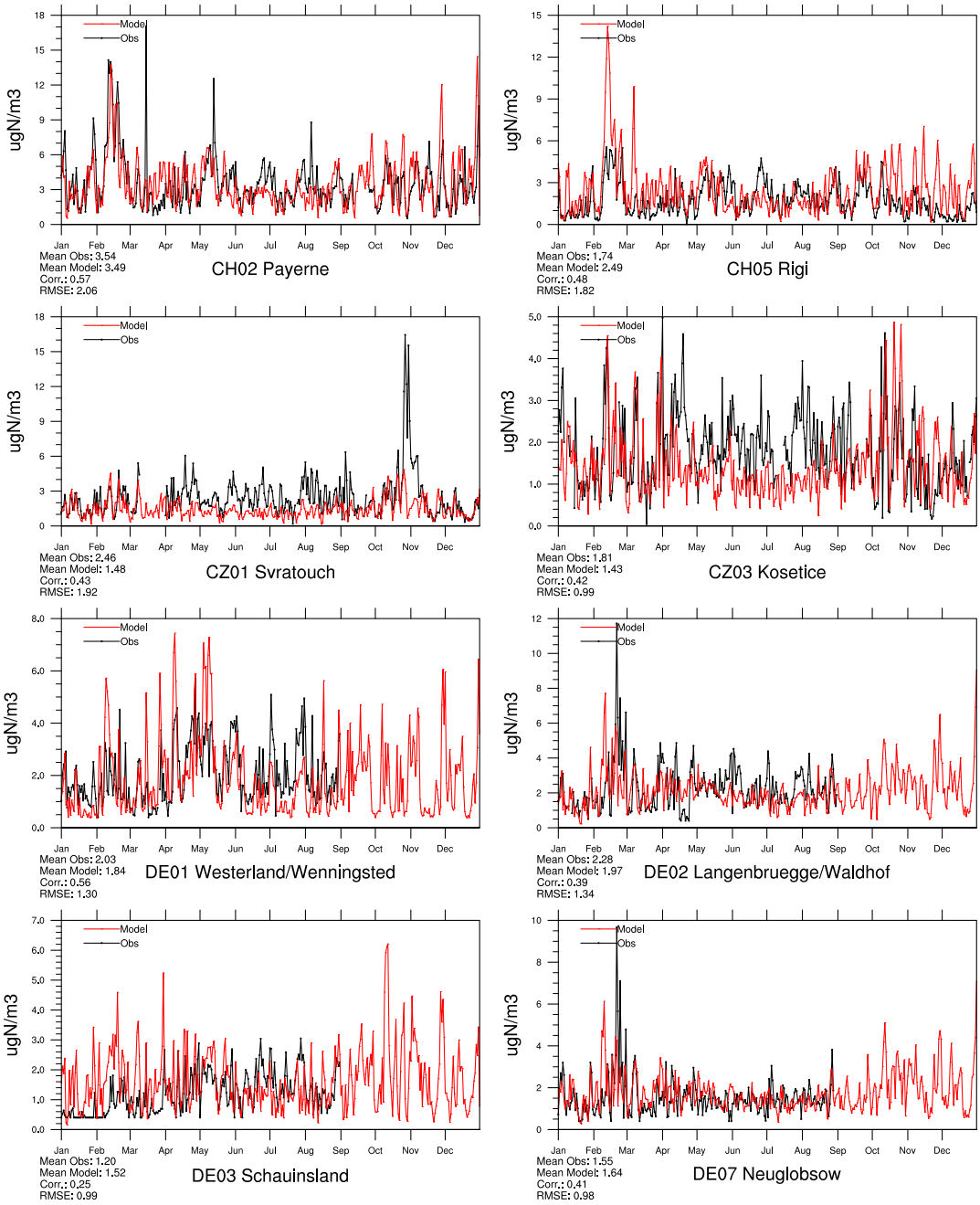

Figure 1.21: Comparison of model results and measurements (daily) total ammonium+ammonia concentrations (μg(N) m^{-3}) for stations that have measured total ammonium+ammo nia in 2008.

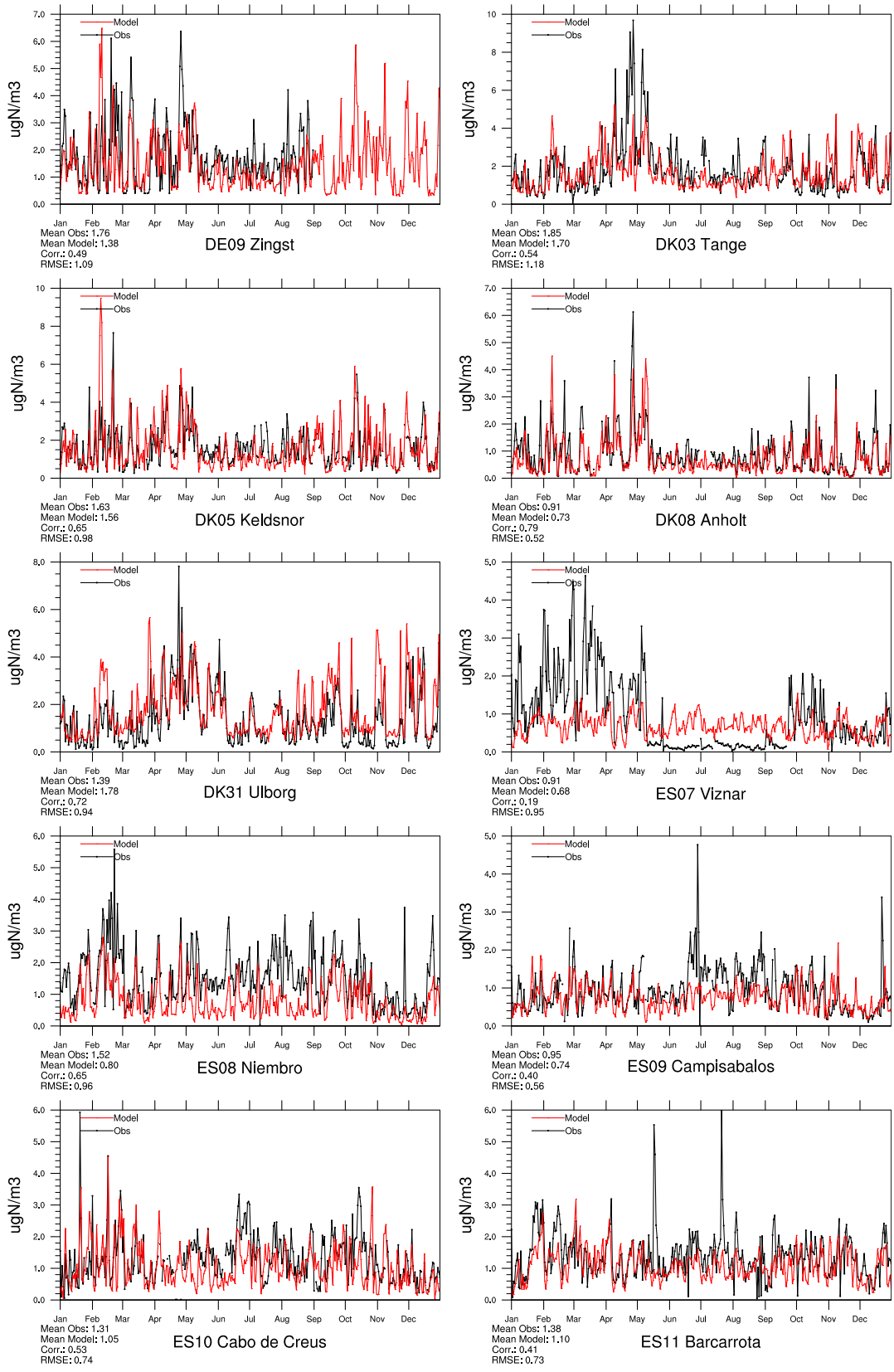

Figure 1.22: Comparison of model results and measurements (daily) total ammonium+ammonia concentrations (μg(N) m^{-3}) for stations that have measured total ammonium+ammo nia in 2008.

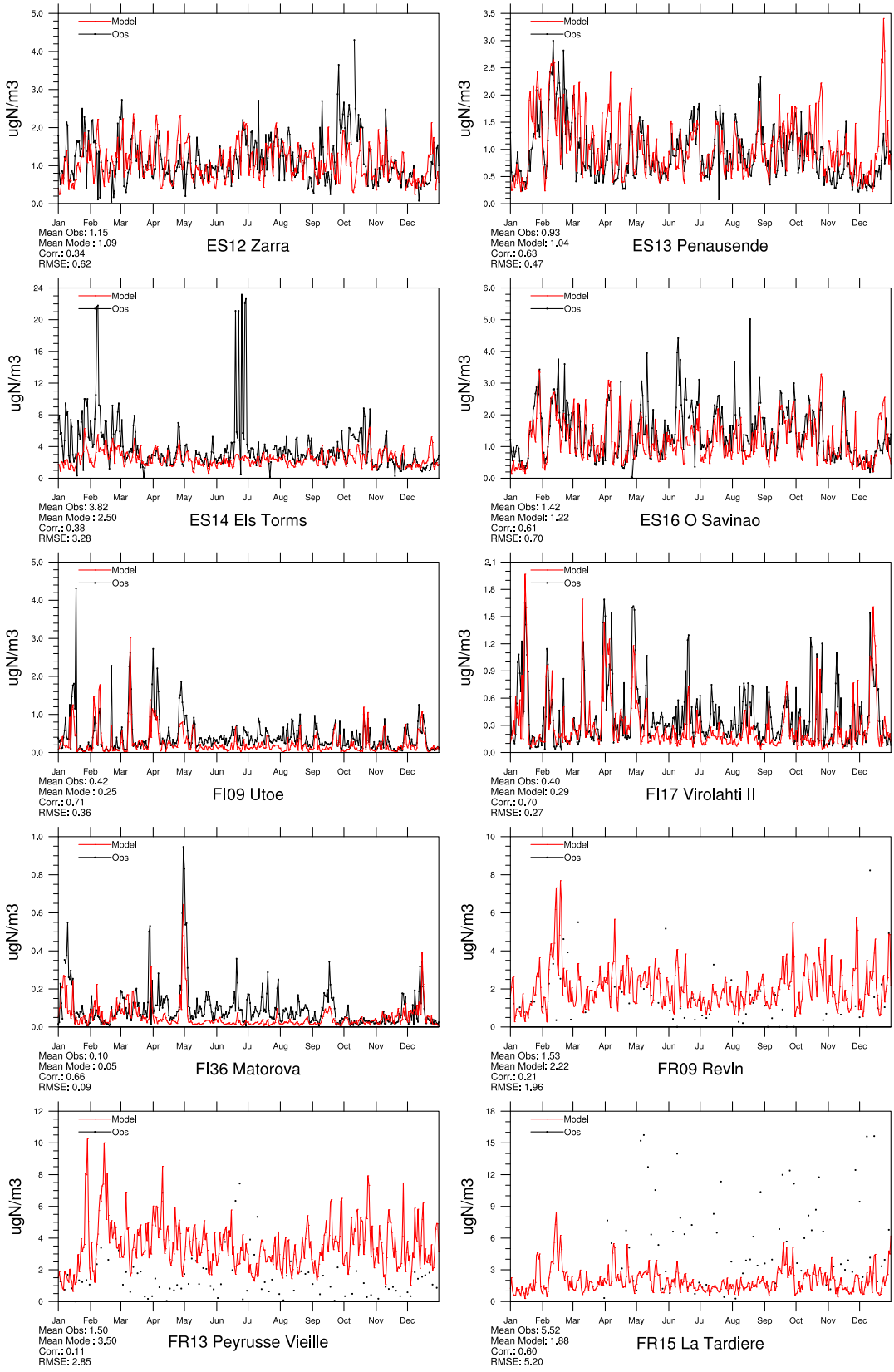

Figure 1.23: Comparison of model results and measurements (daily) total ammonium+ammonia concentrations (μg(N) m^{-3}) for stations that have measured total ammonium+ammo nia in 2008.

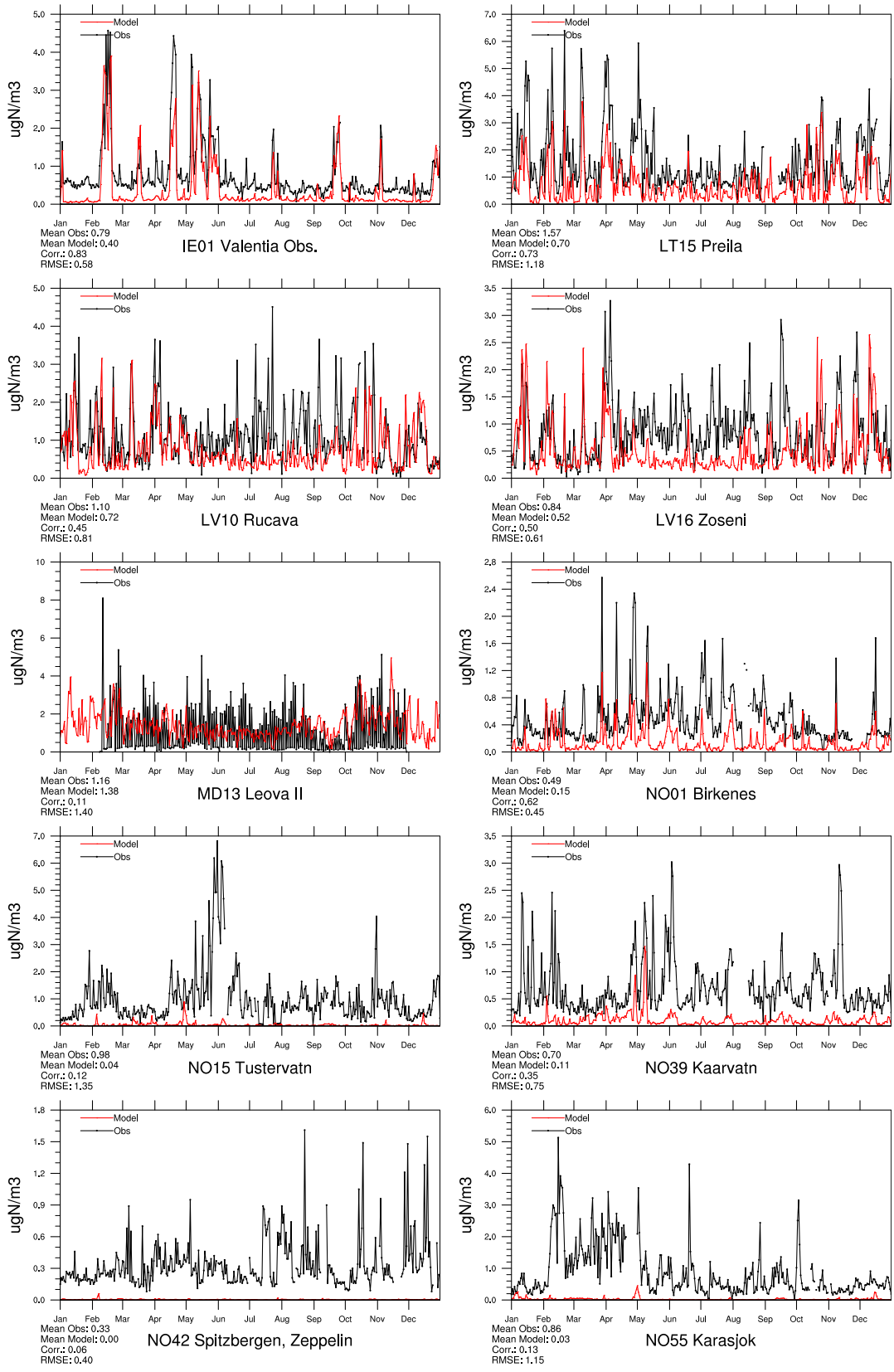

Figure 1.24: Comparison of model results and measurements (daily) total ammonium+ammonia concentrations (μg(N) m^{-3}) for stations that have measured total ammonium+ammo nia in 2008.

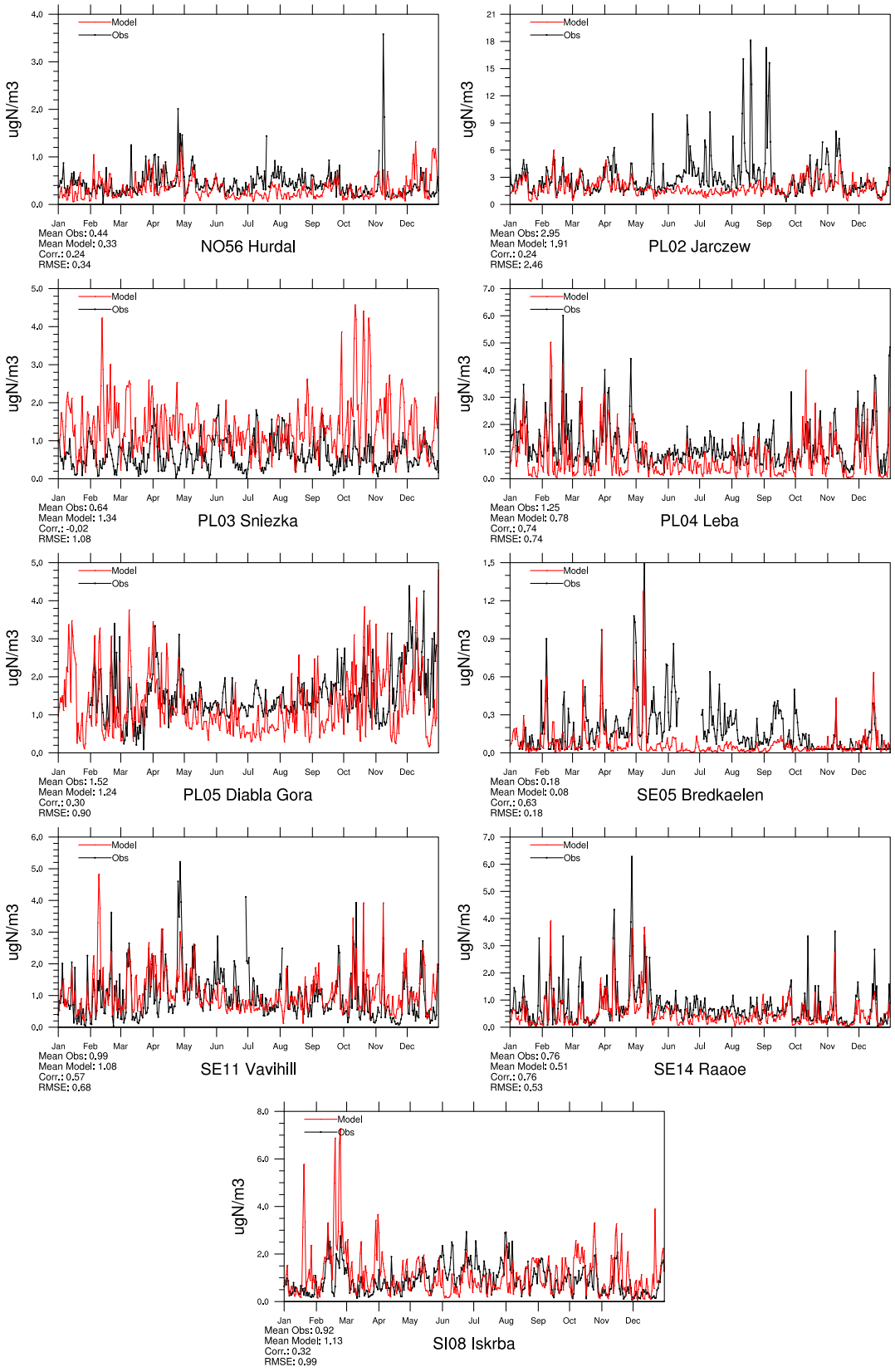

Figure 1.25: Comparison of model results and measurements (daily) total ammonium+ammonia concentrations (μg(N) m^{-3}) for stations that have measured total ammonium+ammo nia in 2008.

Sulphur in precipitation

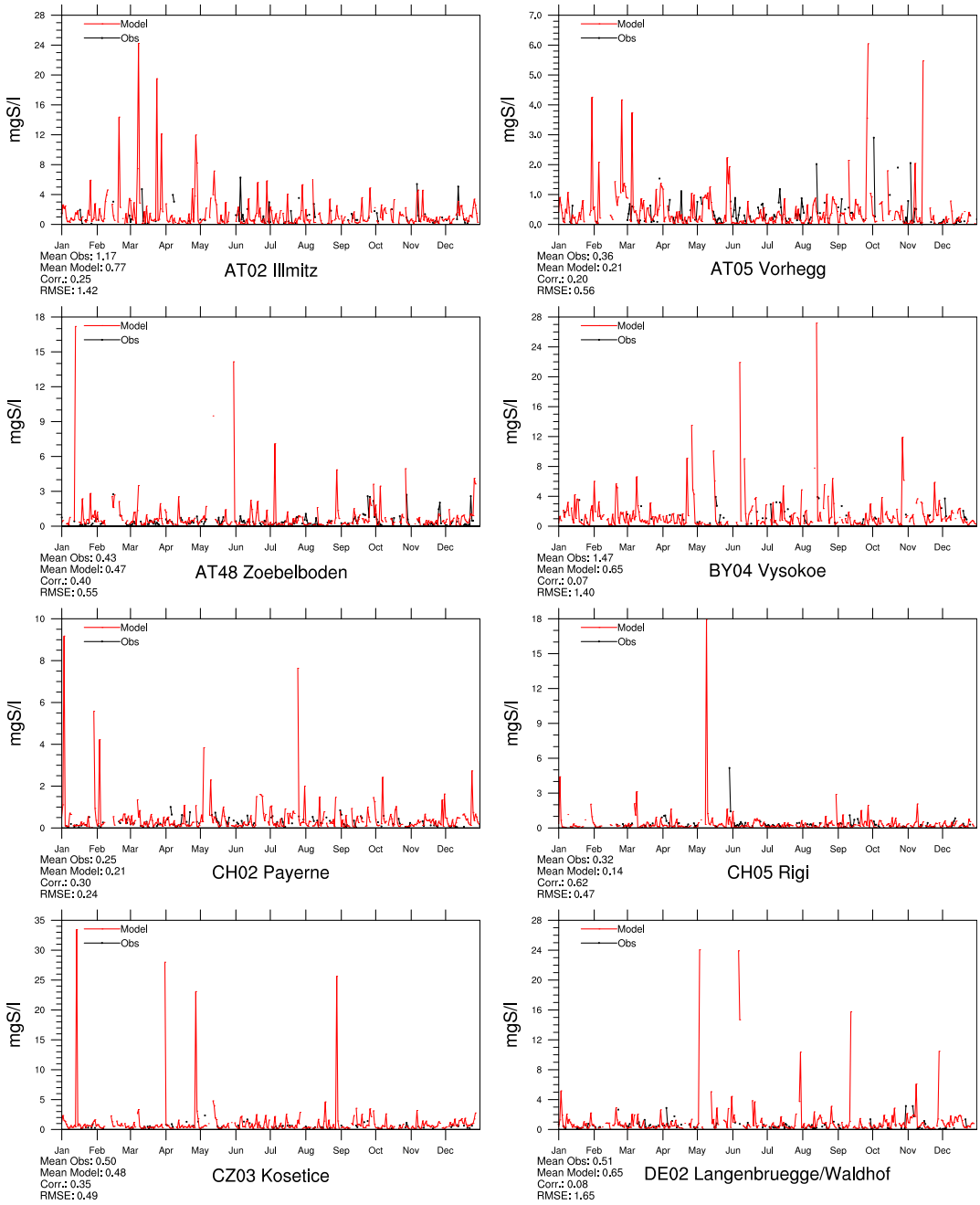

Figure 1.26: Comparison of model results and measurements (daily) for sulphur concentrations in precipitation (μg(S)l^{-1}) in 2008.

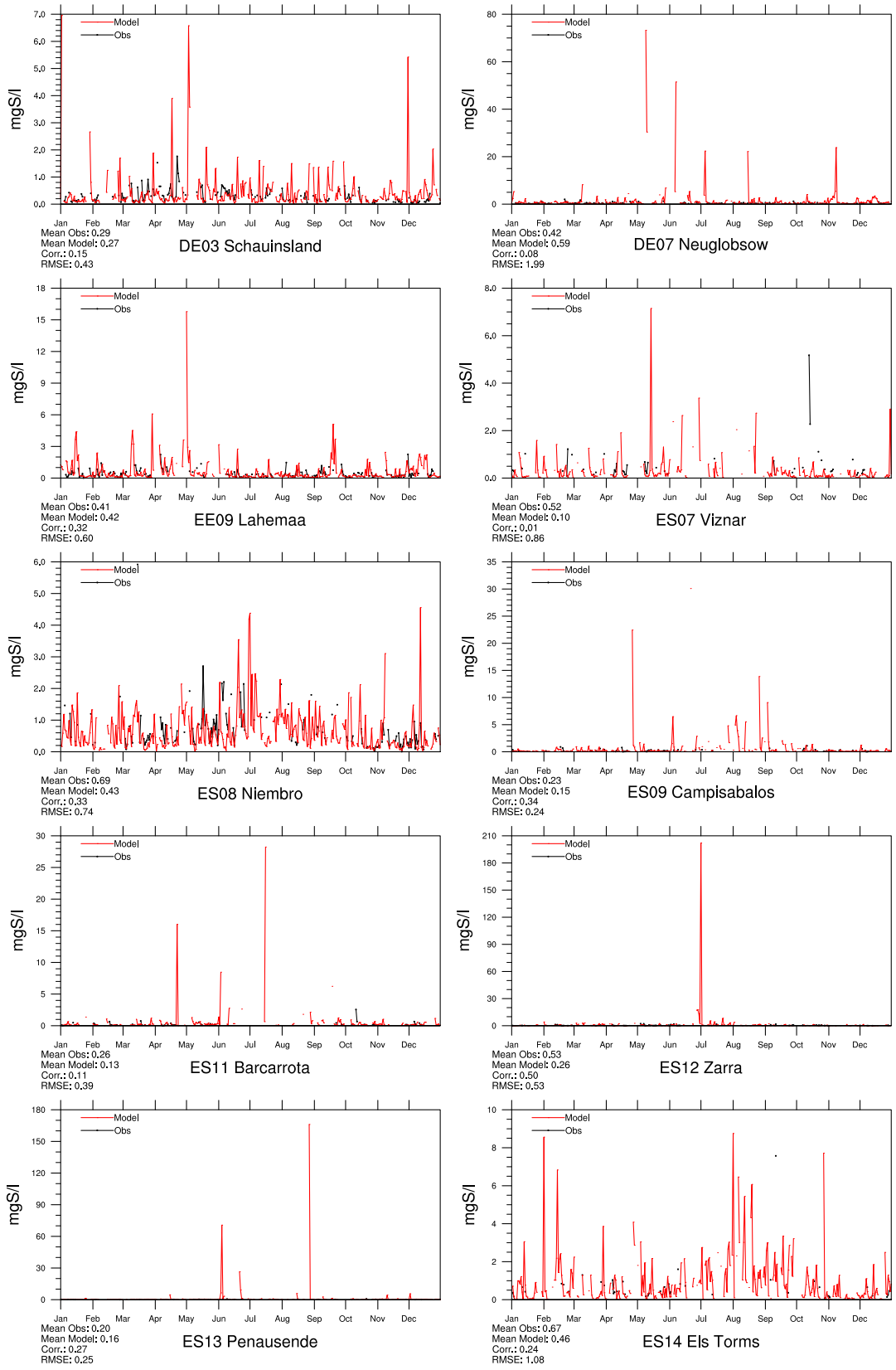

Figure 1.27: Comparison of model results and measurements (daily) for sulphur concentrations in precipitation (μg(S)l^{-1}) in 2008.

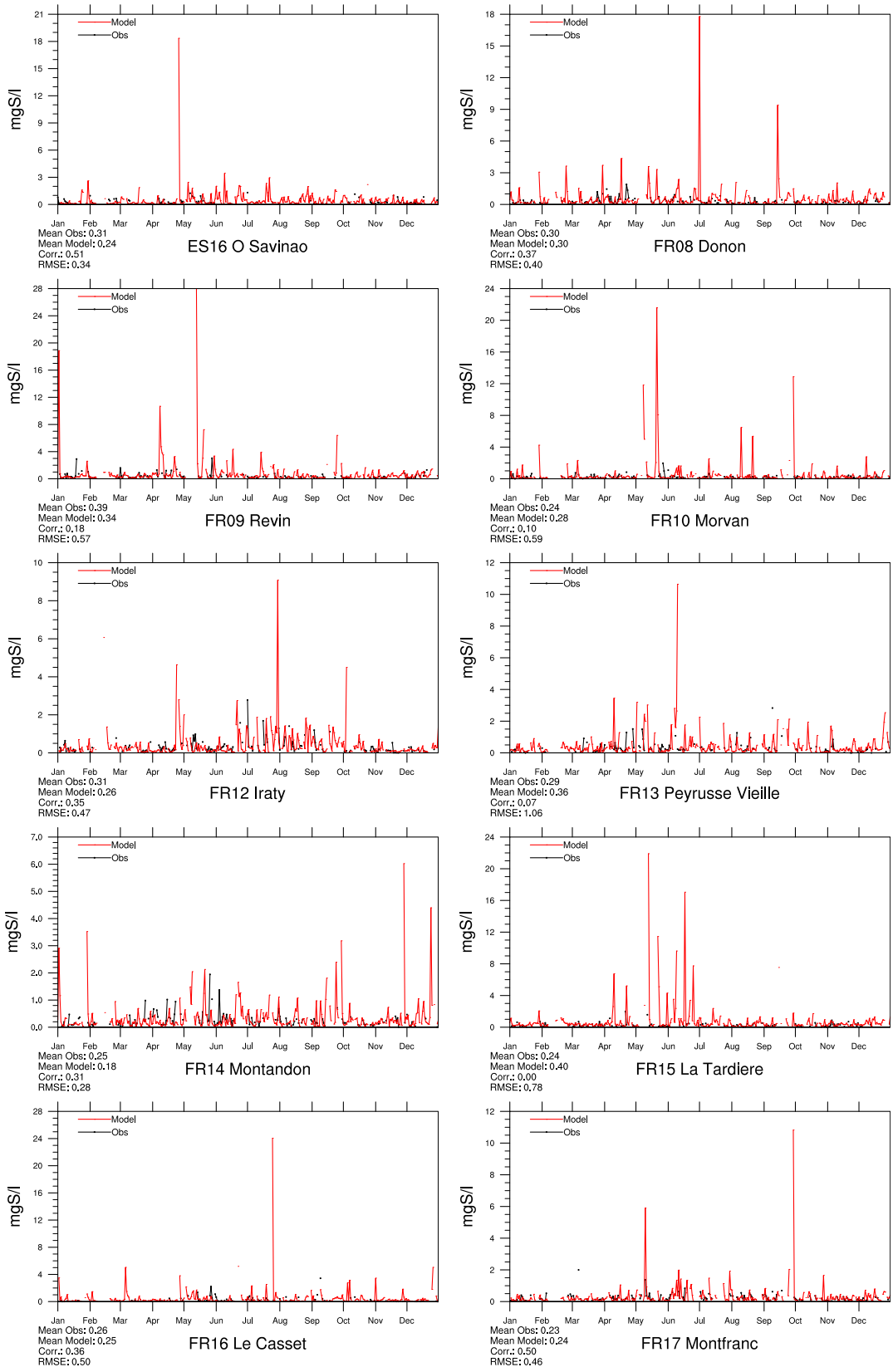

Figure 1.28: Comparison of model results and measurements (daily) for sulphur concentrations in precipitation (μg(S)l^{-1}) in 2008.

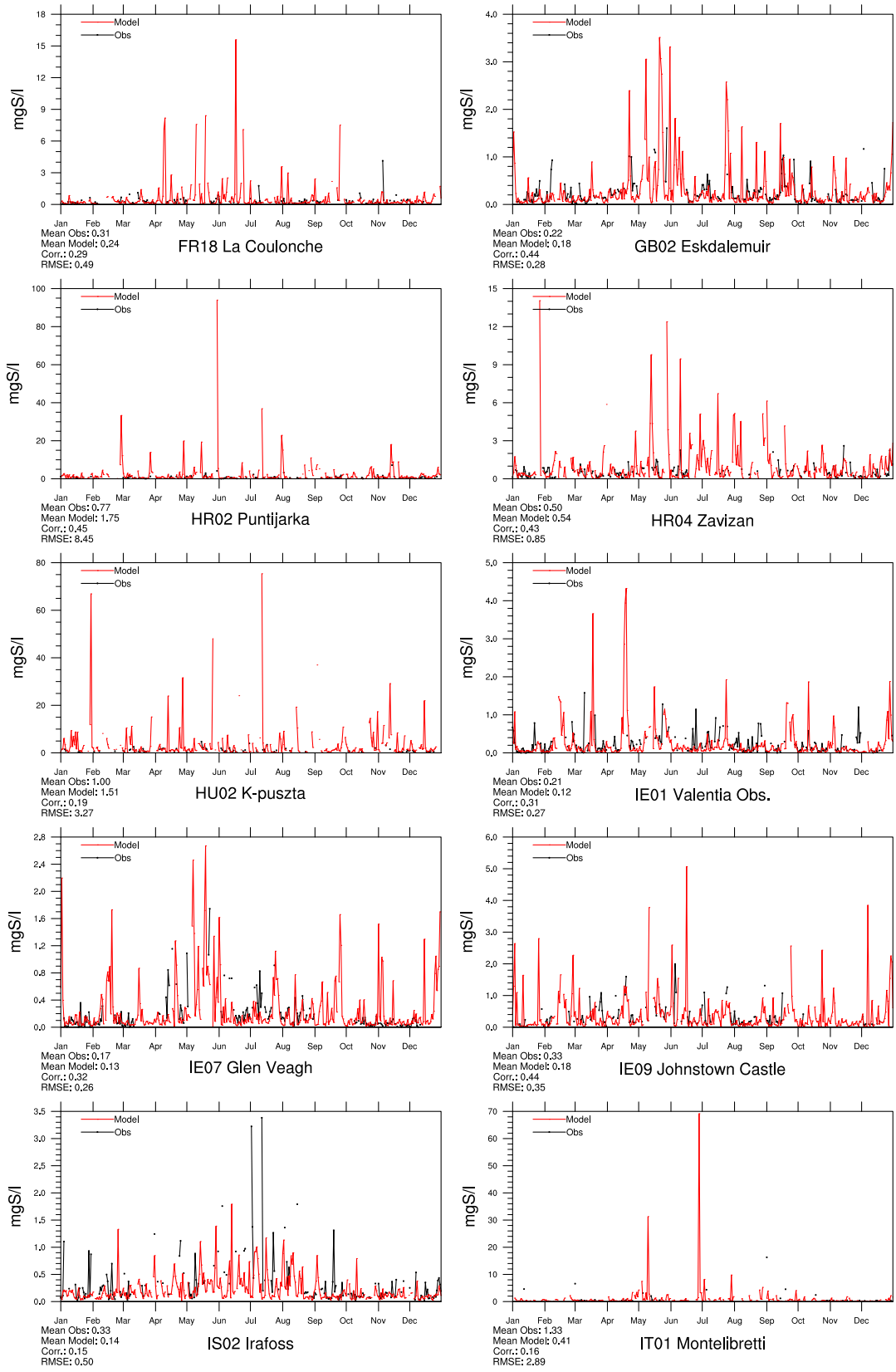

Figure 1.29: Comparison of model results and measurements (daily) for sulphur concentrations in precipitation (μg(S)l^{-1}) in 2008.

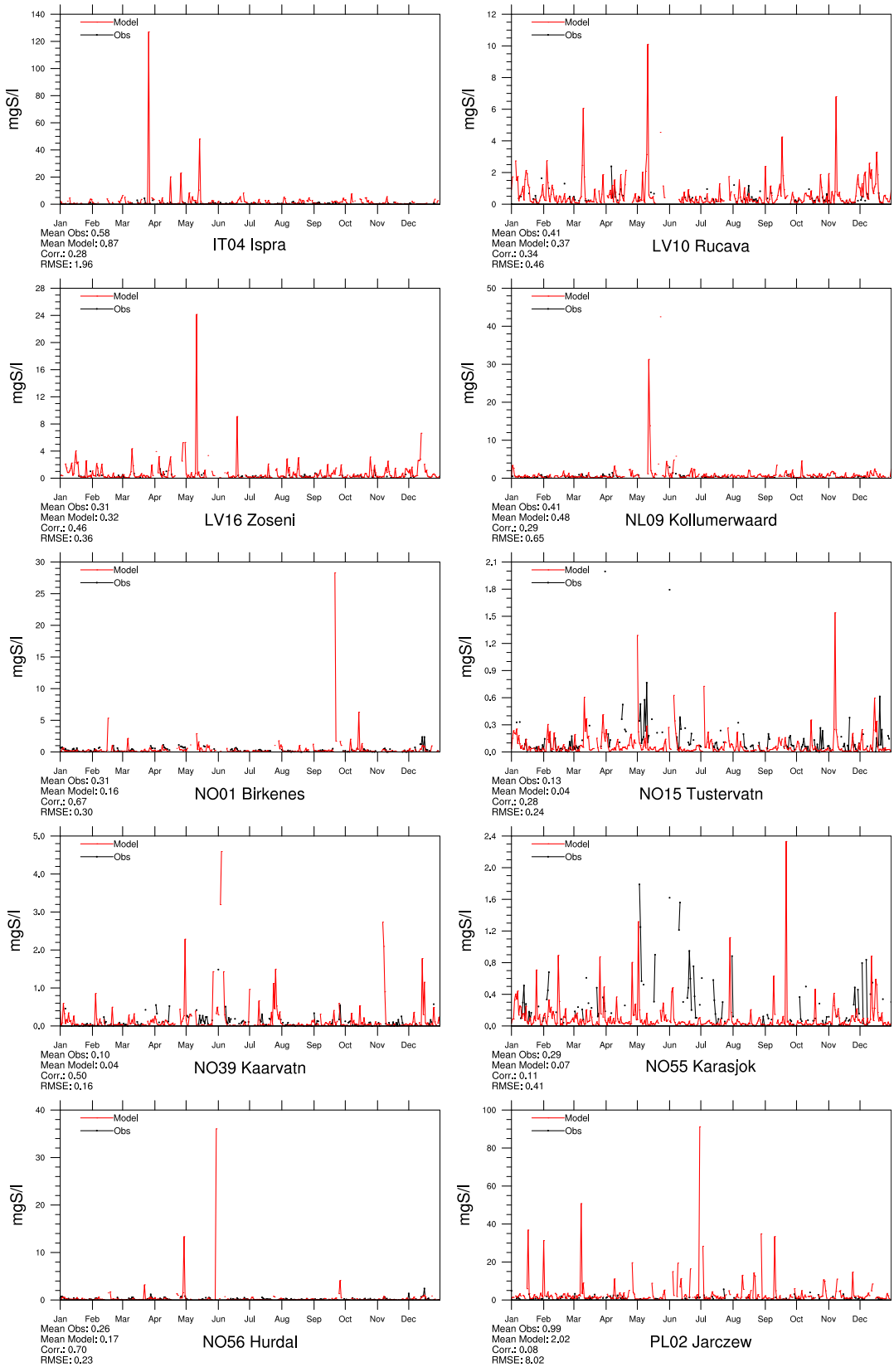

Figure 1.30: Comparison of model results and measurements (daily) for sulphur concentrations in precipitation (μg(S)l^{-1}) in 2008.

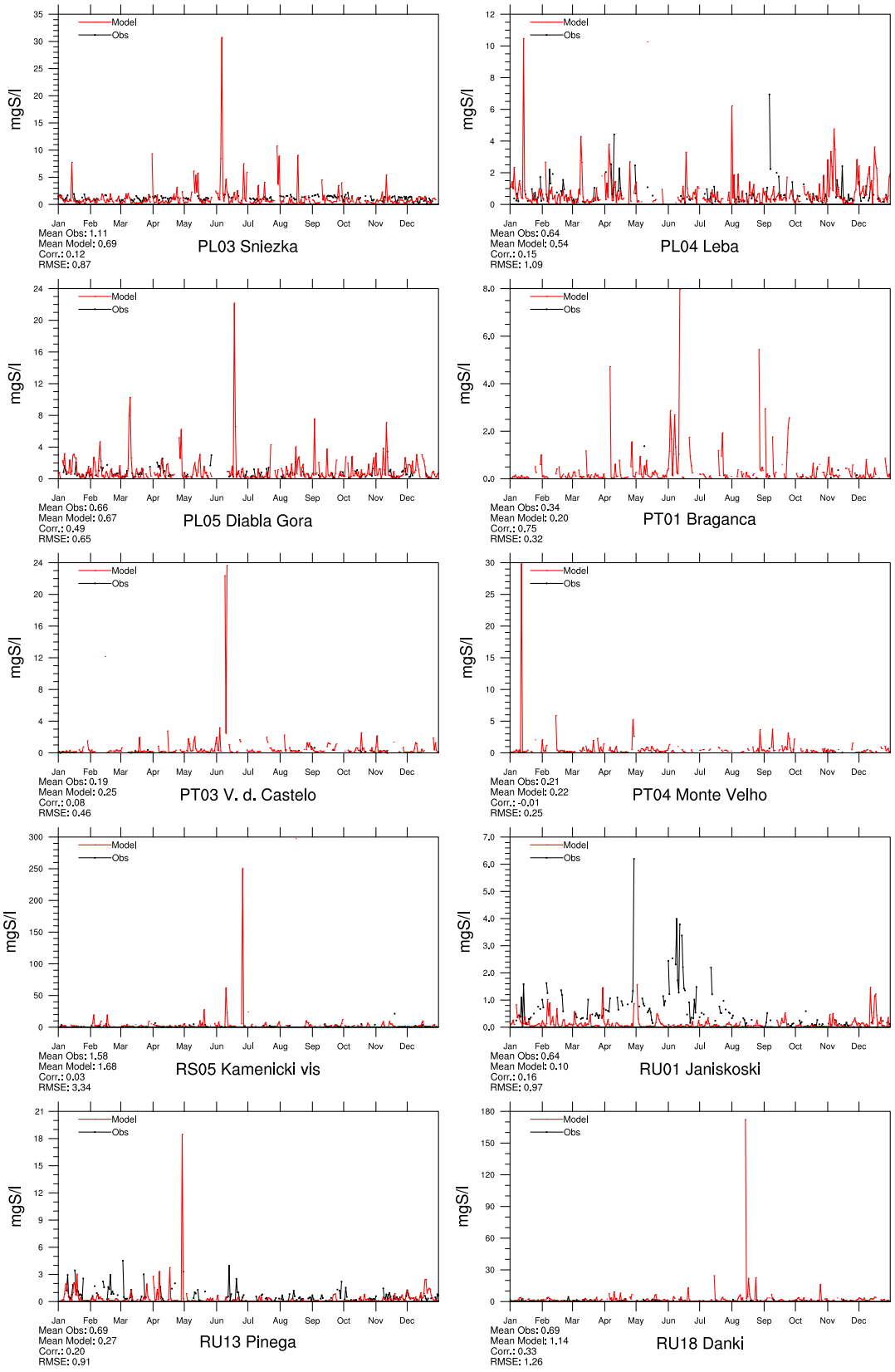

Figure 1.31: Comparison of model results and measurements (daily) for sulphur concentrations in precipitation (μg(S)l^{-1}) in 2008.

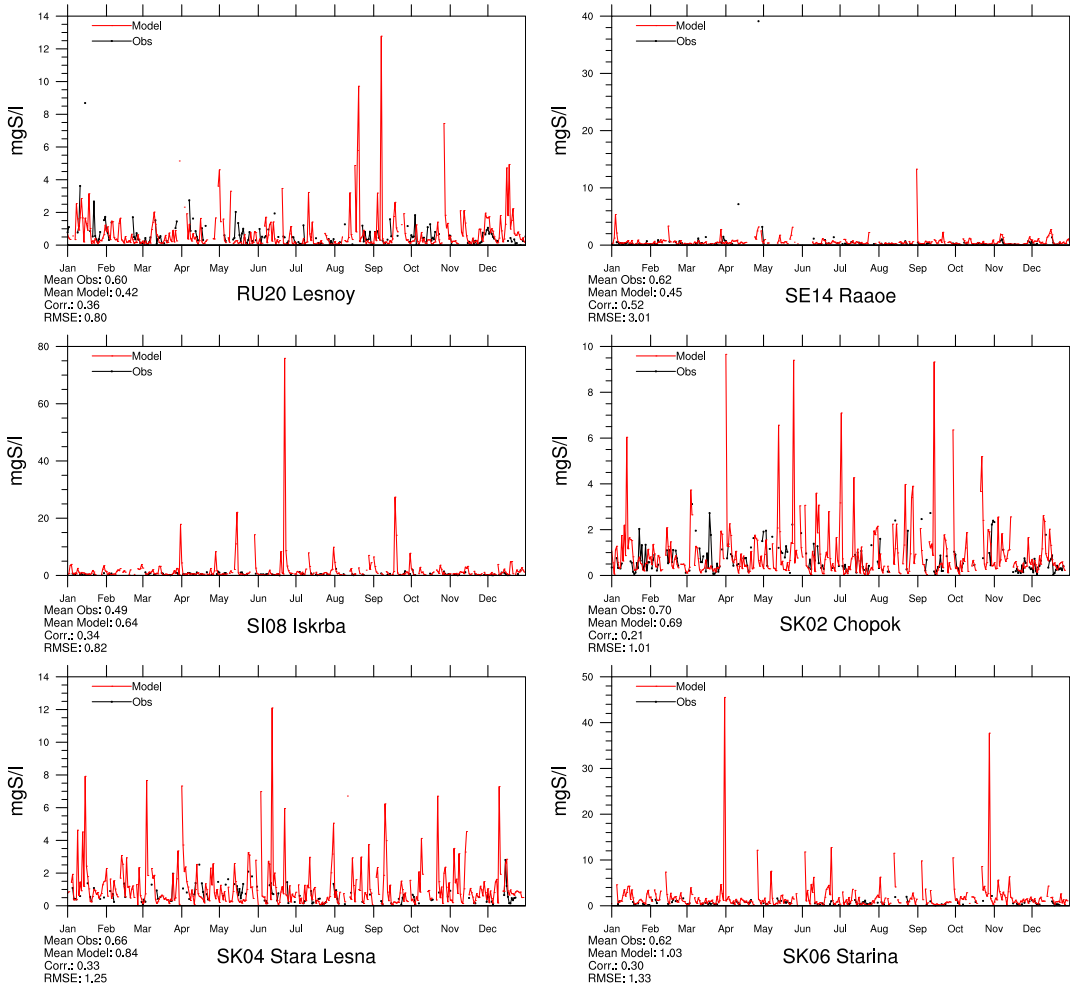

Figure 1.32: Comparison of model results and measurements (daily) for sulphur concentrations in precipitation (μg(S)l^{-1}) in 2008.

Oxidized nitrogen in precipitation

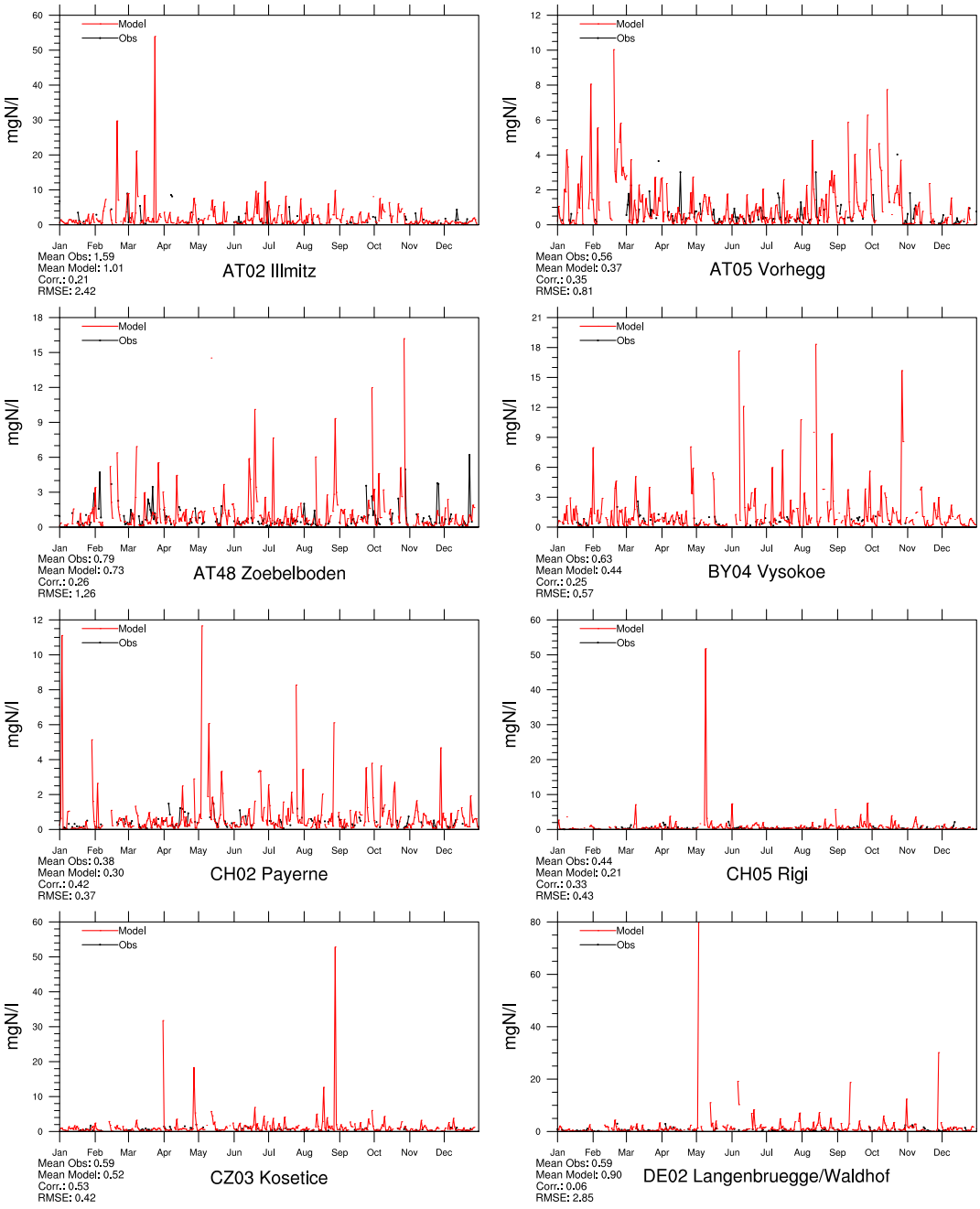

Figure 1.33: Comparison of model results and measurements (daily) for oxidized nitrogen concentrations in precipitation (μg(N)l^{-1}) in 2008.

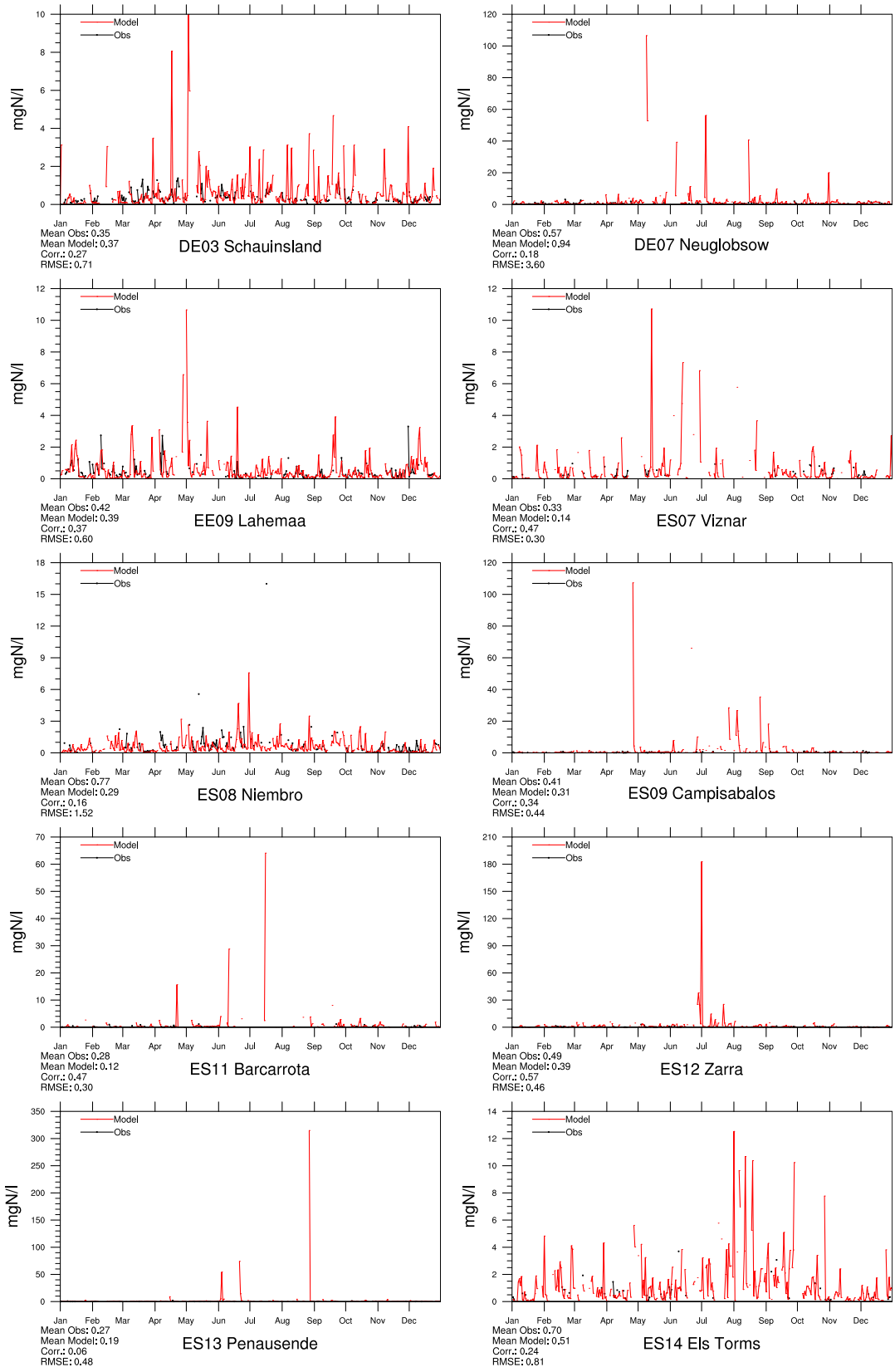

Figure 1.34: Comparison of model results and measurements (daily) for oxidized nitrogen concentrations in precipitation (μg(N)l^{-1}) in 2008.

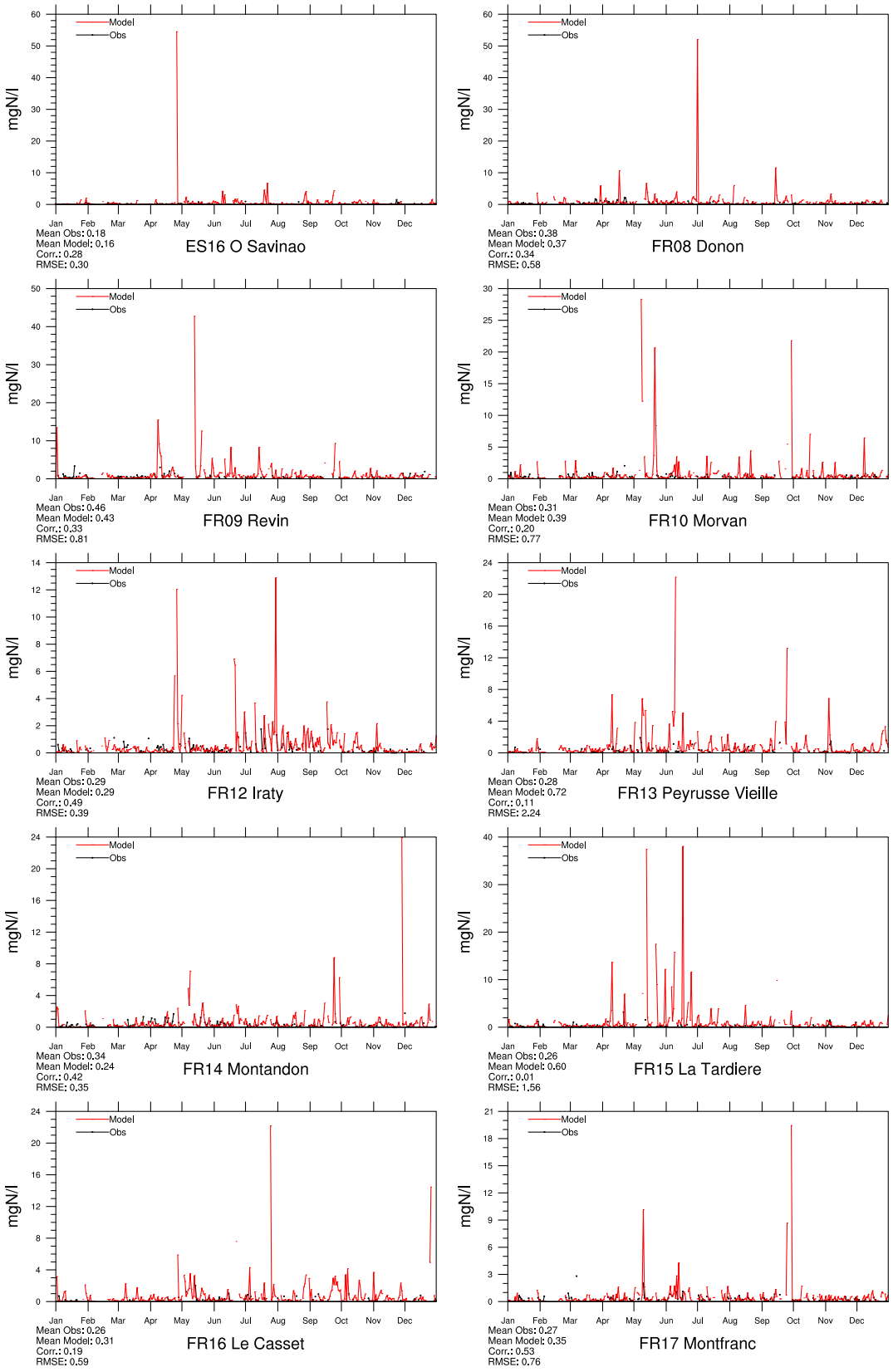

Figure 1.35: Comparison of model results and measurements (daily) for oxidized nitrogen concentrations in precipitation (μg(N)l^{-1}) in 2008.

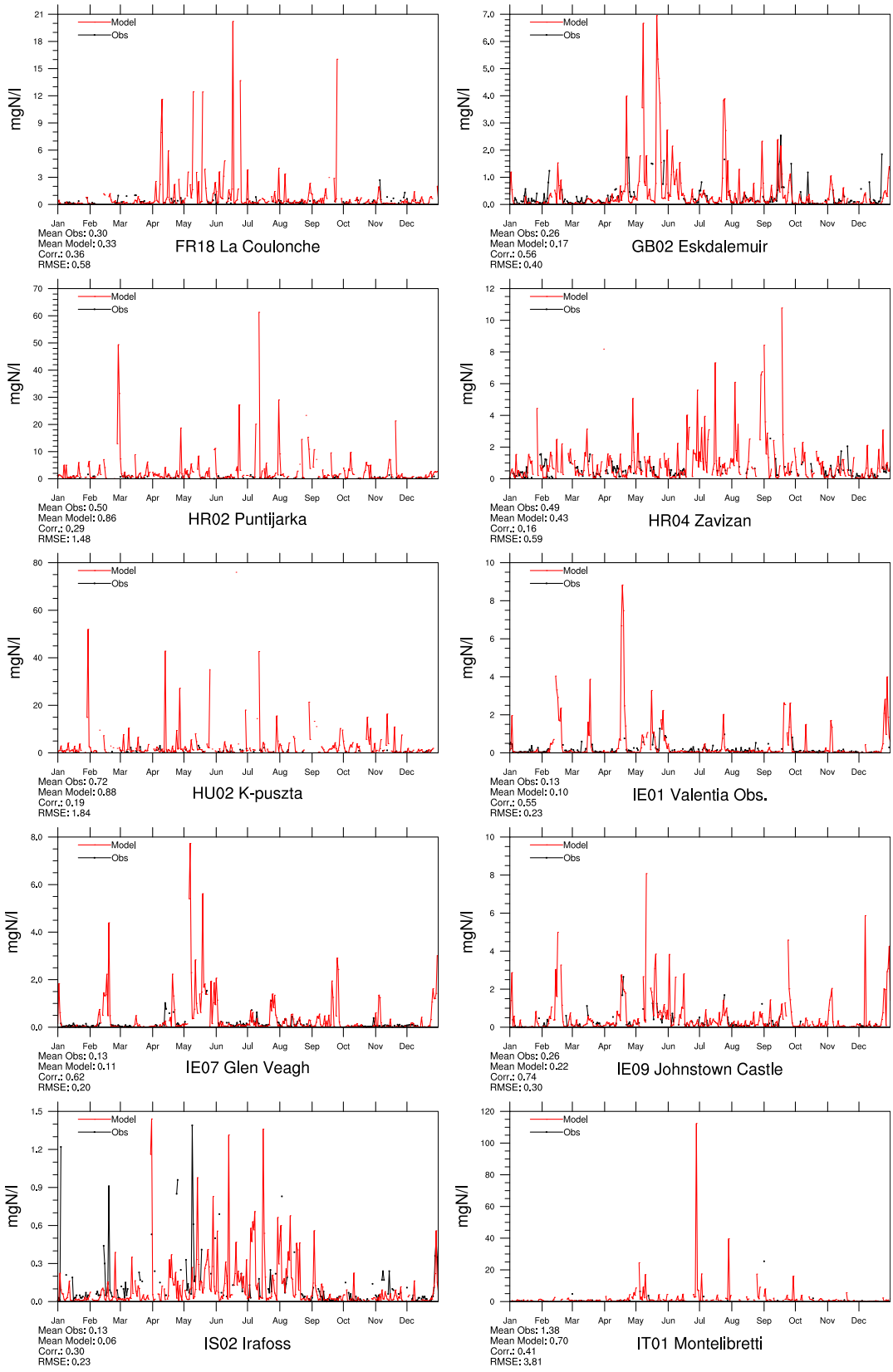

Figure 1.36: Comparison of model results and measurements (daily) for oxidized nitrogen concentrations in precipitation (μg(N)l^{-1}) in 2008.

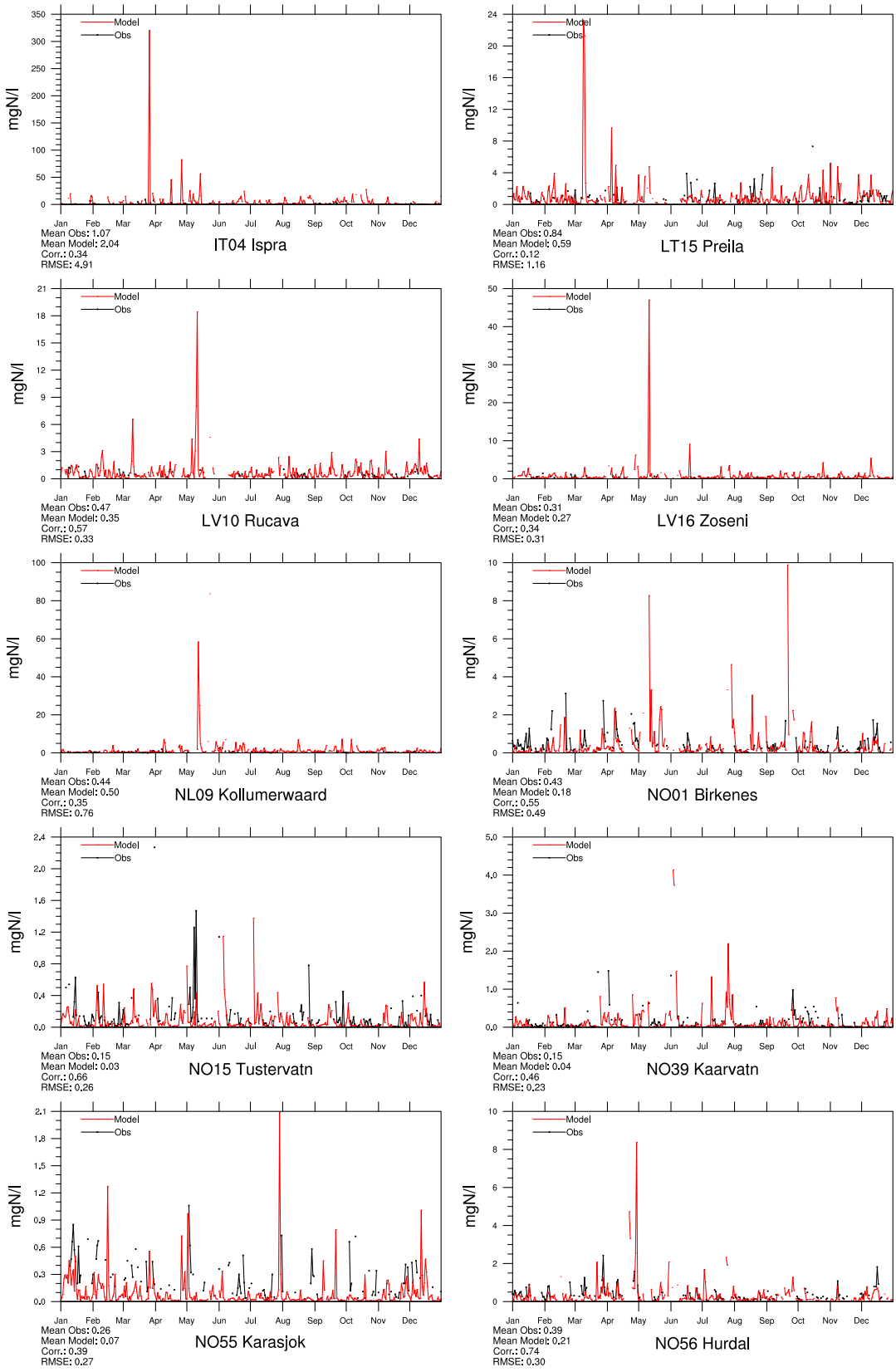

Figure 1.37: Comparison of model results and measurements (daily) for oxidized nitrogen concentrations in precipitation (μg(N)l^{-1}) in 2008.

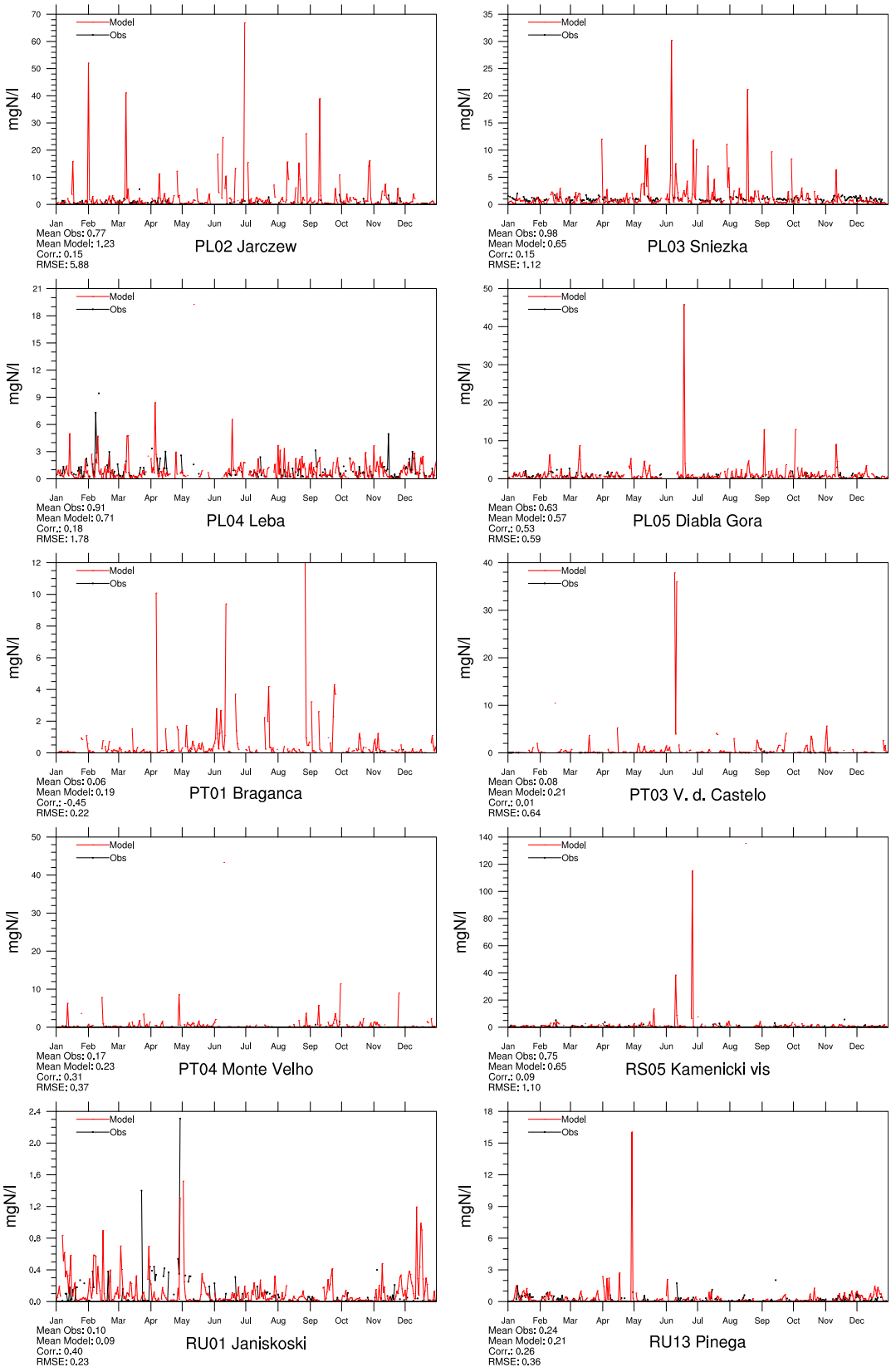

Figure 1.38: Comparison of model results and measurements (daily) for oxidized nitrogen concentrations in precipitation (μg(N)l^{-1}) in 2008.

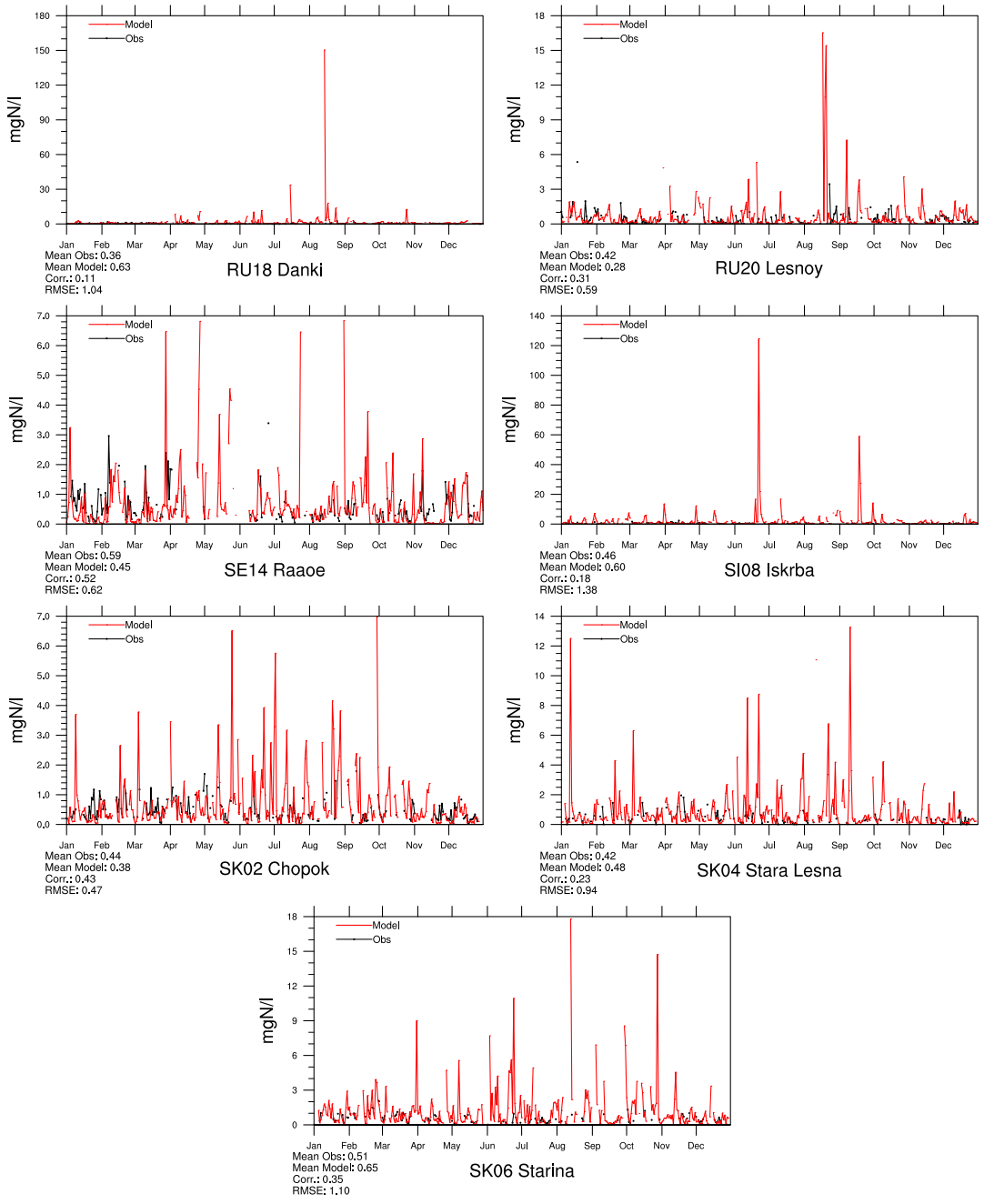

Figure 1.39: Comparison of model results and measurements (daily) for oxidized nitrogen concentrations in precipitation (μg(N)l^{-1}) in 2008.

Reduced nitrogen in precipitation

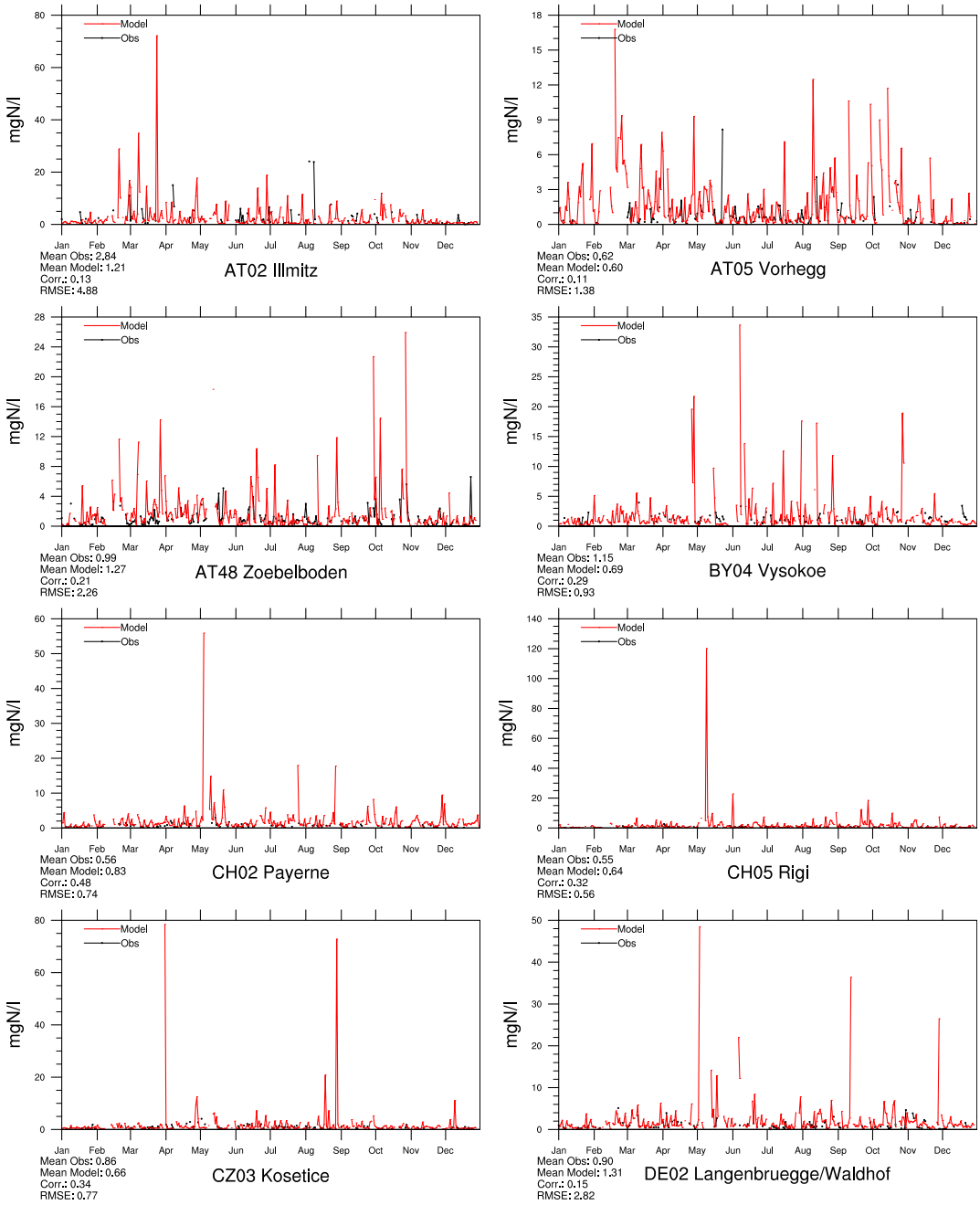

Figure 1.40: Comparison of model results and measurements (daily) for reduced nitrogen concentrations in precipitation (μg(N)l^{-1}) in 2008.

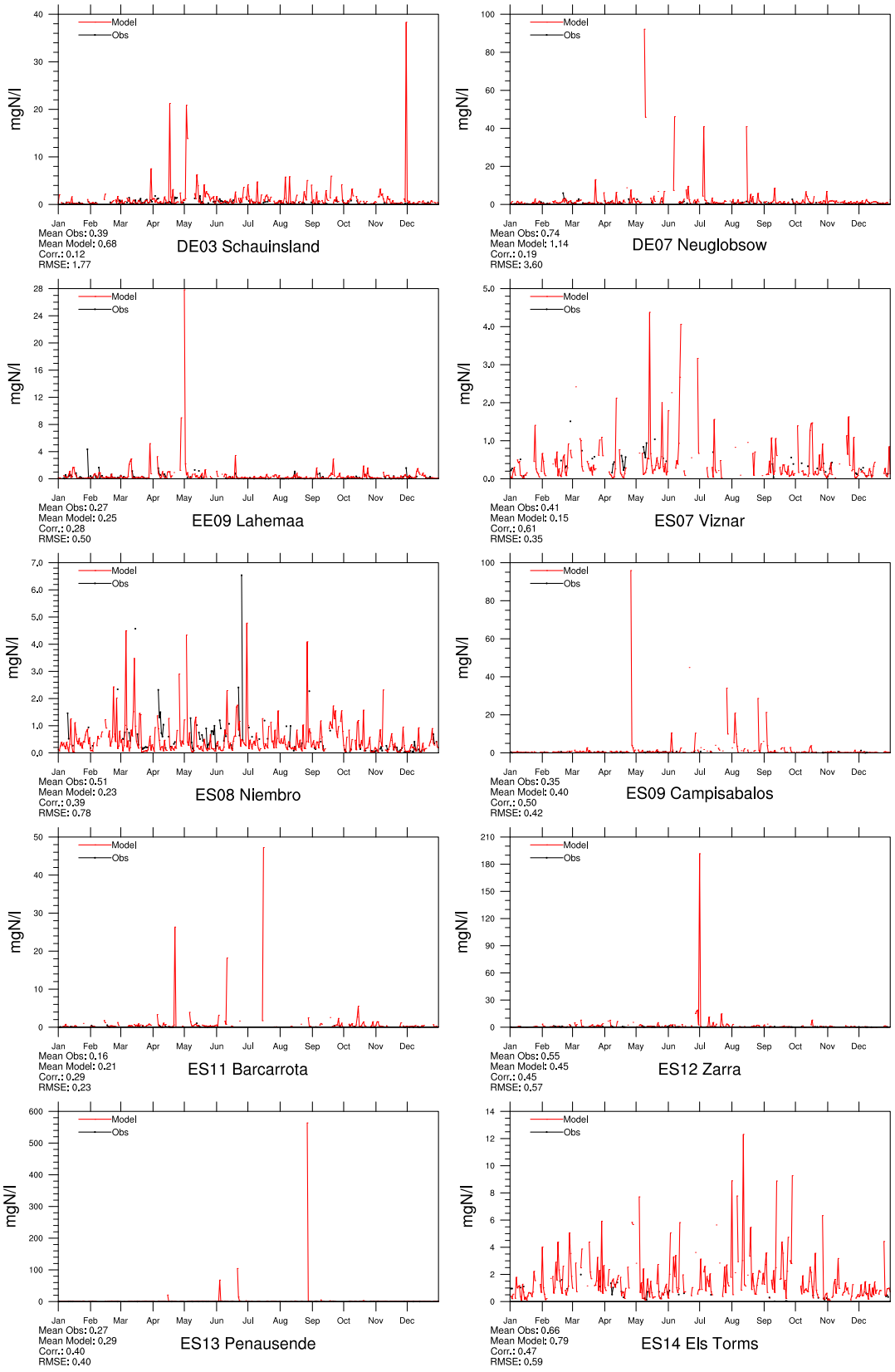

Figure 1.41: Comparison of model results and measurements (daily) for reduced nitrogen concentrations in precipitation (μg(N)l^{-1}) in 2008.

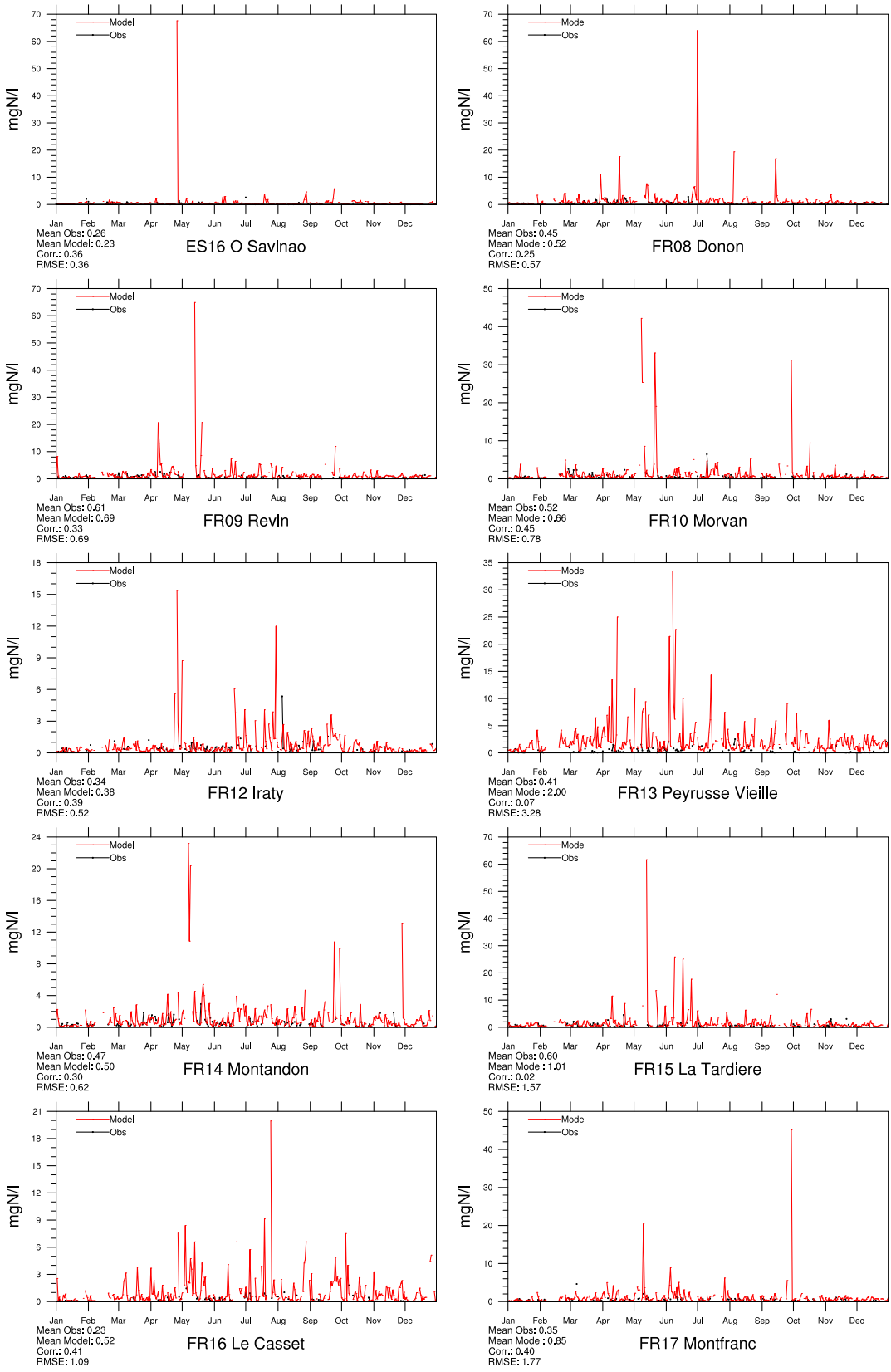

Figure 1.42: Comparison of model results and measurements (daily) for reduced nitrogen concentrations in precipitation (μg(N)l^{-1}) in 2008.

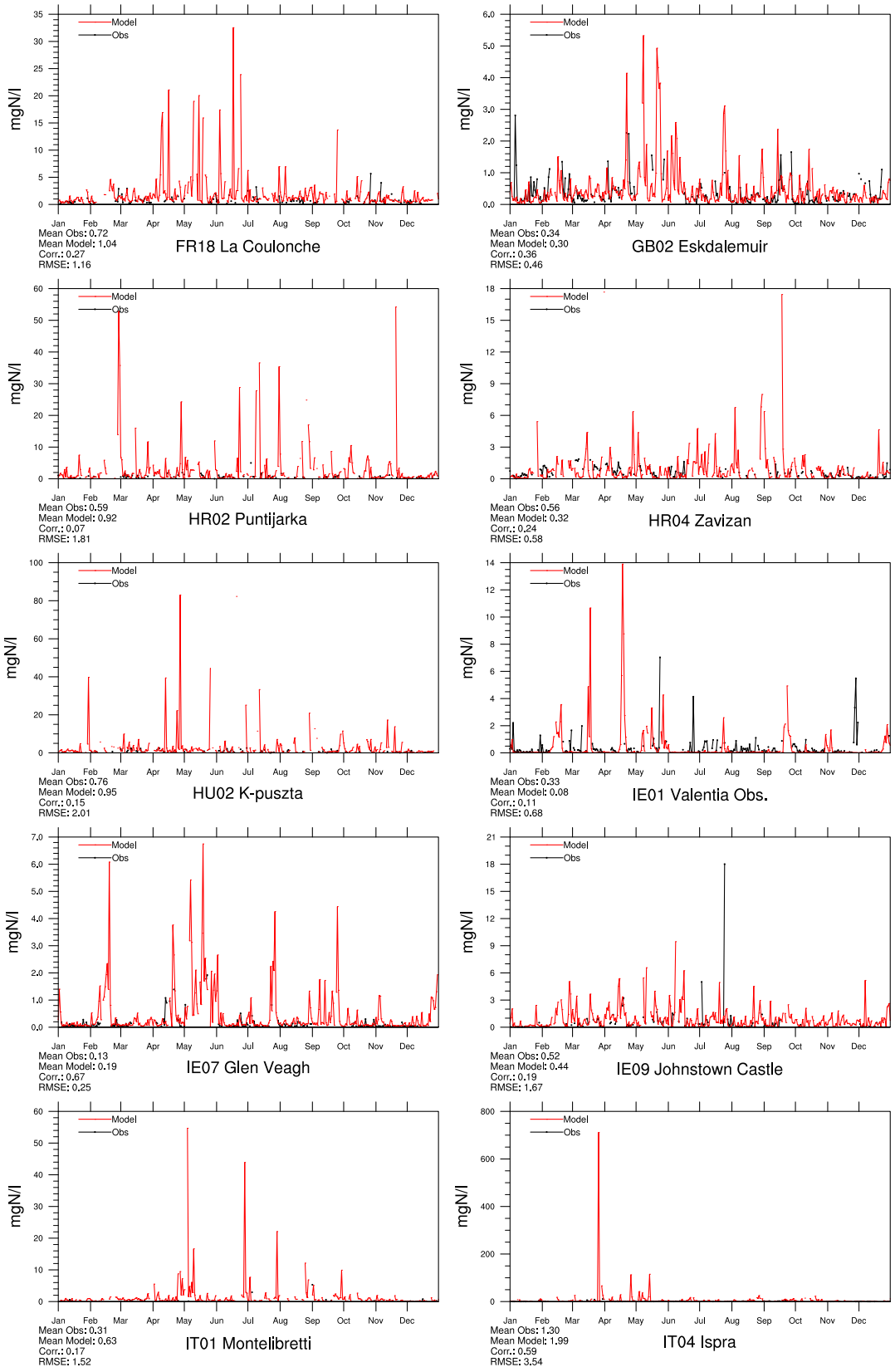

Figure 1.43: Comparison of model results and measurements (daily) for reduced nitrogen concentrations in precipitation (μg(N)l^{-1}) in 2008.

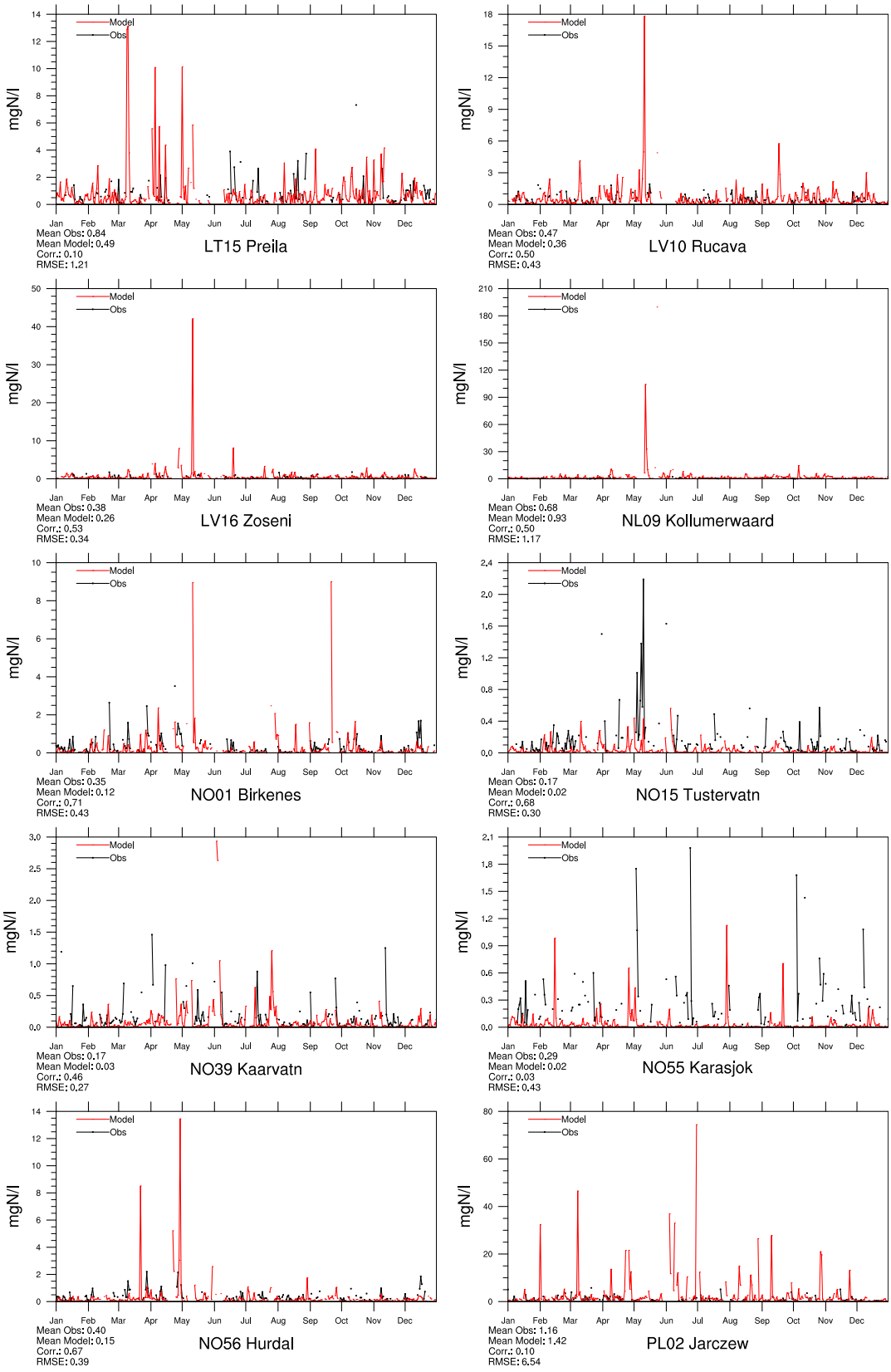

Figure 1.44: Comparison of model results and measurements (daily) for reduced nitrogen concentrations in precipitation (μg(N)l^{-1}) in 2008.

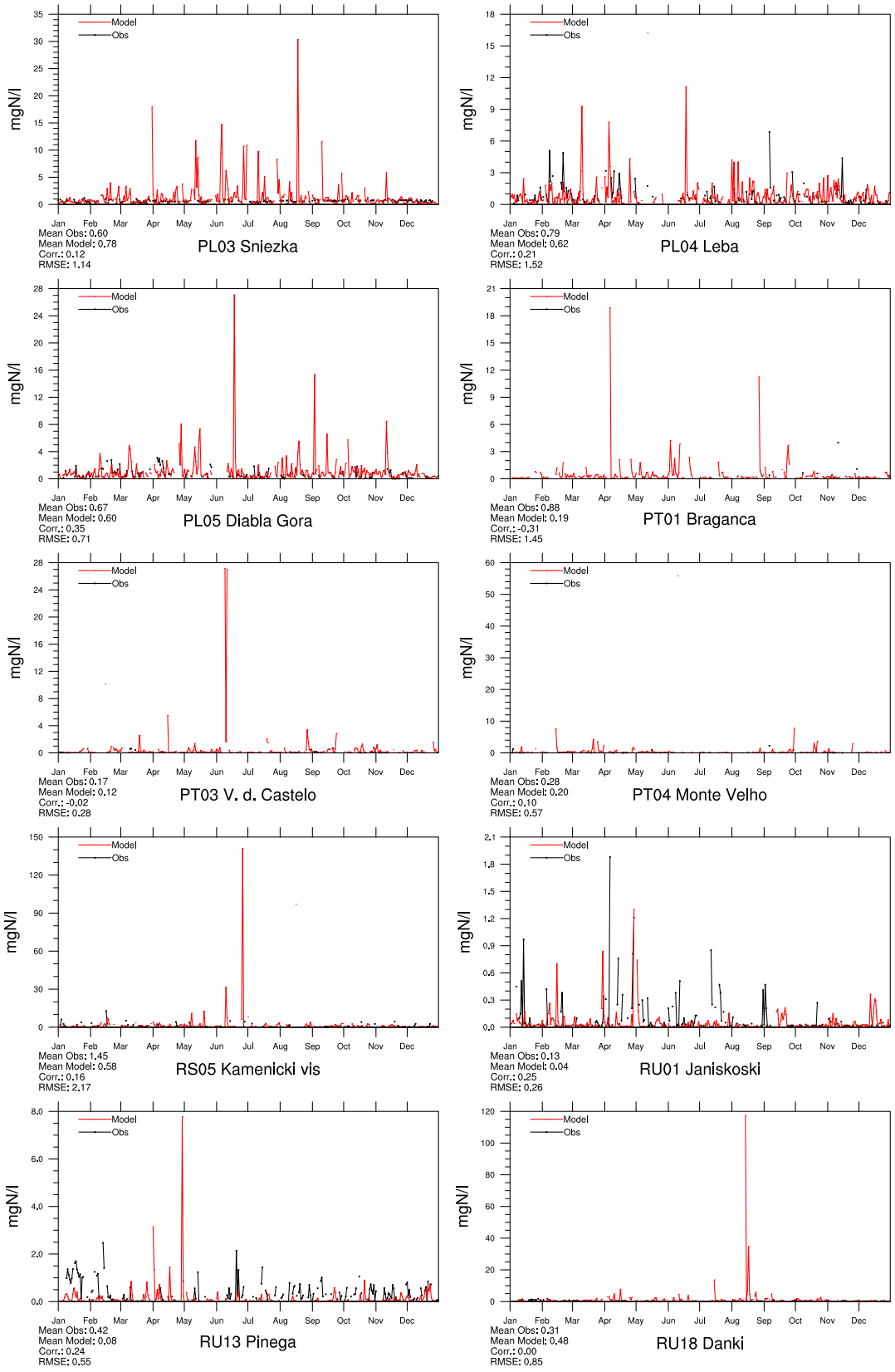

Figure 1.45: Comparison of model results and measurements (daily) for reduced nitrogen concentrations in precipitation (μg(N)l^{-1}) in 2008.

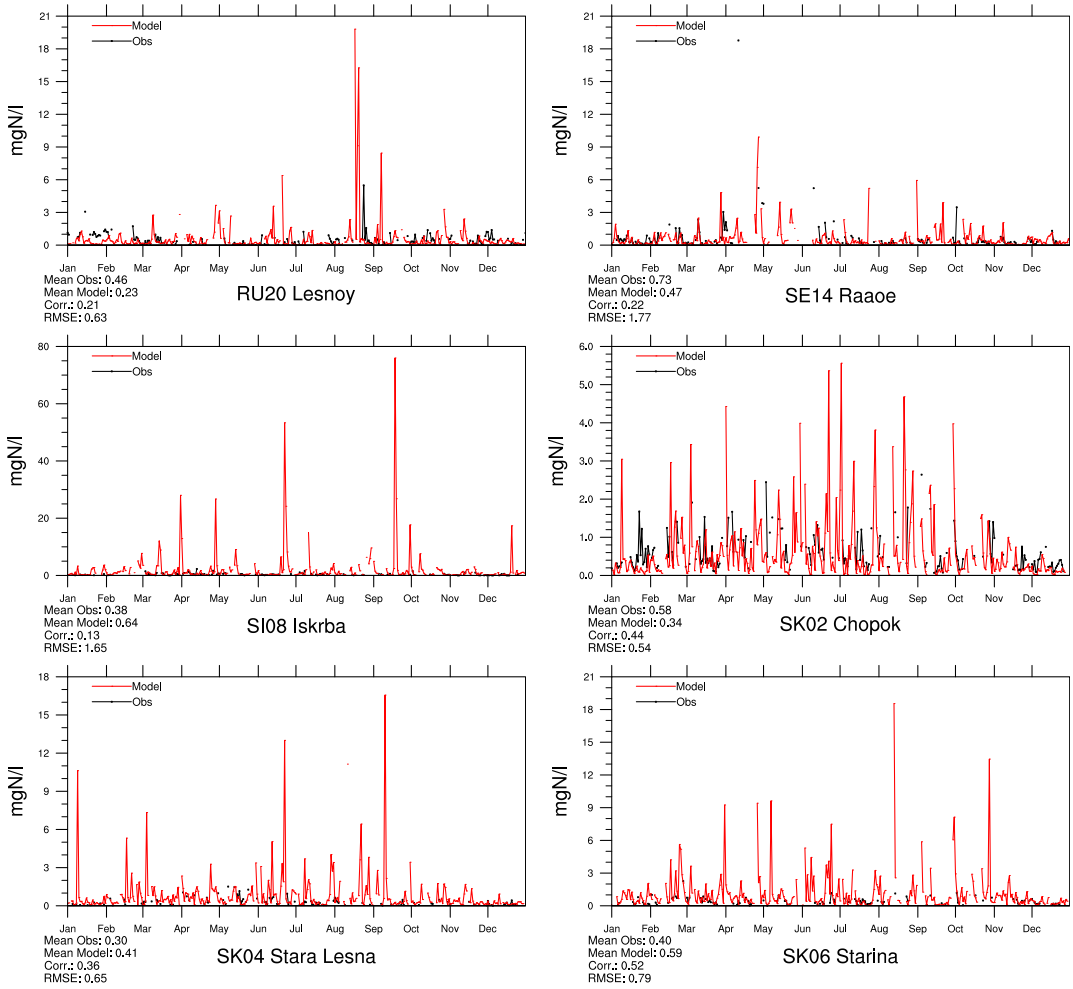

Figure 1.46: Comparison of model results and measurements (daily) for reduced nitrogen concentrations in precipitation (μg(N)l^{-1}) in 2008.

1.3 Combined model results and observations, 2008

In this section, we present the 'best estimates' for air concentrations of SO_2, SO_4^{2-}, NH_3+NH_4^+ and HNO_3+NO_3^- as well as concentrations of oxidized sulphur, oxidized nitrogen and reduced nitrogen in precipitation. The 'best estimates' have been created by using a combination of model results and observations from the EMEP network for 2008. For all measurement points, the difference between the measured value at that point and the modelled value in the corresponding grid cell is calculated. This difference is interpolated spatially using radial basis functions, giving a continuous two-dimensional function describing the difference at any point within the modelled grid. For the interpolated normalized differences (observations-model/(observations+model)), positive values show where the model underpredicts the values, whilst negative values show where the model overpredicts values. The combined maps are derived by adjusting the model results with the interpolated differences, giving large weight to the observed values close to stations, and using the modelled values in areas with no observations. The range of influence of the measured values depends on the component, and has been set to 300 km for NH_3+NH_4^+ and HNO_3+NO_3^- in air, and 500 km for all other components. For each of the components, we present four different figures, visualizing the different steps of the procedure (Figures 1.47 to 1.49). In general, there is good agreement between model results and measurements for 2008 as for previous years. The normalised errors are relatively small, within 18% over large parts of Europe, for all components except SO_4^{2-} where the normalized error shows under-prediction in Northern Europe.

References

EMEP MSC-W & CCC . EMEP Unified model performance for acidifying and eutrophying components and photo-oxidants in 2007. Supplementary material to EMEP Status Report 1/09 . Supplementary material to emep status report 1/2009, available online at `www.emep.int`, The Norwegian Meteorological Institute, Oslo, Norway, 2009.

H. Fagerli. Air concentrations and depositions of acidifying and euthrophying components, status 2002. In *Transboundary acidification, eutrophication and ground level ozone in Europe. EMEP Status Report 1/2004*, pages 77–107. The Norwegian Meteorological Institute, Oslo, Norway, 2004.

H. Fagerli. Acidifying and eutrophying components, status in 2003. In *In Transboundary Acidification, Eutrophication and Ground Level Ozone in Europe. EMEP Status Report 1/2005*, pages 9–30. The Norwegian Meteorological Institute, Oslo, Norway, 2005.

H. Fagerli. Air concentrations and depositions of acidifying and euthrophying com-

ponents, status in 2005. In *Transboundary acidification, eutrophication and ground level ozo ne in Europe in 2005. EMEP Status Report 1/2007*, pages 33–52. The Norwegian Meteorological Institute, Oslo, Norway, 2007.

H. Fagerli and W. Aas. Validation of nitrogen compounds in the emep model. In *Transboundary acidification, eutrophication and ground level ozo ne in Europe in 2005. EMEP Status Report 1/2007*, pages 73–90. The Norwegian Meteorological Institute, Oslo, Norway, 2007.

H. Fagerli and W. Aas. Using the EMEP intensive measurement data to evaluate the performance of the EMEP model for nitrogen compounds. In *In Transboundary Acidification, Eutrophication and Ground Level Ozone in Europe in 2006. EMEP Status Report 1/2008*, pages 109–126. The Norwegian Meteorological Institute, Oslo, Norway, 2008a.

H. Fagerli and A.G. Hjellbrekke. Acidification and eutrophication. In *Transboundary Acidification, Eutrophication and Ground Level Ozone in Europe in 2006. EMEP Status Report 1/2008*, pages 41–56. The Norwegian Meteorological Institute, Oslo, Norway, 2008.

H. Fagerli, D. Simpson, and W. Aas. Model performance for sulphur and nitrogen compounds for the period 1980 to 2000. In L. Tarrasón, editor, *Transboundary Acidification, Eutrophication and Ground Level Ozone in Europe. EMEP Status Report 1/2003, Part II Unified EMEP Model Performance*, pages 1–66. The Norwegian Meteorological Institute, Oslo, Norway, 2003.

Hilde Fagerli and Wenche Aas. Trends of nitrogen in air and precipitation: Model results and observations at emep sites in europe, 1980-2003. *Environ. Poll.*, 154(3): 448–461, August 2008b.

Hilde Fagerli, Peter Wind, Michael Gauss, Ágnes Nyíri, David Simpson, and Svetlana Tsyro. Improved resolution in EMEP models. In *Transboundary Acidification, Eutrophication and Ground Level Ozone in Europe in 2006. EMEP Status Report 1/2008*, pages 89–104. The Norwegian Meteorological Institute, Oslo, Norway, 2008.

Agnes Nyíri and A.-G. Hjellbrekke. Acidifying and eutrophying components: validation and combined maps. Supplementary material to emep status report 1/2009, available online at `www.emep.int`, The Norwegian Meteorological Institute, Oslo, Norway, 2009.

D. Simpson, K. Butterbach-Bahl, H. Fagerli, M. Kesik, U. Skiba, and S. Tang. Deposition and emissions of reactive nitrogen over European forests: A modelling study. *Atmos. Environ.*, 40:5712–5726, 2006a. doi: 10.1016/j.atmosenv.2006.04.063.

D. Simpson, H. Fagerli, S. Hellsten, J.C. Knulst, and O. Westling. Comparison of modelled and monitored deposition fluxes of sulphur and nitrogen to ICP-forest sites in Europe. *Biogeosciences*, 3:337–355, 2006b.

David Simpson, Michael Gauss, Svetlana Tsyro, and Álvaro Valdebenito. Model Updates. In *Transboundary Acidification, Eutrophication and Ground Level Ozone in Europe in 2008. EMEP Status Report 1/2010*. The Norwegian Meteorological Institute, Oslo, Norway, 2010.

Svetlana Tsyro, Haldis Berge, Anna Benedictow, and Michael Gauss. Studying the effect of meteorological input on Unified model results. In *Transboundary Acidification, Eutrophication and Ground Level Ozone in Europe in 2008. EMEP Status Report 1/2010*. The Norwegian Meteorological Institute, Oslo, Norway, 2010.

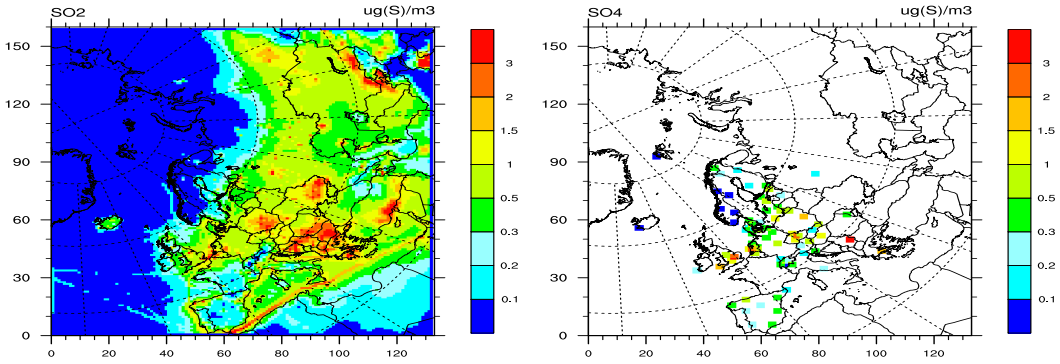

(a) Modelled SO_2 in air

(b) Measured SO_2 in air

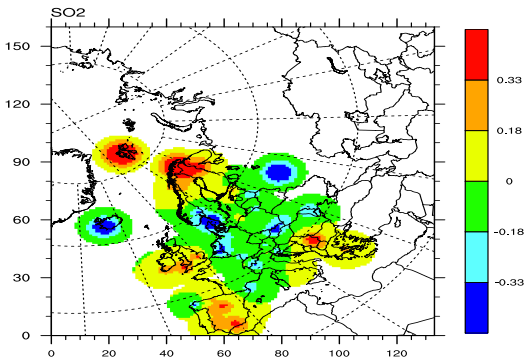

(c) Interpolated normalized differences

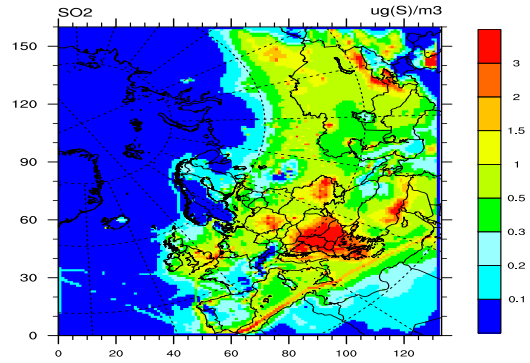

(d) Combined SO_2 in air

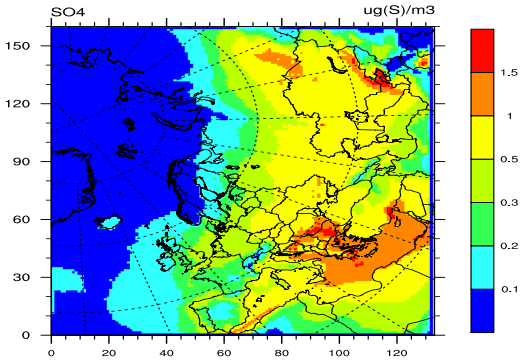

(e) Modelled SO_4^{2-} in air

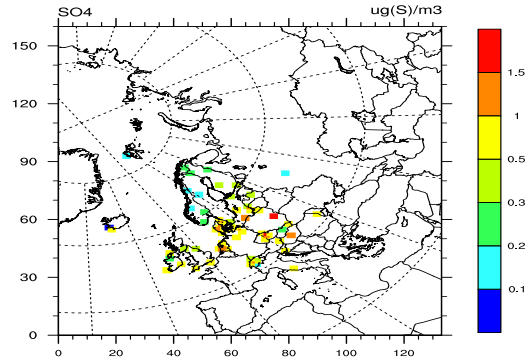

(f) Measured SO_4^{2-} in air

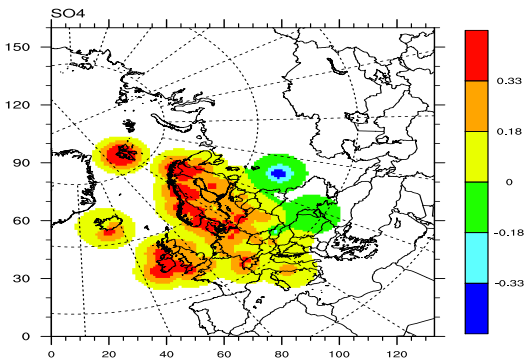

(g) Interpolated normalized differences

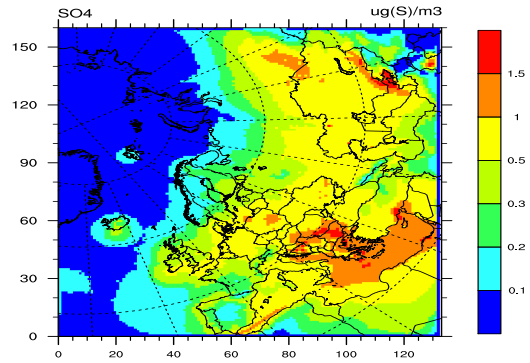

(h) Combined SO_4^{2-} in air

Figure 1.47: Yearly averaged SO_2 (a)-(d) and SO_4^{2-} (e)-(h) concentrations in air [μg(S) m^{-3}] for 2008.

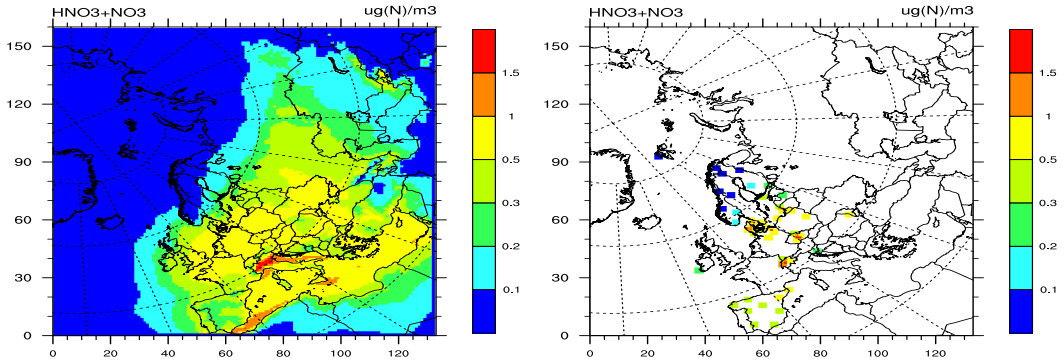

(a) Modelled total nitrate in air (b) Measured total nitrate in air

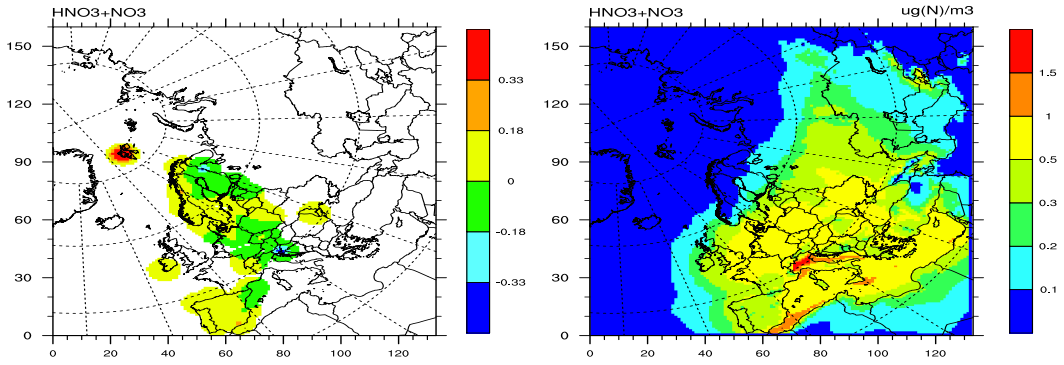

(c) Interpolated normalized differences (d) Combined total nitrate in air

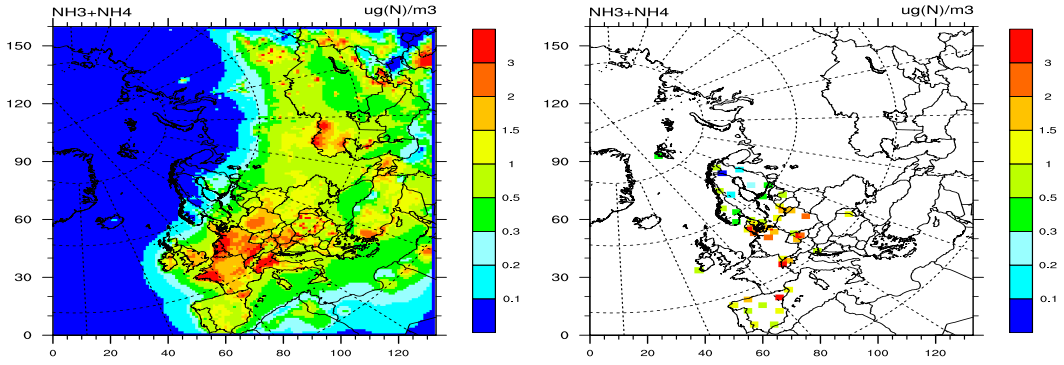

(e) Modelled ammonia+ammonium in air (f) Measured ammonia+ammonium in air

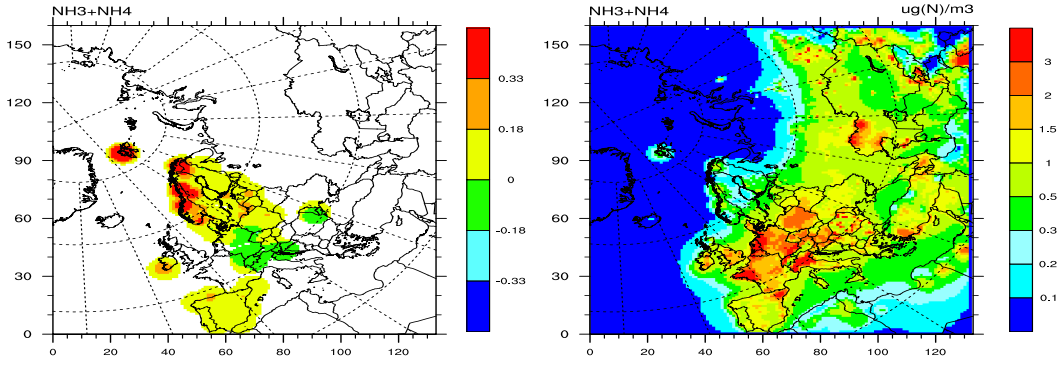

(g) Interpolated normalized differences (h) Combined ammonia+ammonium in air

Figure 1.48: Yearly averaged HNO_3+NO_3^- (a)-(d) and NH_3+NH_4^+ (e)-(h) concentrations in air [μg(N) m^{-3}] for 2008.

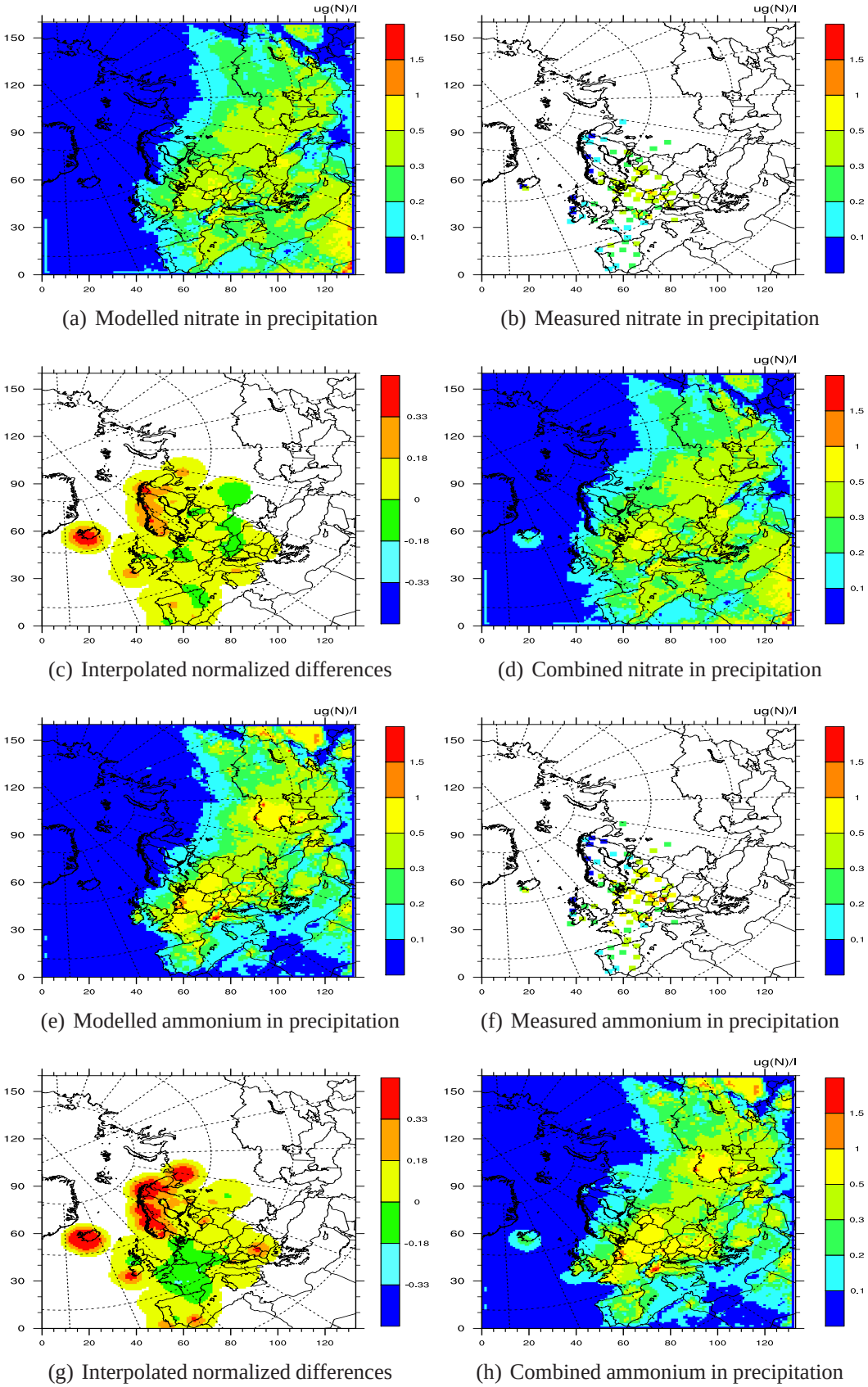

(a) Modelled nitrate in precipitation

(b) Measured nitrate in precipitation

(c) Interpolated normalized differences

(d) Combined nitrate in precipitation

(e) Modelled ammonium in precipitation

(f) Measured ammonium in precipitation

(g) Interpolated normalized differences

(h) Combined ammonium in precipitation

Figure 1.49: Yearly averaged oxidized nitrogen (a)-(d) and reduced nitrogen (e)-(h) concentrations in precipitation [μg(N)l^{-1}] for 2008.

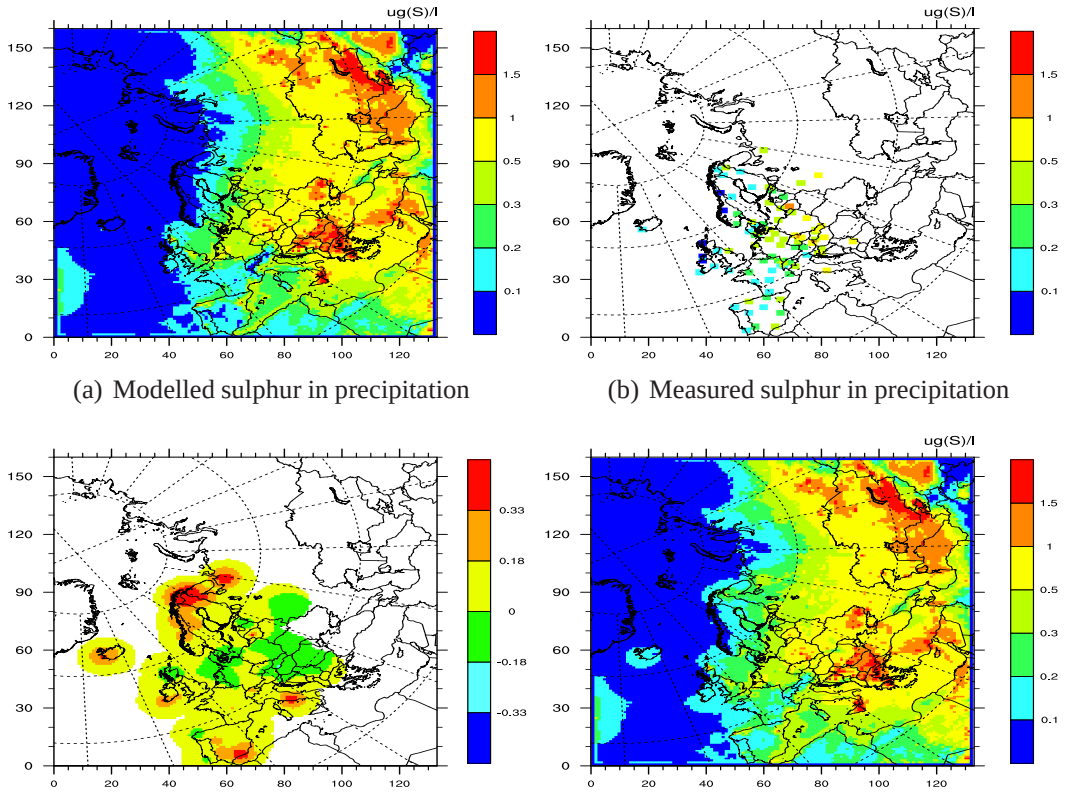

(a) Modelled sulphur in precipitation

(b) Measured sulphur in precipitation

(c) Interpolated normalized differences

(d) Combined sulphur in precipitation

Figure 1.50: Yearly averaged sulphur concentrations in precipitation [μg(S)l^{-1}] for 2008.

CHAPTER 2

Photo-oxidants: validation and combined maps

Haldis Berge, Michael Gauss and Anne-Gunn Hjellbrekke

In this chapter the Unified EMEP model is evaluated with respect to surface ozone and NO_2. In section 2.1 we present time-series plots for selected stations to illustrate the performance of the EMEP model for the year 2008. In section 2.2 we present 'best estimate' maps of ozone and NO_2 for 2008, created by combining measurements and model results.

2.1 Validation

Daily maximum ozone values have been validated for all stations supplying data to EMEP CCC. Table 2.1 summarises these comparisons, and Figures 2.1-2.17 show time-series plots for stations representing the different regions of Europe. This year for the first time we introduce root mean square error (RMSE) and index of agreement (IOA). IOA varies between 0 and 1. A value of 1 corresponds to perfect agreement between model and observations and 0 is the theoretical minimum.

Table 2.1: Comparison of modelled versus observed ozone for year 2008. Concentrations are given as means of daily maximum ozone values (ppb). The numbers in parentheses show the deviation (ppb) from the average over all measurements within the 5-year period 2003-2007. Correlation coefficients (r), root mean square erroe (RMSE), and index of agreement (IOA) are included to judge the model's agreement with observation (for details see start of this section)

Code	Station	Obs. (ppb)	Mod. (ppb)	r	RMSE	IOA
		Nordic Countries				
DK05	Keldsnor	36.98 (-0.97)	40.34	0.71	8.45	0.81
DK31	Ulborg	40.82 (1.68)	41.27	0.87	5.64	0.93
DK41	Lille Valby	37.85 (N.A.)	40.36	0.82	6.96	0.89
FI09	Utoe	38.31 (N.A.)	42.60	0.72	8.12	0.80
FI17	Virolahti II	35.25 (-0.26)	38.13	0.67	8.57	0.79
FI22	Oulanka	32.40 (-0.85)	34.12	0.81	5.34	0.89
FI37	Aehtaeri II	34.52 (-1.04)	36.26	0.77	6.85	0.86
FI96	Pallas	36.66 (-0.66)	33.95	0.72	6.60	0.82
NO01	Birkenes	38.64 (-0.02)	41.91	0.76	7.95	0.81
NO15	Tustervatn	39.04 (0.73)	39.60	0.79	5.31	0.88
NO39	Kaarvatn	36.69 (0.06)	42.66	0.72	8.62	0.75
NO42	Spitzbergen, Zeppelin	37.19 (0.03)	38.98	0.61	6.38	0.77
NO43	Prestebakke	36.94 (0.02)	41.04	0.81	7.52	0.85
NO52	Sandve	40.50 (2.74)	42.35	0.68	6.94	0.80
NO55	Karasjok	35.70 (-0.10)	34.34	0.72	6.15	0.83
NO56	Hurdal	34.42 (0.40)	38.70	0.82	7.57	0.85
SE05	Bredkaelen	33.78 (-2.84)	36.93	0.79	6.21	0.86
SE11	Vavihill	35.35 (-3.45)	40.46	0.77	9.60	0.82
SE12	Aspvreten	37.07 (-1.65)	39.76	0.84	6.40	0.89
SE13	Esrange	36.68 (-0.24)	35.19	0.73	6.59	0.83
SE14	Raaoe	38.64 (0.62)	39.40	0.69	7.60	0.81
SE32	Norra-Kvill	37.26 (0.05)	40.09	0.79	7.05	0.86
SE35	Vindeln	33.66 (-0.15)	36.69	0.80	6.55	0.85
SE39	Grimsoe	35.16 (-1.31)	38.14	0.84	6.63	0.88
		Eastern European Countries				
BG53	Rojen peak	47.06 (-1.99)	49.80	0.62	8.89	0.75
CZ01	Svratouch	40.45 (1.70)	44.33	0.79	9.88	0.85
CZ03	Kosetice	41.29 (0.27)	44.83	0.83	8.21	0.89
EE09	Lahemaa	36.14 (-0.64)	38.48	0.68	8.56	0.80
HU02	K-puszta	45.98 (-1.63)	47.71	0.87	7.98	0.92
LT15	Preila	36.71 (-1.35)	44.47	0.71	11.30	0.74
LV10	Rucava	38.06 (3.41)	42.09	0.76	8.91	0.82
LV16	Zoseni	34.52 (N.A.)	37.92	0.74	7.44	0.83

continued on next page

Code	Station	Obs.	Mod.	r	RMSE	IOA
PL02	Jarczew	37.56 (-5.35)	41.97	0.83	8.88	0.88
PL03	Sniezka	48.82 (-5.23)	43.89	0.75	9.64	0.82
PL04	Leba	40.03 (-1.74)	43.45	0.78	8.11	0.85
PL05	Diabla Gora	37.66 (-1.98)	40.31	0.80	8.27	0.87
SK02	Chopok	52.47 (0.06)	47.67	0.75	8.76	0.80
SK04	Stara Lesna	48.73 (2.91)	46.93	0.65	8.77	0.79
SK06	Starina	42.19 (-1.02)	44.43	0.77	7.81	0.86
SK07	Topolniky	44.96 (1.16)	46.97	0.82	9.03	0.90
		Central and NW European Countries				
AT02	Illmitz	42.26 (-1.68)	47.26	0.83	9.74	0.88
AT05	Vorhegg	43.15 (-3.38)	50.08	0.67	12.07	0.76
AT30	Pillersdorf	41.27 (-2.78)	45.20	0.84	9.33	0.89
AT32	Sulzberg	47.78 (-0.11)	50.78	0.72	9.58	0.83
AT34	Sonnblick	53.83 (-2.65)	54.53	0.61	7.69	0.78
AT37	Zillertalen Alpen	49.23 (-2.70)	56.81	0.63	11.22	0.68
AT38	Gerlitzen	50.95 (-2.31)	50.79	0.73	8.55	0.84
AT40	Masenberg	45.81 (-3.38)	47.50	0.78	8.20	0.87
AT41	Haunsberg	42.20 (-1.71)	47.87	0.81	9.86	0.86
AT42	Heidenreichstein	42.26 (-1.08)	45.30	0.83	8.57	0.88
AT43	Forsthof	38.29 (-6.14)	46.69	0.81	11.80	0.82
AT44	Graz Platte	44.66 (-1.91)	48.13	0.81	9.21	0.88
AT45	Dunkelsteinerwald	40.91 (-1.68)	45.49	0.82	10.82	0.87
AT46	Gaenserndorf	40.85 (-1.83)	45.92	0.84	10.02	0.89
AT47	Stixneusiedl	41.58 (-1.72)	46.02	0.84	9.74	0.89
AT48	Zoebelboden	44.18 (-1.10)	46.42	0.75	9.18	0.85
AT49	Grebenzen	49.36 (-0.44)	48.69	0.67	9.12	0.79
BE01	Offagne	38.66 (0.42)	43.54	0.77	9.26	0.83
BE32	Eupen	35.88 (2.37)	40.67	0.77	9.88	0.85
BE35	Vezin	35.36 (0.41)	41.72	0.80	10.55	0.84
CH01	Jungfraujoch	41.34 (-0.61)	56.37	0.52	17.81	0.45
CH02	Payerne	40.32 (-1.50)	47.94	0.74	12.89	0.78
CH03	Taenikon	40.68 (-1.07)	49.53	0.68	14.97	0.73
CH04	Chaumont	46.77 (-0.75)	47.93	0.73	8.37	0.85
CH05	Rigi	46.76 (-0.89)	50.79	0.71	10.03	0.81
DE01	Westerland/Wenningsted	41.84 (0.33)	42.70	0.79	6.95	0.87
DE02	Langenbruegge/Waldhof	37.94 (-0.48)	40.67	0.85	9.41	0.89
DE03	Schauinsland	46.00 (-1.44)	47.27	0.66	9.05	0.80
DE07	Neuglobsow	39.79 (0.61)	40.43	0.87	8.77	0.90
DE08	Schmuecke	42.39 (0.54)	42.70	0.73	9.29	0.85
DE09	Zingst	36.27 (-0.18)	40.59	0.78	8.74	0.83
FR08	Donon	42.70 (-2.39)	44.90	0.74	9.11	0.85
FR09	Revin	37.94 (-0.34)	43.37	0.79	9.51	0.84

continued on next page

Code	Station	Obs.	Mod.	r	RMSE	IOA
FR10	Morvan	39.54 (0.93)	44.44	0.76	8.26	0.82
FR12	Iraty	47.31 (-2.45)	46.56	0.73	6.28	0.84
FR13	Peyrusse Vieille	39.57 (1.67)	42.31	0.43	10.86	0.64
FR14	Montandon	38.12 (-1.30)	46.73	0.69	12.21	0.73
FR15	La Tardiere	39.57 (1.39)	42.43	0.72	8.99	0.82
FR16	Le Casset	51.64 (-1.92)	49.40	0.68	9.27	0.79
FR17	Montfranc	41.59 (-0.28)	44.79	0.67	7.58	0.79
FR18	La Coulonche	40.03 (N.A.)	42.21	0.82	6.23	0.89
GB02	Eskdalemuir	36.57 (0.73)	42.01	0.81	7.78	0.81
GB06	Lough Navar	33.39 (1.56)	42.00	0.84	9.86	0.75
GB13	Yarner Wood	38.30 (0.33)	43.15	0.79	7.77	0.83
GB14	High Muffles	37.46 (2.87)	42.13	0.71	9.58	0.76
GB15	Strath Vaich Dam	42.99 (2.83)	42.33	0.83	5.46	0.89
GB31	Aston Hill	41.12 (2.34)	42.84	0.81	5.78	0.89
GB32	Bottesford	35.78 (1.51)	39.73	0.81	7.96	0.87
GB33	Bush	36.75 (1.59)	40.65	0.79	6.88	0.84
GB34	Glazebury	34.64 (1.04)	37.97	0.81	7.60	0.86
GB35	Great Dun Fell	34.61 (-2.25)	42.53	0.72	10.35	0.72
GB36	Harwell	34.50 (0.16)	40.59	0.81	8.93	0.83
GB37	Ladybower	37.73 (2.59)	40.12	0.81	6.56	0.88
GB38	Lullington Heath	39.10 (2.34)	43.10	0.74	8.55	0.82
GB39	Sibton	41.97 (7.04)	42.57	0.66	9.01	0.79
GB43	Narberth	37.72 (3.72)	42.28	0.76	7.84	0.82
GB45	Wicken Fen	38.06 (-2.08)	41.05	0.82	7.42	0.89
GB48	Auchencorth Moss	37.57 (N.A.)	40.56	0.81	6.33	0.87
GB49	Weybourne	40.80 (N.A.)	41.40	0.73	7.88	0.84
GB50	St. Osyth	37.56 (N.A.)	38.59	0.77	7.37	0.86
GB51	Market Harborough	38.52 (N.A.)	40.47	0.81	7.08	0.88
GB52	Lerwick	40.44 (N.A.)	43.46	0.68	6.82	0.79
GB53	Charlton Mackrell	31.88 (N.A.)	35.59	0.80	5.87	0.83
IE31	Mace Head	43.24 (1.08)	43.59	0.80	5.03	0.89
NL07	Eibergen	29.61 (-0.48)	40.18	0.82	13.27	0.78
NL09	Kollumerwaard	34.56 (-3.23)	41.22	0.84	9.49	0.84
NL10	Vreedepeel	31.22 (-0.80)	40.27	0.84	12.13	0.83
NL11	Cabauw	29.71 (N.A.)	38.75	0.84	11.74	0.82
NL91	De Zilk	33.22 (N.A.)	43.13	0.76	13.14	0.75
		Mediterranean Countries and Portugal				
ES07	Viznar	51.42 (-2.02)	48.99	0.66	7.39	0.77
ES08	Niembro	42.29 (-0.47)	46.73	0.78	7.10	0.82
ES09	Campisabalos	50.84 (5.35)	47.87	0.78	8.49	0.82
ES10	Cabo de Creus	44.42 (-1.33)	49.77	0.78	8.83	0.83
ES11	Barcarrota	44.70 (0.39)	46.43	0.73	7.43	0.79

continued on next page

Code	Station	Obs.	Mod.	r	RMSE	IOA
ES12	Zarra	47.84 (1.74)	47.98	0.79	7.57	0.87
ES13	Penausende	48.94 (0.76)	45.79	0.73	7.54	0.80
ES14	Els Torms	47.57 (-0.92)	47.83	0.83	7.26	0.90
ES16	O Savinao	40.93 (-2.08)	44.34	0.68	8.48	0.76
GR02	Finokalia	51.98 (N.A.)	54.78	0.69	8.19	0.77
IT01	Montelibretti	49.21 (-0.78)	53.06	0.84	10.35	0.88
IT04	Ispra	40.40 (6.89)	62.40	0.75	26.28	0.67
MT01	Giordan lighthouse	53.61 (4.30)	53.86	0.66	6.90	0.81
SI08	Iskrba	42.46 (7.23)	48.01	0.76	12.09	0.81
SI31	Zarodnje	40.93 (-3.65)	50.11	0.82	11.84	0.79
SI32	Krvavec	53.45 (-1.31)	49.90	0.75	9.54	0.82
SI33	Kovk	39.73 (-3.50)	47.89	0.74	12.53	0.78

Nordic sites

In addition to the statistics for the Nordic sites listed in Table 2.1, measured and modelled ozone levels are compared for Nordic sites in Figures 2.1-2.3. The model performance is similar to previous years (Simpson 2006, Jonson et al. 2007, Simpson and Hjellbrekke 2008, Gauss and Hjellbrekke 2009). At Spitzbergen (NO42), which is far away from the major emission sources, the model has some problems capturing the sudden drop in ozone observed in April. The correlation at this station is among the lowest in the Nordic area (0.61). Other stations where the correlation with model data is relatively low are Kaarvatn (NO39), Sandve (NO52), Aehtaeri II (FI37) and Raae (SE14). These stations, except SE14 and NO52 are also the only stations with an index of agreement below 0.8. Generally the performance is relatively good with high correlations and low biases. It is also worth noting that the ozone values are close to the 5-year mean at nearly all stations. The same can be said about the other regions, discussed in the following paragraphs.

Eastern European sites

Measured and modelled maximum ozone levels for sites in the Eastern European region are shown in Figures 2.4 and 2.5. These sites are mostly typical continental sites with a clear summer maximum, reflecting local/regional ozone production in summer, and a winter minimum. In general the model performance is rather good, and in line with the performance in previous years. However this year the model has higher concentration than observed at all Eastern European stations except Chopok (SK02), Stara Lesna (SK04) and Sniezka (PL03). The overestimation of ozone is highest during autumn. Relatively high bias are found at Preila (LT15), with the model overestimating ozone. The index of agreement (IOA) is below 0.74 at this station.

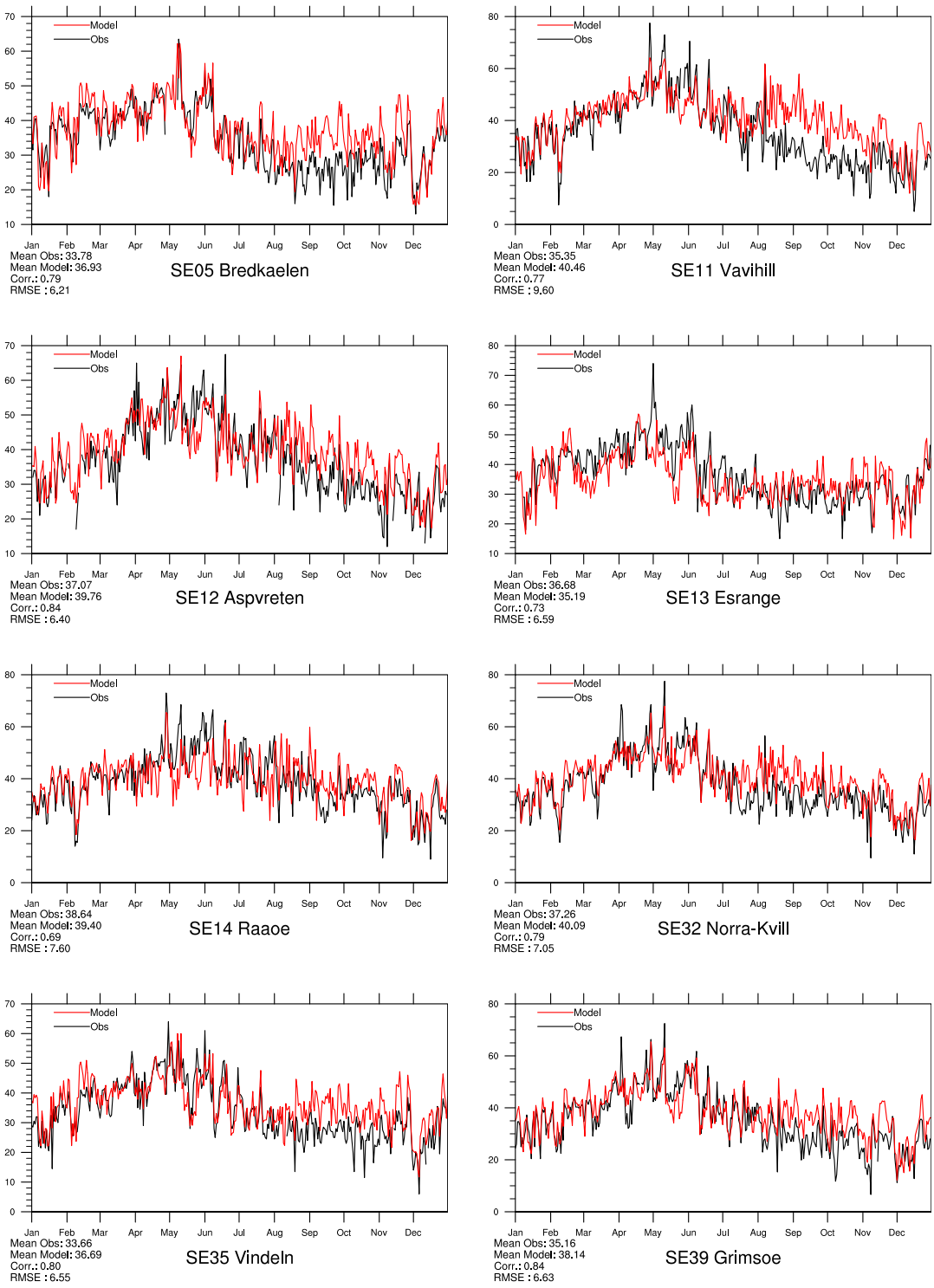

Figure 2.1: Modelled versus Observed Daily Maximum Ozone (ppb) at Swedish sites for 2008. Note that in some plots the vertical axis does not start at zero.

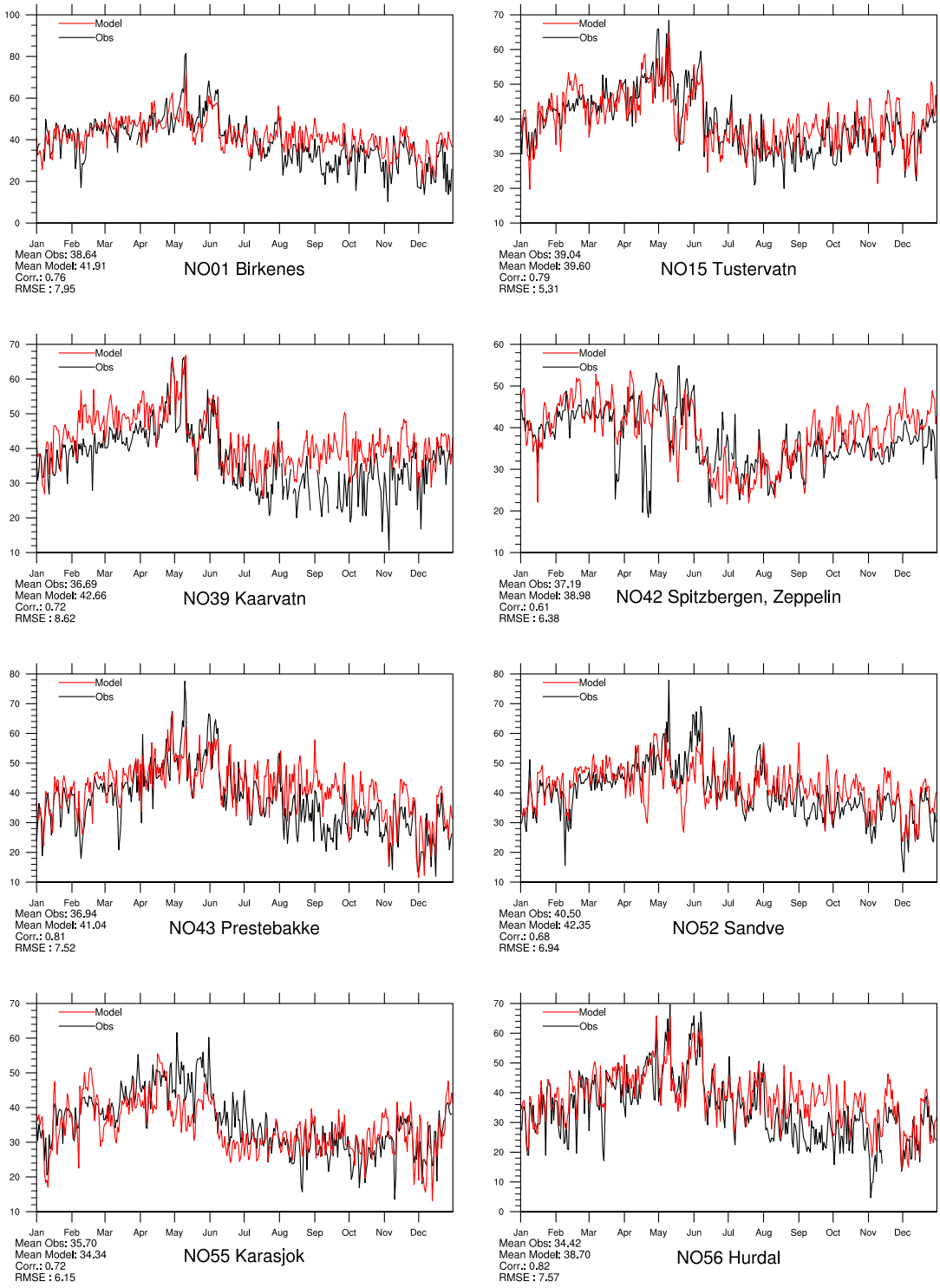

Figure 2.2: Modelled versus Observed Daily Maximum Ozone (ppb) at Norwegian sites for 2008. Note that in some plots the vertical axis does not start at zero.

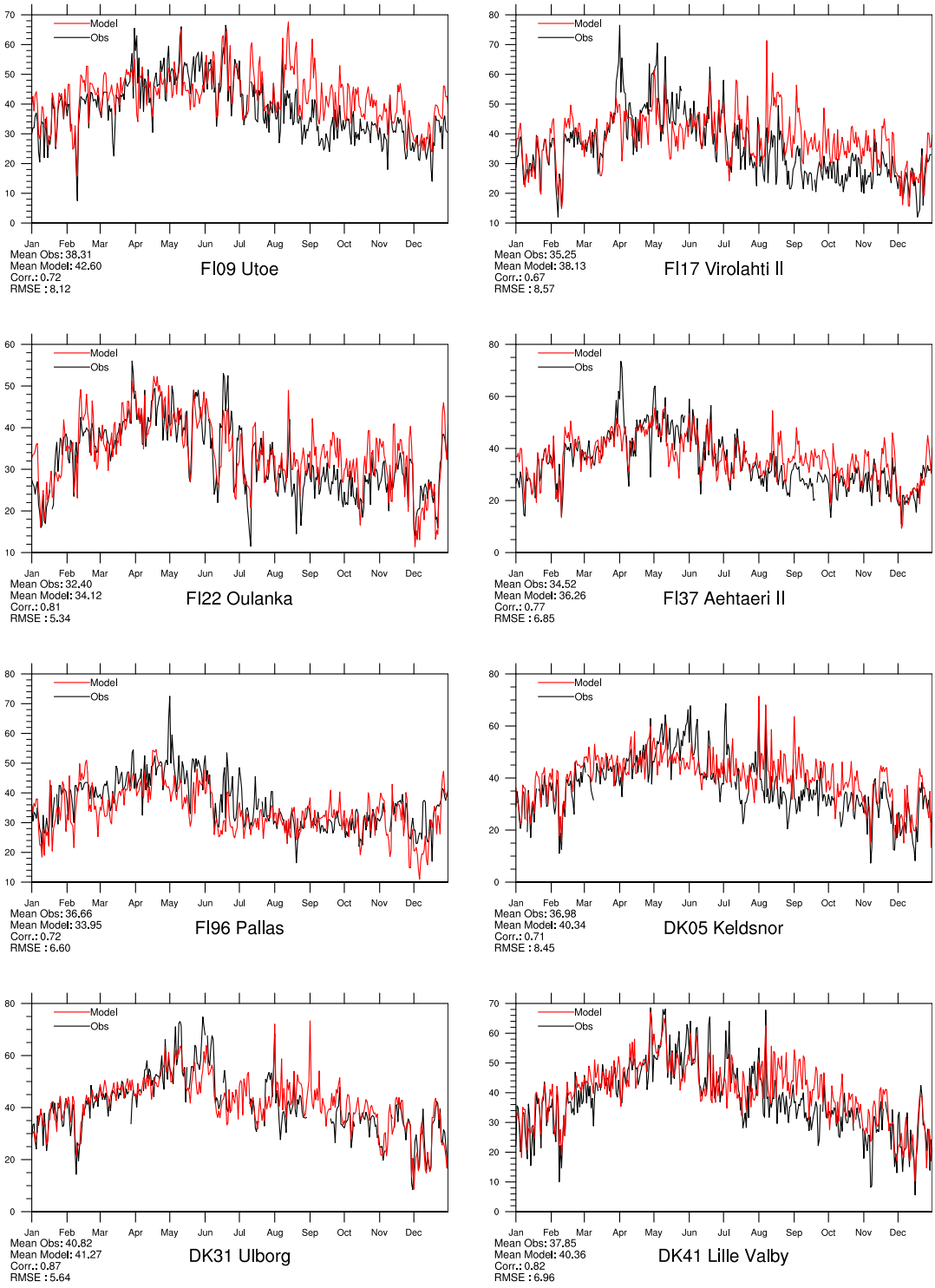

Figure 2.3: Modelled versus Observed Daily Maximum Ozone (ppb) at Danish and Finnish sites for 2008. Note that in some plots the vertical axis does not start at zero.

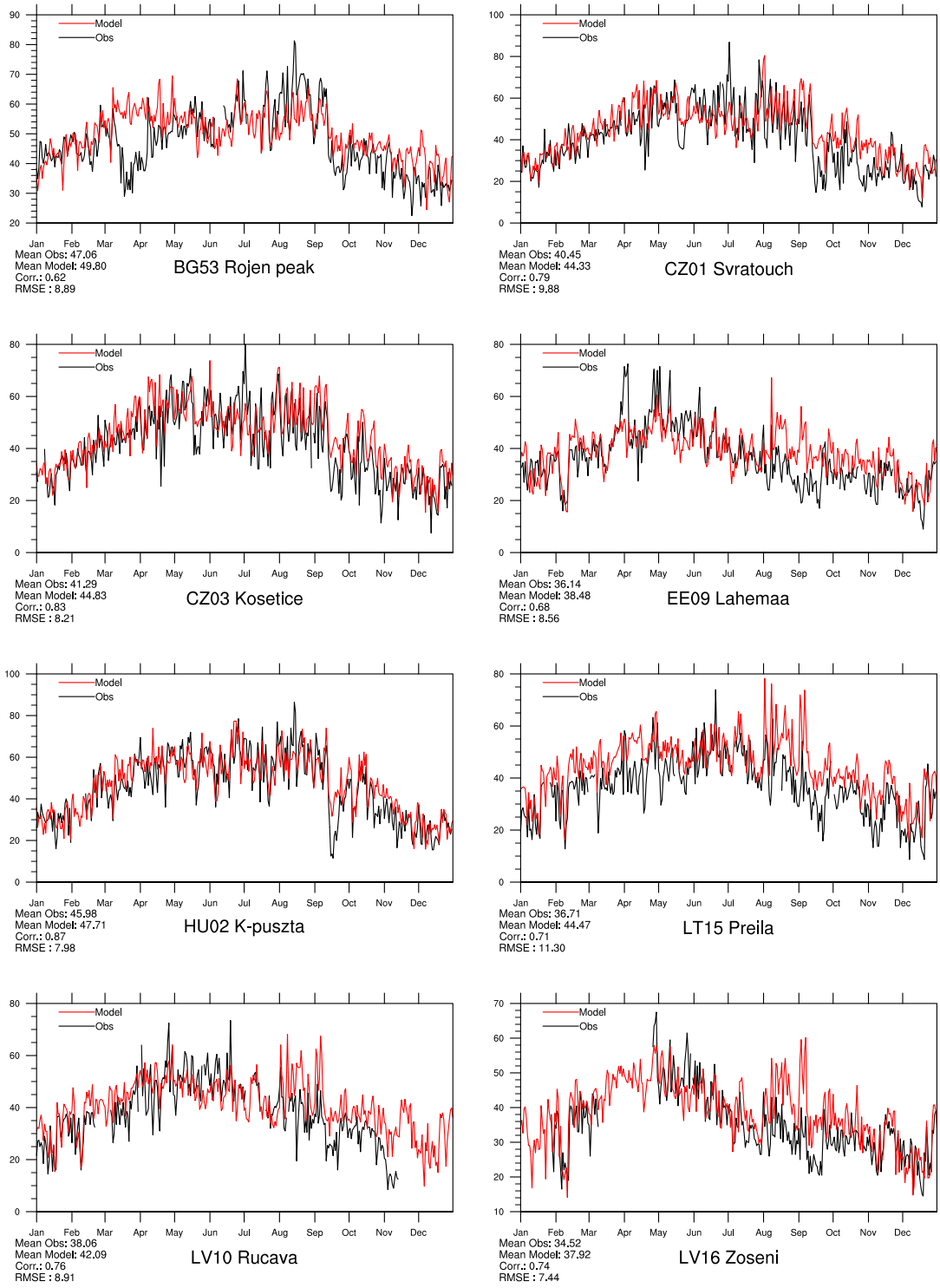

Figure 2.4: Modelled versus Observed Daily Maximum Ozone (ppb) at Eastern European sites for 2008. Note that in some plots the vertical axis does not start at zero.

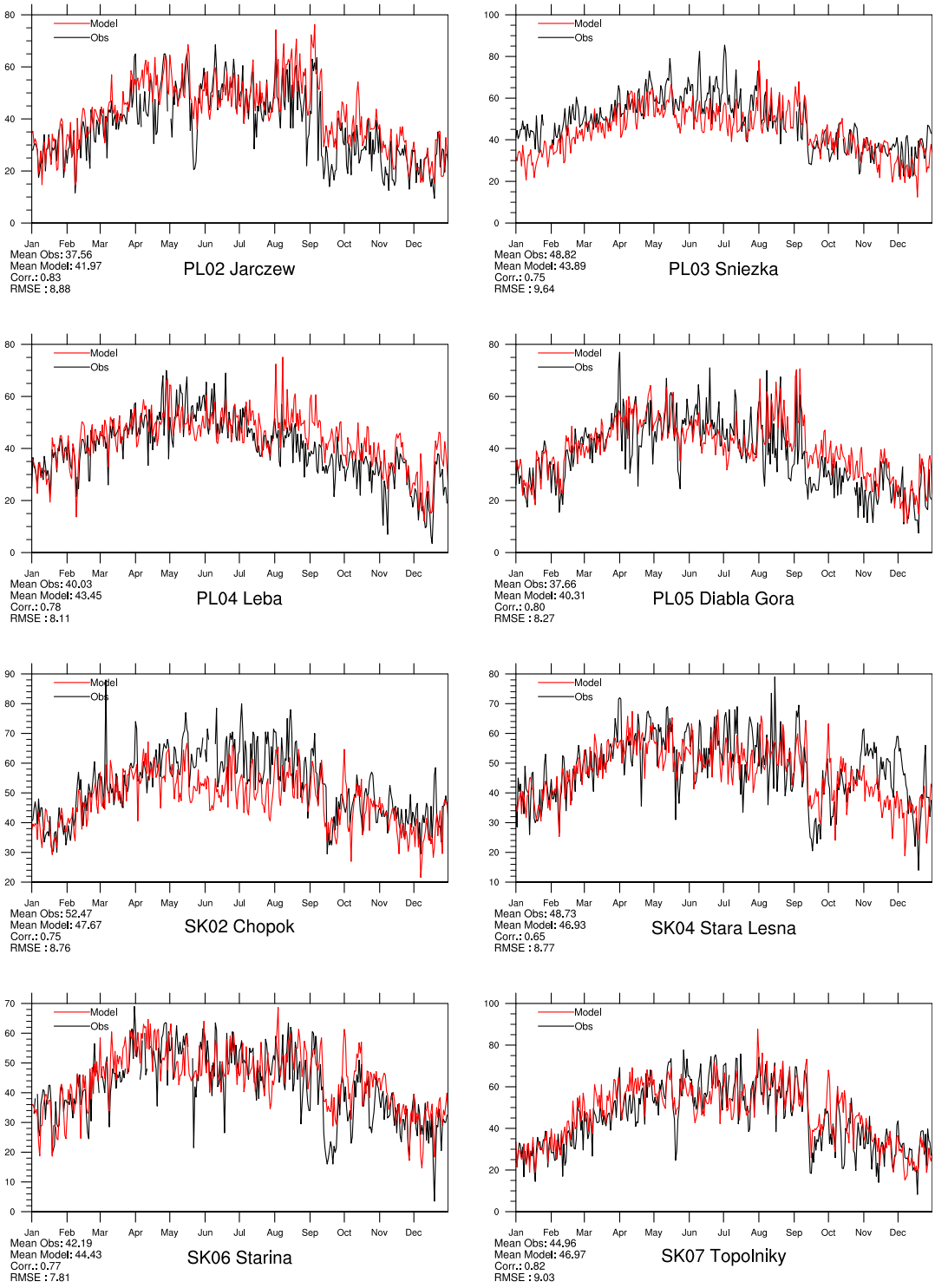

Figure 2.5: Modelled versus Observed Daily Maximum Ozone (ppb) at Eastern European sites for 2008. Note that in some plots the vertical axis does not start at zero.

Central and Northwestern European sites

Measured and modelled maximum ozone levels for selected sites in Central and Northwestern Europe are shown in Figures 2.6-2.14. These sites are mainly typical continental sites with a clear summer maximum, reflecting local/regional ozone production in summer, and a winter minimum. Concentrations at the site Mace Head in Ireland are partly used to specify background conditions for the EMEP model, so good performance for the seasonal cycle is guaranteed.

The overall model performance is very good in this area with many correlations better than 0.8 and small biases. However, there are some exceptions with low correlations, such as Jungfraujoch (CH01) and Peyrusse Vieille (FR13). At Jungfraujoch the index of agreement is low and bias is high, which might be explained by the fact that this is a mountain site (3578 m.a.s). Because of its high elevation, for a long-term run, this site will often be above the boundary layer, especially in the winter. With the coarse topography in the regional scale model, this cannot be well captured by the model. Overestimations of ozone are seen at the Dutch stations, but these show a good correlation ($>$0.8 except NL91 r=0.76). This year there are lower measured ozone concentrations compared to the measured 5 year's mean (Table 2.1).

Mediterranean sites

A special section about the Mediterranean has been included in this year's status report (Aas et al. 2010) Measured and modelled ozone levels for selected sites in the Mediterranean region are shown in Figures 2.15 and 2.17. The meteorological situation in and around the Mediterranean basin differs considerably from the rest of Europe. This region also receives more solar radiation resulting in conditions favourable for ozone production. Hence these sites have some of the highest ozone levels in Europe. In general the model performance is good for most sites in this region.

Relatively high biases are found at Zarodnje (SI31), Kovk (SI33) and Ispra (IT04), with the model overestimating ozone in all three cases. The index of agreement (IOA) is below 0.8 at all these three stations.

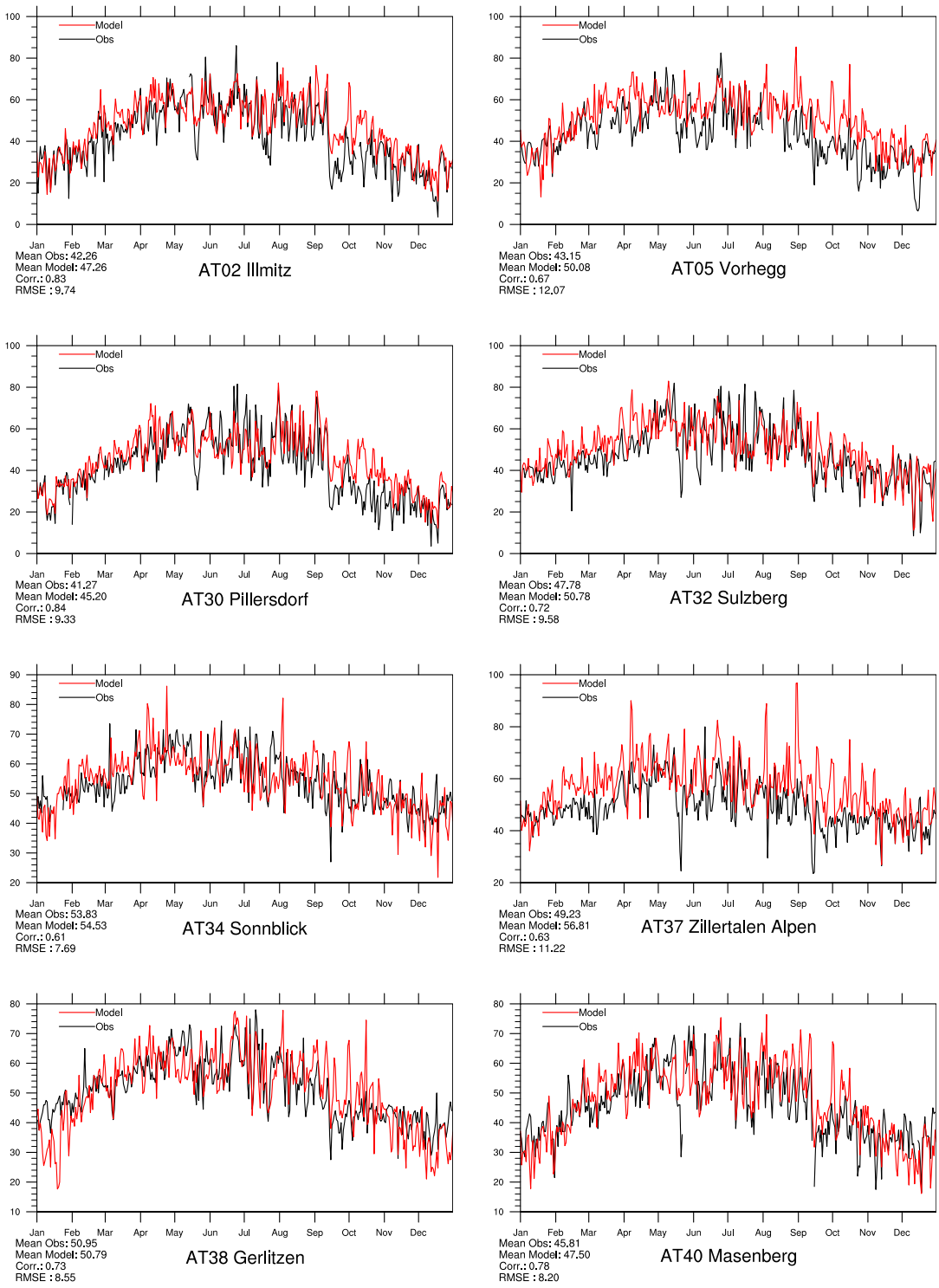

Figure 2.6: Modelled versus Observed Daily Maximum Ozone (ppb) at Austrian sites for 2008. Note that in some plots the vertical axis does not start at zero.

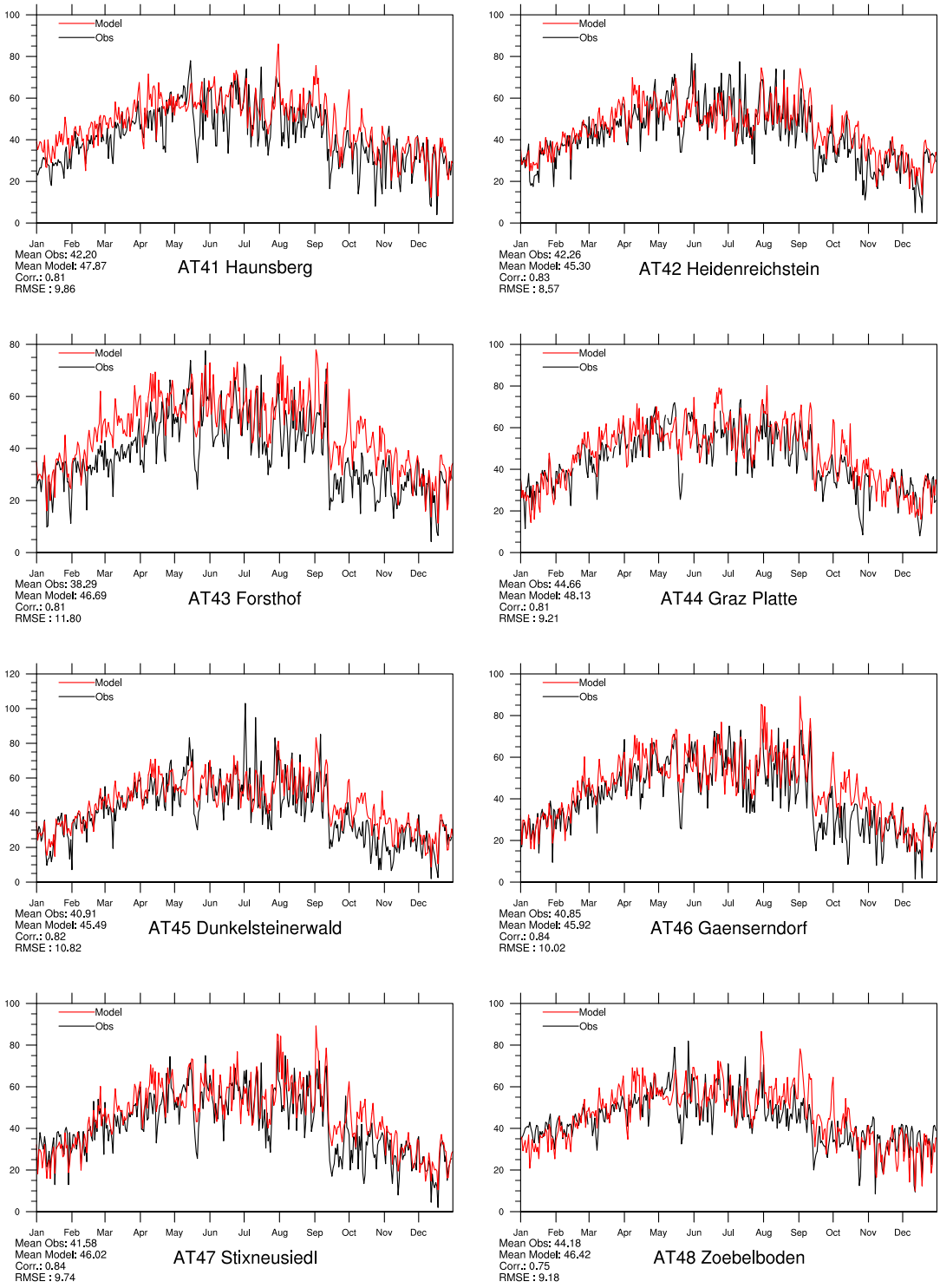

Figure 2.7: Modelled versus Observed Daily Maximum Ozone (ppb) at Austrian sites for 2008. Note that in some plots the vertical axis does not start at zero.

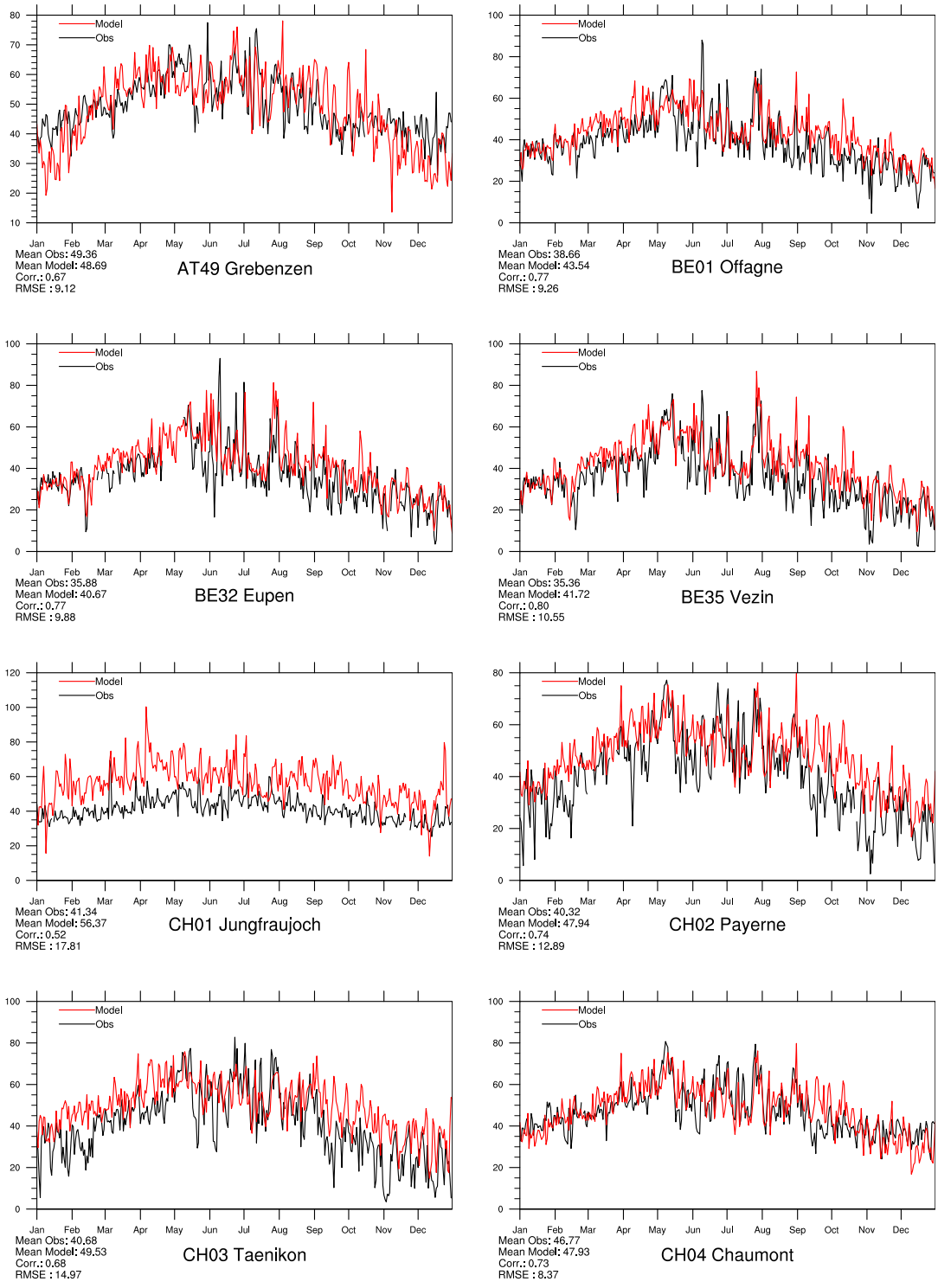

Figure 2.8: Modelled versus Observed Daily Maximum Ozone (ppb) at sites in Austria, Belgium, and Switzerland for 2008. Note that in some plots the vertical axis does not start at zero.

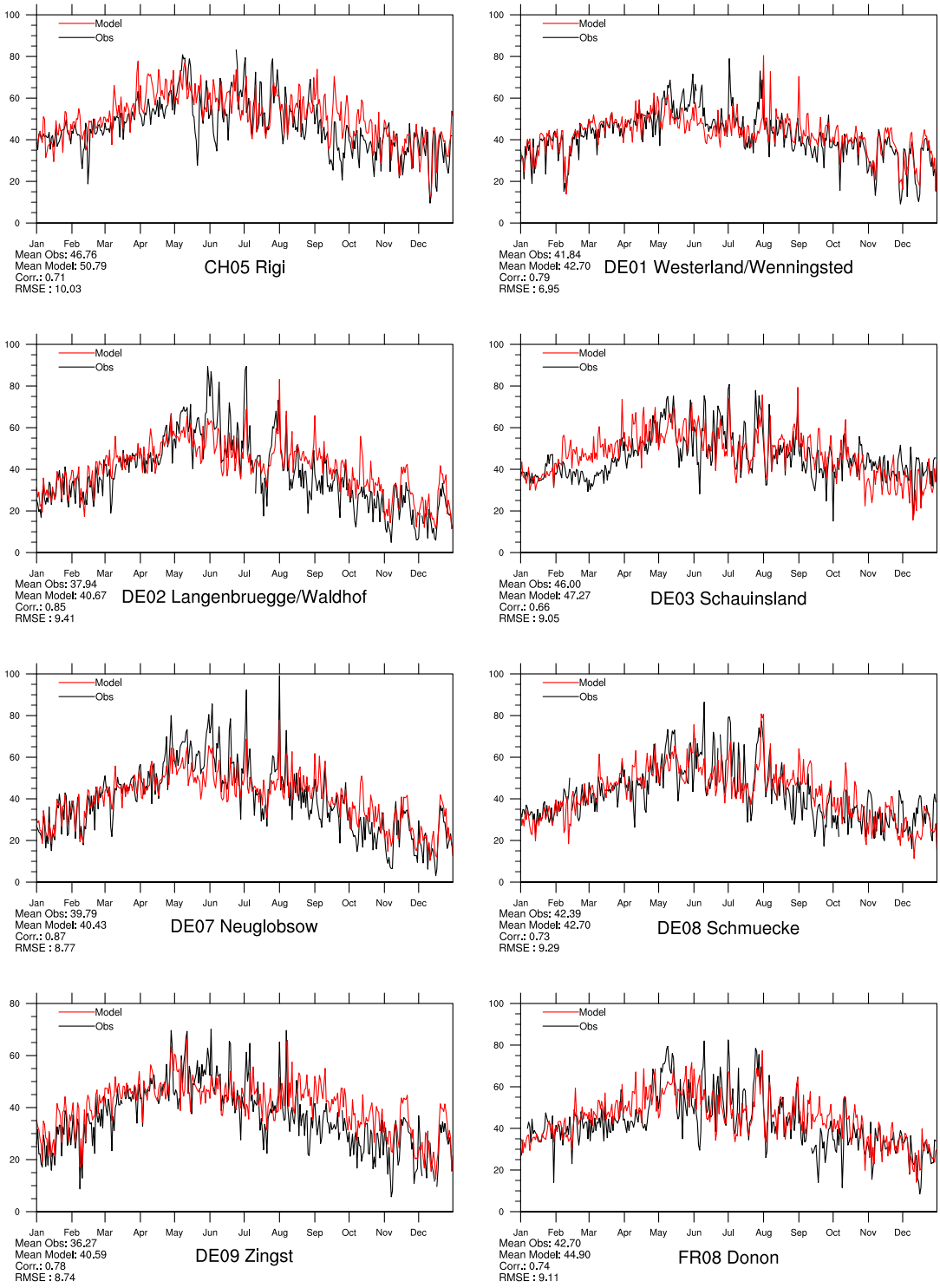

Figure 2.9: Modelled versus Observed Daily Maximum Ozone (ppb) at sites in Switzerland, Germany, and France for 2008. Note that in some plots the vertical axis does not start at zero.

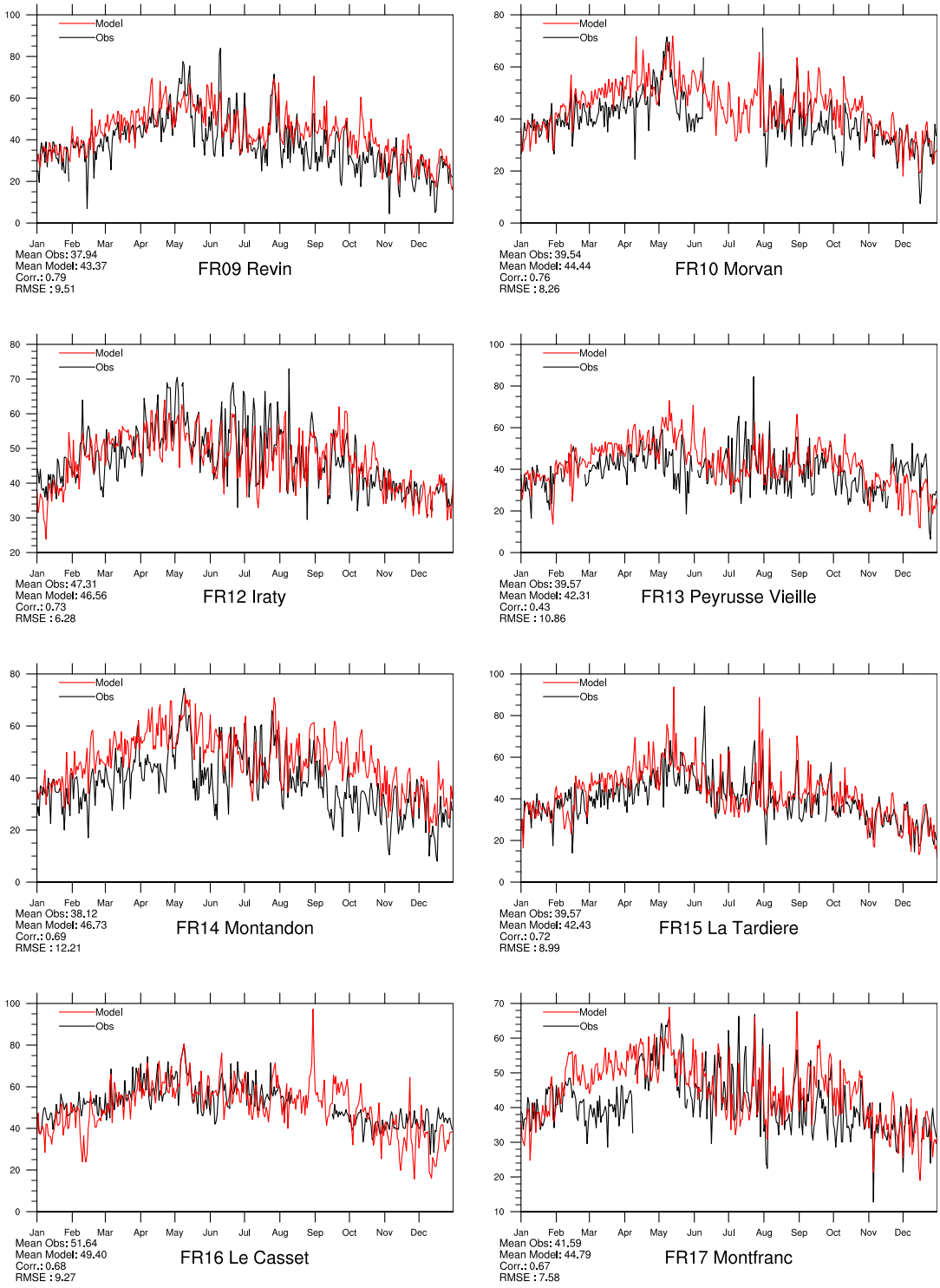

Figure 2.10: Modelled versus Observed Daily Maximum Ozone (ppb) at French sites for 2008. Note that in some plots the vertical axis does not start at zero.

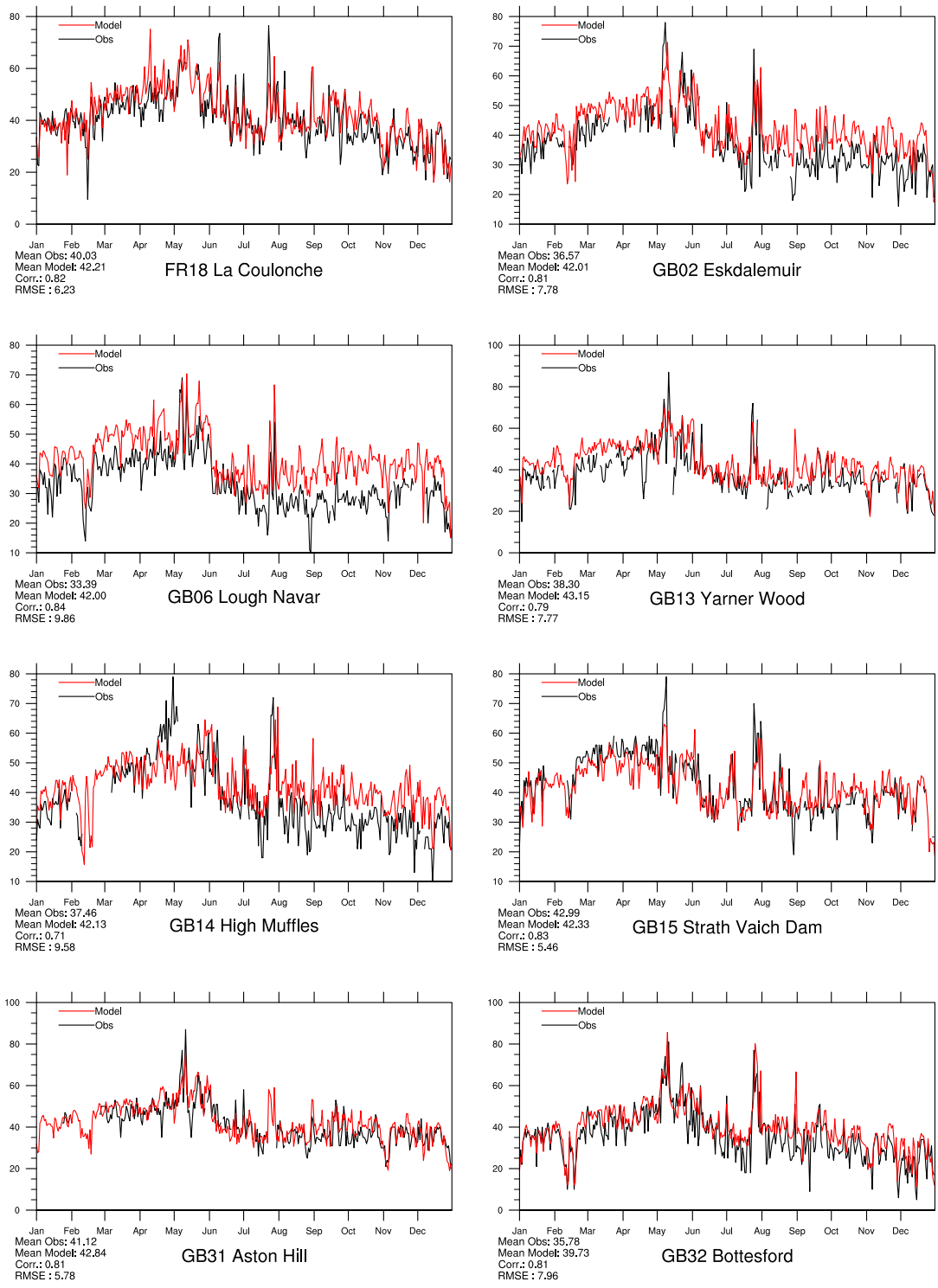

Figure 2.11: Modelled versus Observed Daily Maximum Ozone (ppb) at French and British sites for 2008. Note that in some plots the vertical axis does not start at zero.

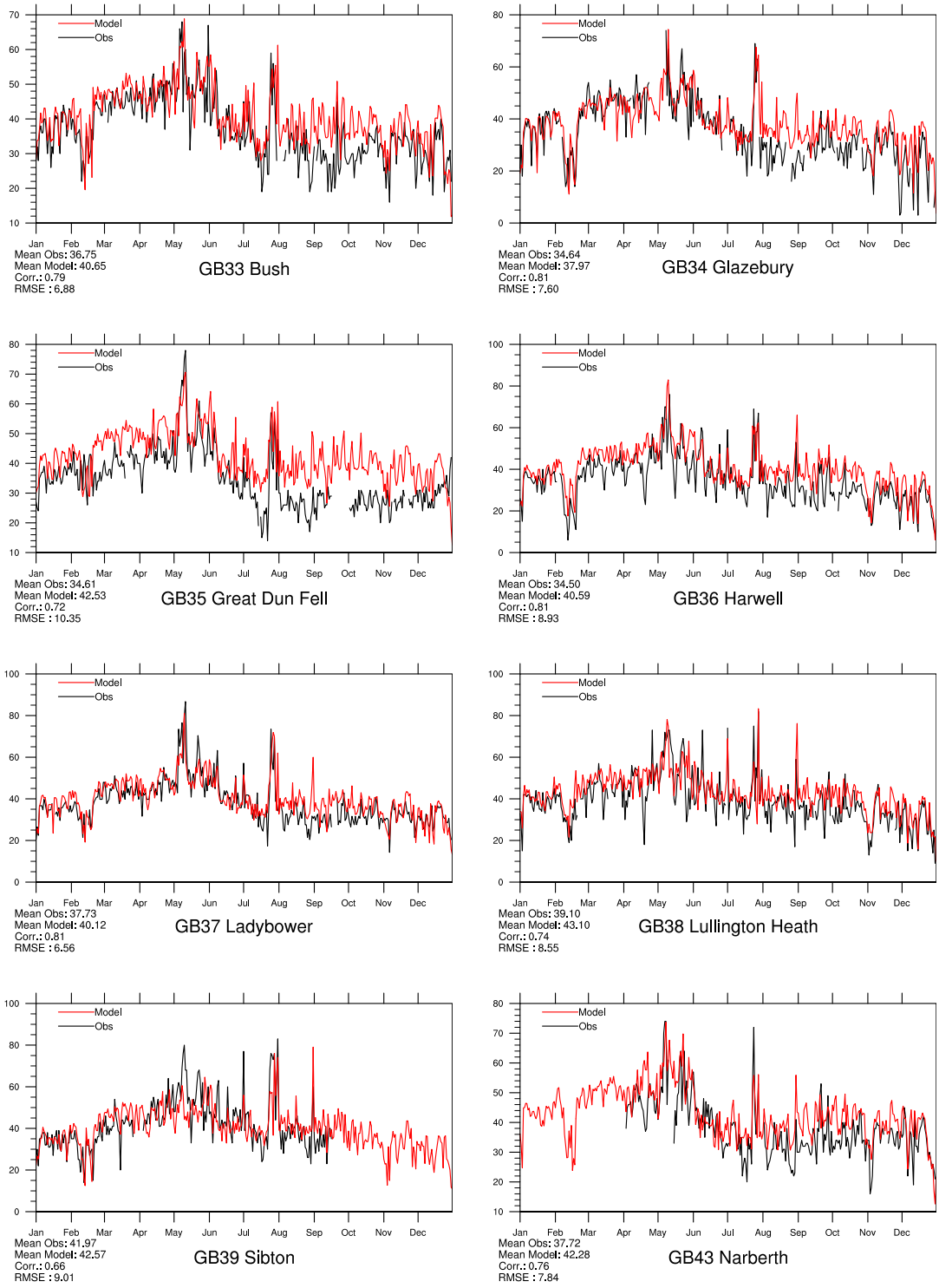

Figure 2.12: Modelled versus Observed Daily Maximum Ozone (ppb) at British sites for 2008. Note that in some plots the vertical axis does not start at zero.

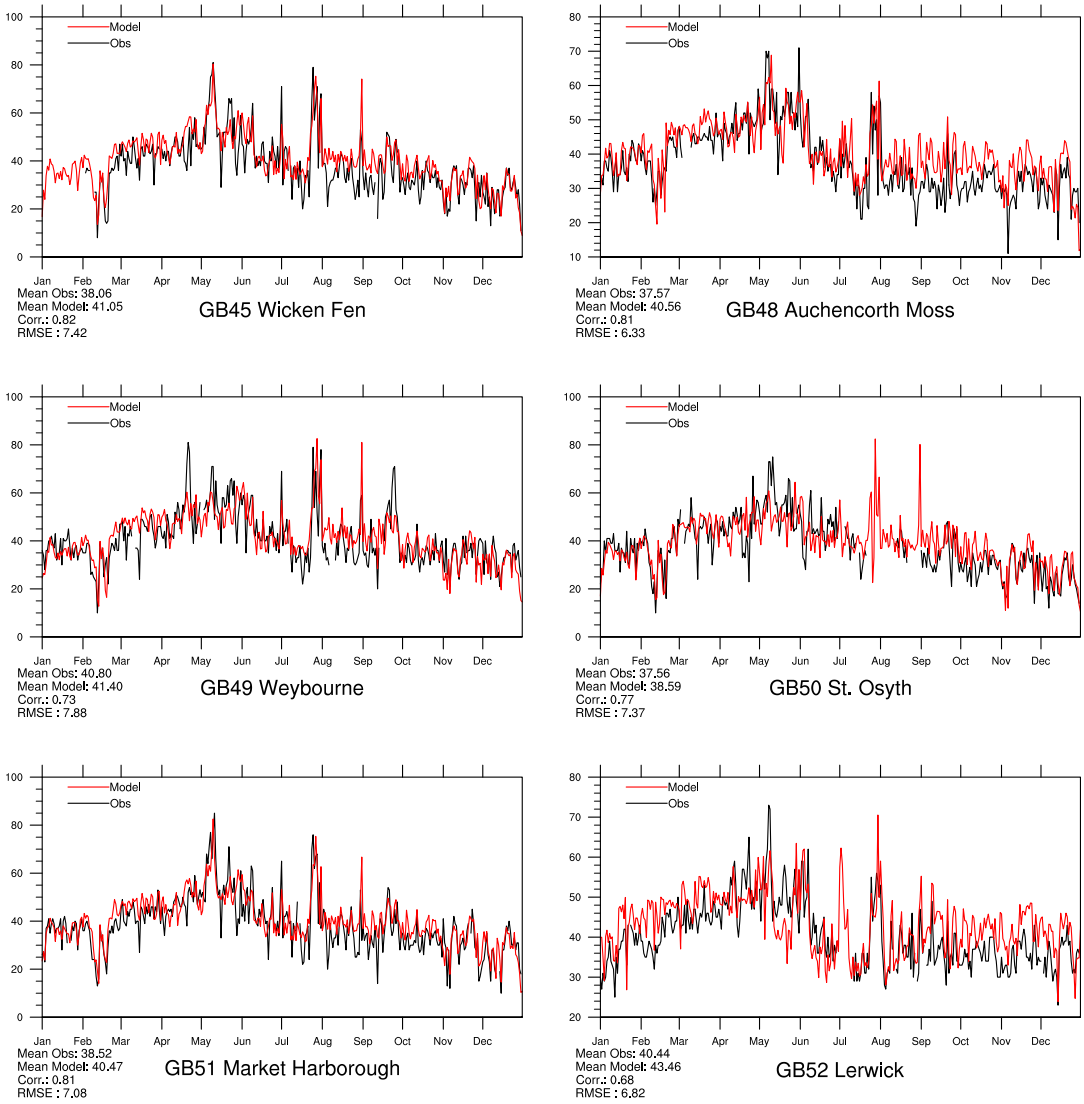

Figure 2.13: Modelled versus Observed Daily Maximum Ozone (ppb) at British sites for 2008. Note that in some plots the vertical axis does not start at zero.

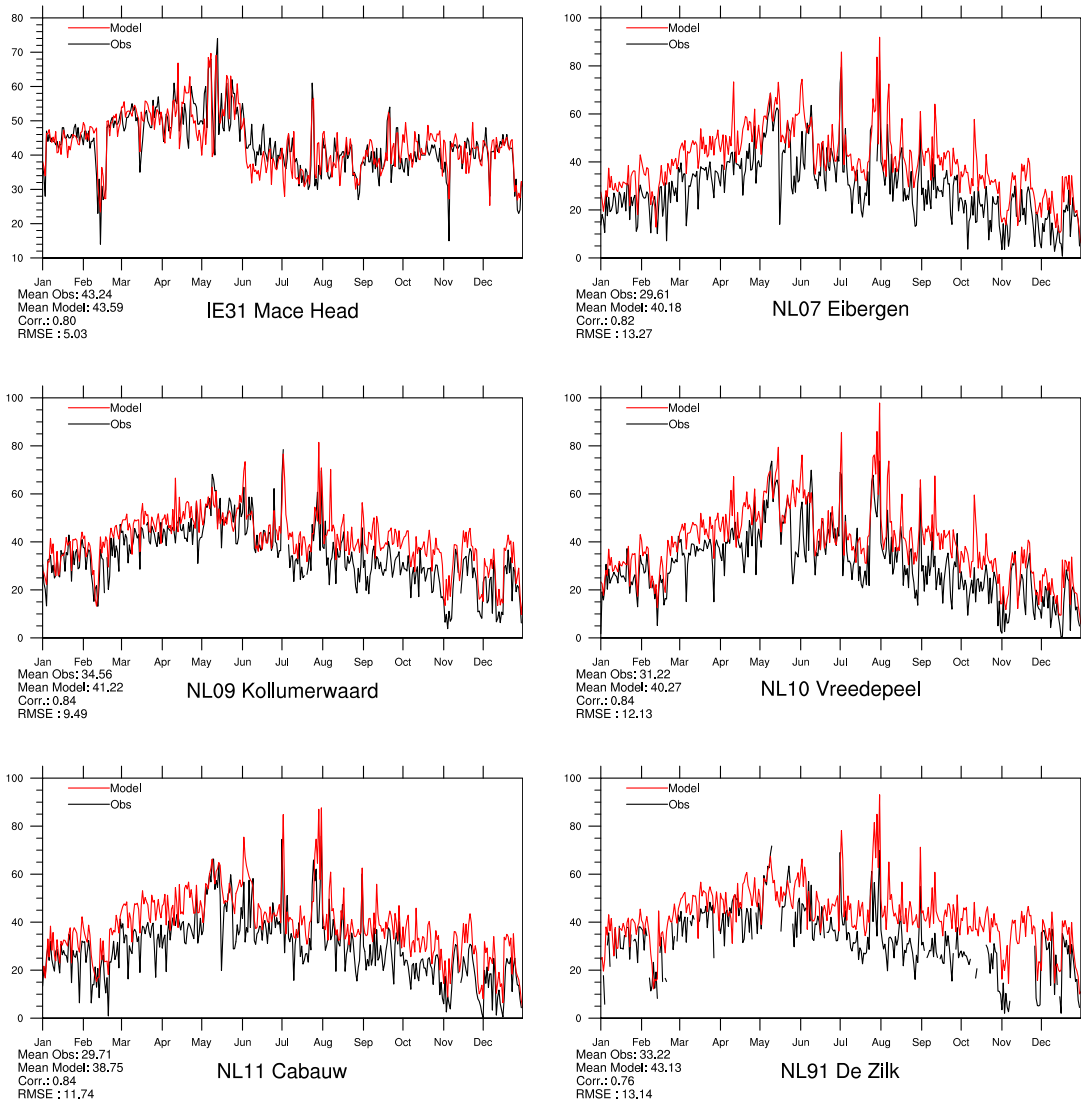

Figure 2.14: Modelled versus Observed Daily Maximum Ozone (ppb) at sites in Ireland and the Netherlands for 2008. Note that in some plots the vertical axis does not start at zero.

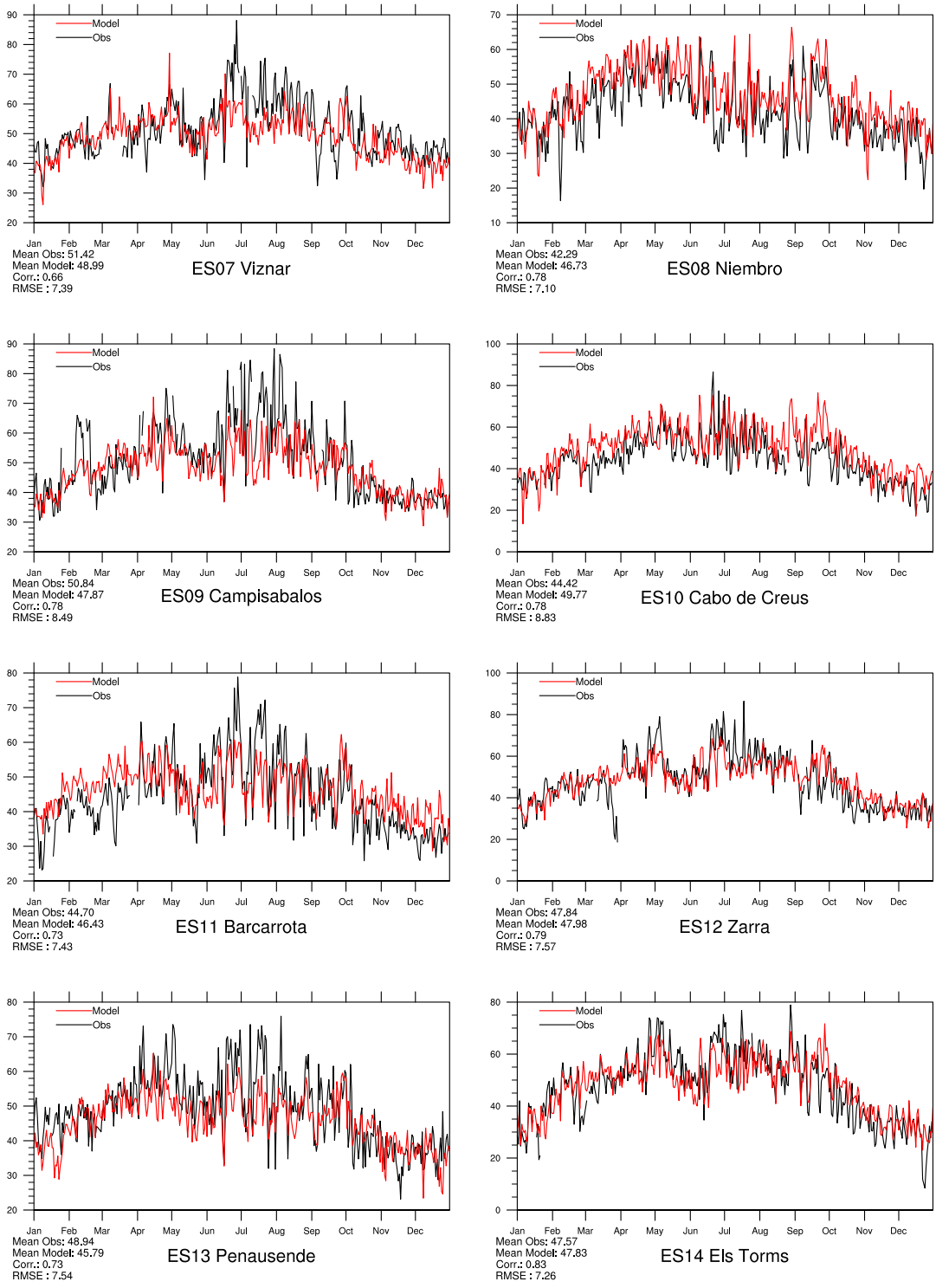

Figure 2.15: Modelled versus Observed Daily Maximum Ozone (ppb) at Spanish sites for 2008. Note that in some plots the vertical axis does not start at zero.

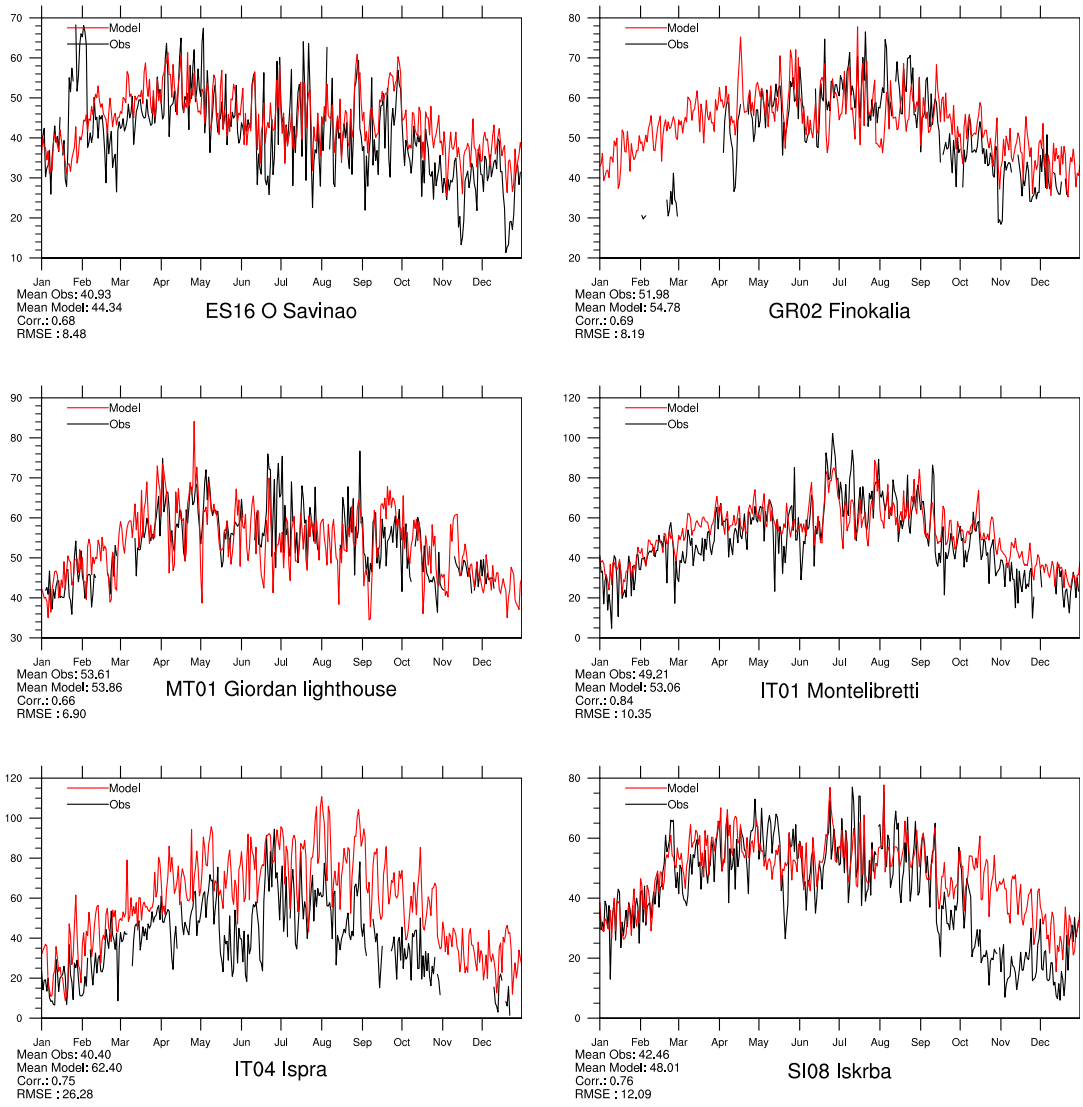

Figure 2.16: Modelled versus Observed Daily Maximum Ozone (ppb) at Mediterranean Sites for 2008. Note that in some plots the vertical axis does not start at zero.

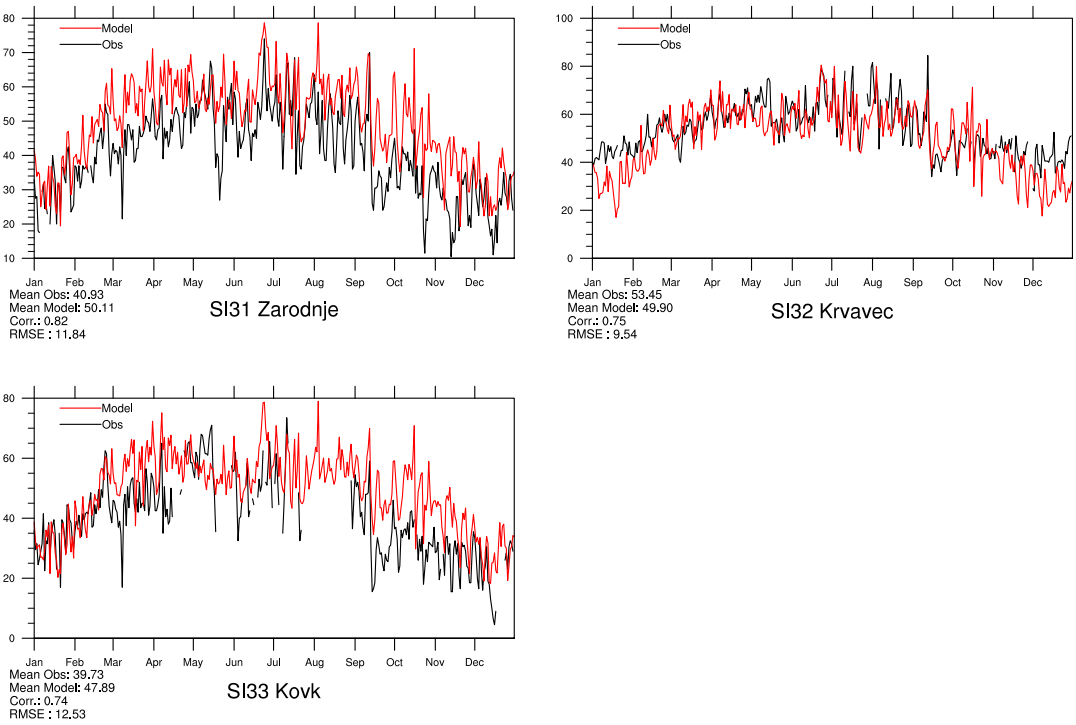

Figure 2.17: Modelled versus Observed Daily Maximum Ozone (ppb) at Mediterranean Sites for 2008. Note that in some plots the vertical axis does not start at zero.

2.2 Combined model results and observations, 2008

In this section we present 'best estimates' for concentrations of ozone and NO_2. The 'best estimates' have been created by using a combination of model results and observations from the EMEP network for 2008 and are shown in Figures 2.19-2.20.

2.2.1 Method

For all measurement points, the difference between the measured value at that point and the modelled value in the corresponding grid cell is calculated. This difference is interpolated spatially using radial basis functions, giving a continuous two-dimensional function describing the difference at any point within the modelled grid. The combined maps are derived adjusting the model calculations with the interpolated differences, giving large weight to the observed values close to stations, and using the modelled values in areas with no observations. The range of influence of the measured values depends on the component, but has been set to 500 km for ozone and NO_2.

2.2.2 Ozone

Figure 2.18 shows maps of modelled and combined model-obs daily maximum ozone levels, as annual averages. The normalised error is also shown. In general the normalised errors are relatively small, within 5% over large parts of Europe, and almost always within 10%.

2.2.3 NO_2

Figure 2.20 shows maps of model calculated and combined model-observed annually averaged daily mean NO_2 concentrations, along with the normalised error. NO_2 is a difficult compound, in that it has a short lifetime in the atmosphere, and the variability within the 50×50 km^2 grid is large. Normalised errors are larger than for ozone, but still most areas of Europe show normalised errors within the $\pm$18% band shown in Figure 2.20(c). The influence of a few sites is very evident though, e.g. in southern Greece or Turkey where the model significantly under-predicts the observed NO_2 concentrations.

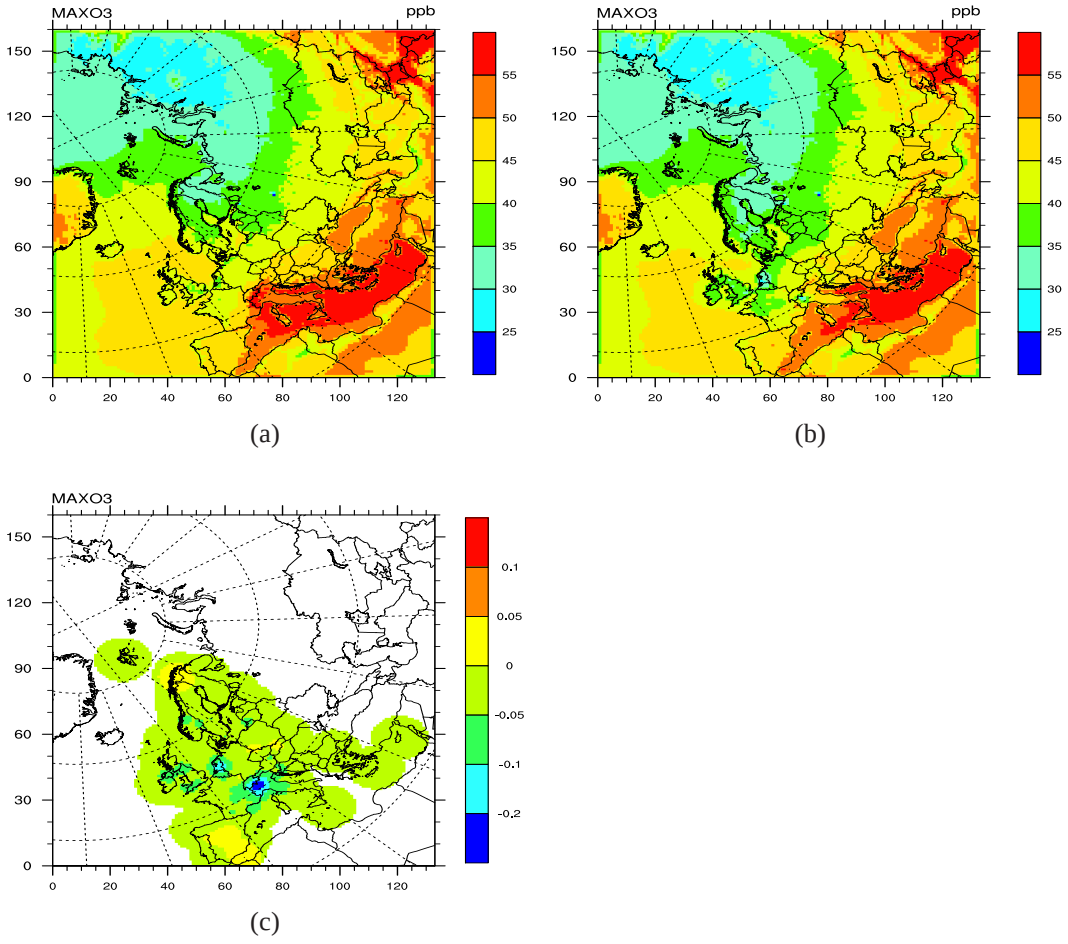

Figure 2.18: Average of daily maximum ozone in 2008. a: modelled concentrations, b: 'combined' (model+obs.) concentrations, and c: normalised errors. Concentration maps have units of ppb. For the maps of normalised error, positive values denote model under-prediction, and negative values model over-prediction.

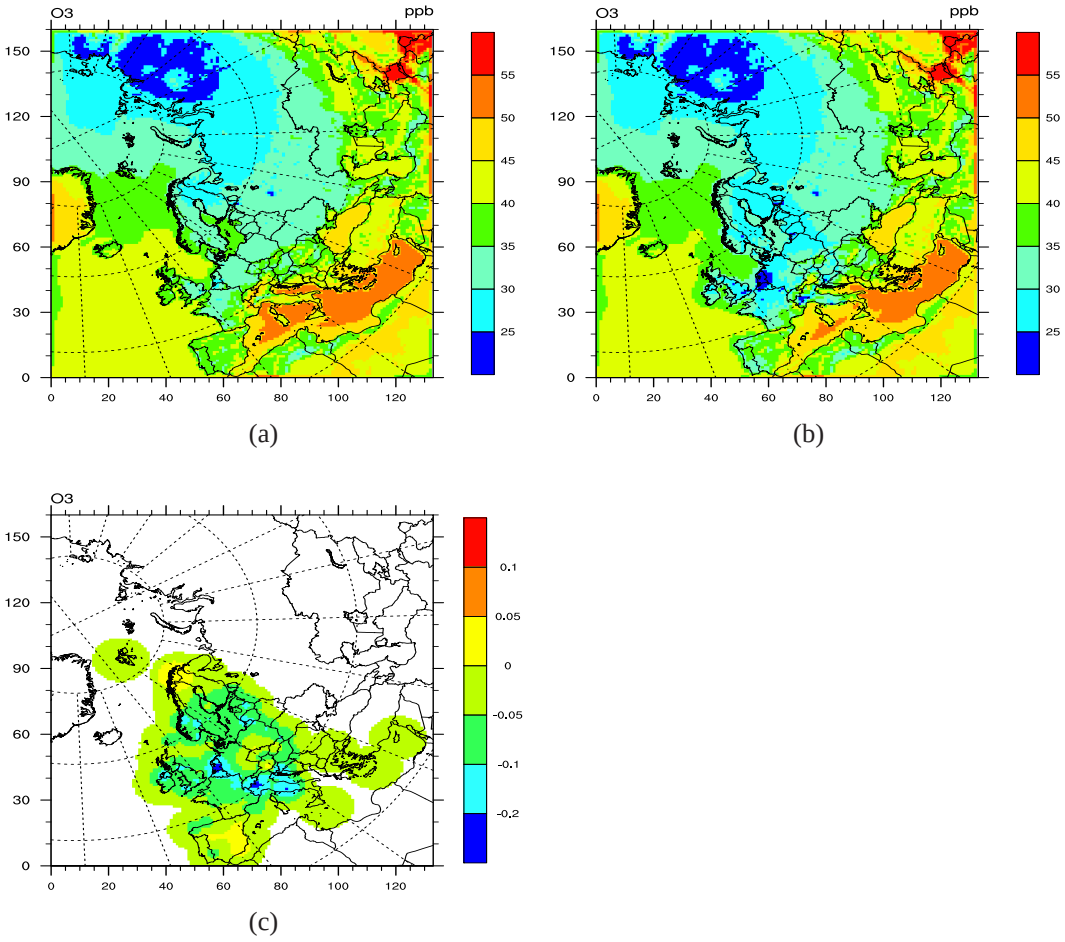

Figure 2.19: Daily mean ozone in 2008. a: modelled concentrations, b: 'combined' (model+obs.) concentrations, and c: normalised errors. Concentration maps have units of ppb. For the maps of normalised error, positive values denote model under-prediction, and negative values model over-prediction.

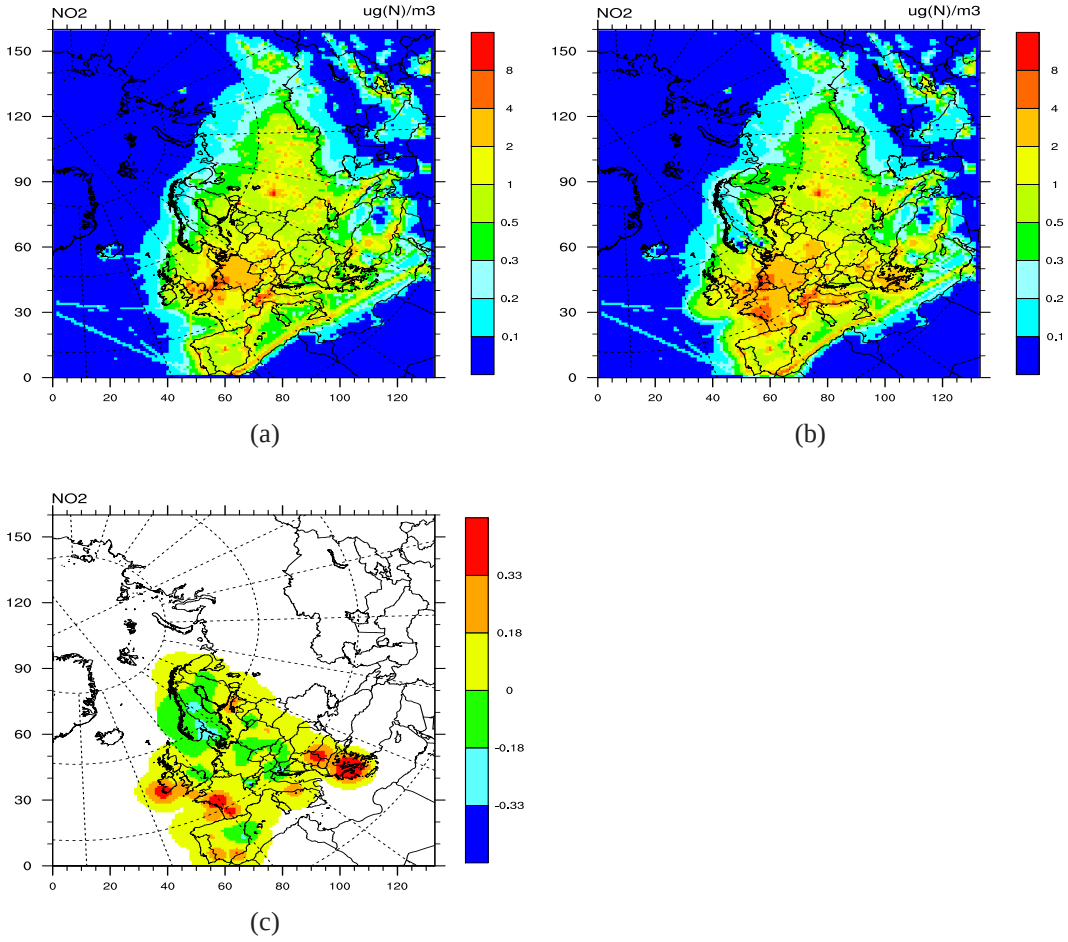

Figure 2.20: NO_2 in 2008. a: modelled concentrations, b: 'combined' (model+obs.) concentrations, and c: normalised errors. Concentration maps have units of μg(N) m^{-3}. For the maps of normalised error, positive values denote model under-prediction, and negative values model over-prediction.

References

Wenche Aas, Sverre Solberg, Michael Gauss, and David Simpson. The Mediterranean region. In *Transboundary Acidification, Eutrophication and Ground Level Ozone in Europe in 2008. EMEP Status Report 1/2010*. The Norwegian Meteorological Institute, Oslo, Norway, 2010.

M. Gauss and A.-G. Hjellbrekke. Photo-oxidants: validation and combined maps. Supplementary material to emep status report 1/2009, available online at `www.emep.int`, The Norwegian Meteorological Institute, Oslo, Norway, 2009.

J.E. Jonson, L. Tarrasón, A. Benedictow, and A.G. Hjeĺbrekke. Photo-oxidants, status in 2005. In *In Transboundary Acidification, Eutrophication and Ground Level Ozone in Europe. EMEP Status Report 1/2007*, pages 53–69. The Norwegian Meteorological Institute, Oslo, Norway, 2007.

D. Simpson and A.G. Hjellbrekke. Photo-oxidants: validation and combined maps. In *In Transboundary Acidification, Eutrophication and Ground Level Ozone in Europe in 2006. EMEP Status Report 1/2008*, pages 53–66. The Norwegian Meteorological Institute, Oslo, Norway, 2008.

David Simpson. Ozone. In *Transboundary Acidification, Eutrophication and Ground Level Ozone in Europe since 1990 to 2004, EMEP Status Report 1/2006*, pages 53–62. The Norwegian Meteorological Institute, Oslo, Norway, 2006.